Spring 1995

An investigation of the Speed and Power Limitations of a Copper-Doped Gallium Arsenide Photoconductive Switch

David Clifton Stoudt
Old Dominion University

AN INVESTIGATION OF THE SPEED AND POWER LIMITATIONS OF A COPPER-DOPED GALLIUM ARSENIDE PHOTOCONDUCTIVE SWITCH

by

David Clifton Stoudt

B.S.E.E. December 1987, Old Dominion University
M.S.E.E. December 1989, Old Dominion University

A Dissertation Submitted to the Faculty of
Old Dominion University in Partial Fulfillment of the
Requirements for the Degree of

DOCTOR OF PHILOSOPHY

ELECTRICAL ENGINEERING

OLD DOMINION UNIVERSITY
May, 1995

Approved by:

_____
Karl H. Schoenbach (Director)

_____

_____

_____

ABSTRACT

AN INVESTIGATION OF THE SPEED AND POWER LIMITATIONS OF A COPPER-DOPED GALLIUM ARSENIDE PHOTOCONDUCTIVE SWITCH

David Clifton Stoudt
Old Dominion University, 1995
Director: Dr. Karl H. Schoenbach

The processes of persistent photoconductivity followed by photo-quenching are demonstrated in copper-compensated, silicon-doped, semi-insulating gallium arsenide. These processes allow a switch to be developed that can be closed by the application of one laser pulse (λ=1.06 μm) and opened by the application of a second laser pulse with a wavelength equal to twice that of the first laser (λ=2.13 μm). Switch closure is primarily achieved by elevating electrons from a deep copper center which has been diffused into the material. The opening phase is a two-step process which relies initially on the absorption of the 2-μm laser causing electrons to be elevated from the valence band back into the copper center, and finally on the recombination of electrons in the conduction band with holes in the valence band. The second step requires a sufficient concentration of recombination centers in the material for opening to occur in the subnanosecond regime. Both an experimental and a theoretical investigation of the generation of recombination centers in copper-doped gallium arsenide material, for the purpose of enabling the switch to close as well as open in the subnanosecond regime, is presented. These recombination centers were generated in the bulk GaAs material by fast-neutron irradiation (~1-MeV). An enhanced recombination

center density also allows the copper-compensated GaAs switches to open against average electric fields of up to 36 kV/cm corresponding to a switch voltage of 18 kV. Finally, a new high-power radio-frequency (RF) source topology is introduced which uses two copper-doped gallium arsenide switches to synthesize frequency-agile RF waveforms. These waveforms may have considerable advantages when used in high-power-microwave applications.

ACKNOWLEDGEMENTS

I would like to express by sincere appreciation to Dr. Karl H. Schoenbach for his insightful discussions and continual support during the course of my research. I would also like to thank Drs. Linda L. Vahala, Ravindra P. Joshi, and Gary E. Copeland for their comments on this manuscript and for being on my committee. I would also like to thank Mr. Michael A. Richardson for his efforts in performing many of the experiments reported in this dissertation. My thanks also go to the Naval Surface Warfare Center for allowing me to participate in the Navy Fellowship Program, and to the Space and Naval Warfare Systems Command (SPAWAR 332) for their financial support of this research.

To my parents, I offer my gratitude for providing me with the mental capacity and the strong will that allowed me to complete this undertaking. You always said that I could accomplish anything I set my mind to.

Finally, to my wife Kerry, I offer my deepest appreciation for your unwavering support, encouragement, and understanding during the course of this endeavor. The love and affection that I received from you, and our daughters Jennifer and Jessica, made all the difference in my being able to complete this work. I only hope that, by completing this dissertation, I will be able to repay you for the many days and nights that we were separated.

TABLE OF CONTENTS

Page

ACKNOWLEDGEMENTS ..... *ii*

TABLE OF CONTENTS ..... *iii*

LIST OF TABLES ..... *v*

LIST OF FIGURES ..... *vi*

Chapter

I. INTRODUCTION 1

A. The BOSS Switch Concept 4
B. Historical Background 9
C. Overview 11

II. DEVICE MODELING 13

A. The Semiconductor Rate Equations 13
B. Initial Numerical Results 16
C. Effect of the Circuit 23
D. Summary 24

III. SAMPLE PREPARATION AND CHARACTERIZATION 25

A. Fast-Neutron Irradiation 25
B. Sample Preparation 27
C. Sample Characterization 30
1. Majority-Carrier Mobility 30
2. Majority-Carrier Concentration 32
3. DC I-V Characteristics 33
D. Summary 37

TABLE OF CONTENTS - concluded

Page

IV. EXPERIMENTAL SETUP 39

A. Two-Wavelength Laser Source 39
B. Video-Pulse Circuit Configuration 42
C. Monocycle Circuit Configuration 46
D. Summary 50

V. EXPERIMENTAL RESULTS 51

A. Effects of a Low Neutron Fluence 52
B. Effects of an Excessive Neutron Fluence 54
C. Effect of Annealing 57
D. Electrical Pulse-Width Agility 60
E. High-Repetition-Rate Capability 64
F. Monocycle RF Generation 68
F. Summary 72

VI. DISCUSSION OF RESULTS 74

A. Recombination-Center Density vs. Neutron Fluence 75
B. Analysis of the Minimum Electrical Pulse Width 77
C. Variation of the Turn-Off-Laser Energy and Pulse Width 86
D. High-Repetition-Rate Self-Opening Switches 93
E. High-Power Capability 101
F. Summary 105

VII. CONCLUSIONS 107

LIST OF REFERENCES 112

Appendix

A. POTENTIAL RF OUTPUT OF A PSO GENERATOR 119

LIST OF TABLES

Table		*Page*
1.	Deep-level parameters used in the simulation	17
2.	Deep-level concentrations and energy levels	17
3.	Group designations and fluences of BOSS devices being investigated	29

LIST OF FIGURES

Figure		*Page*
1.	Energy-level diagram showing the dominant impurity levels of the semiconductor material used in the BOSS switch (GaAs:Si:Cu)	5
2.	The basic geometry of the BOSS switch (a); the resulting current delivered to the load during the BOSS switching cycle (b); the initial high-resistivity state of the material prior to the first laser pulse (c); the optical excitation of electrons from the Cu_B center to the conduction band (d); the slow decay of electrons during the on state (e); and the fast photo-induced quenching of the photoconductivity	7
3.	Simulated current response of a BOSS switch with the density of recombination centers as a variable parameter	18
4.	Simulated temporal variation of free carriers, and bound electrons at the Cu_B level for $N_{RC}=6.0x10^{15}$ cm^{-3}	20
5.	Simulated temporal variation of free carriers, and bound electrons at the Cu_B level for $N_{RC}=4.0x10^{15}$ cm^{-3}	21
6.	The effect of fast-neutron irradiation on the majority-carrier mobility in n-type gallium arsenide	31
7.	Effect of neutron irradiation on the dc I-V characteristics of copper-doped GaAs material	34
8.	The dc I-V characteristics of devices from the third neutron-irradiation run	36
9.	Schematic diagram of the flash-lamp-pumped Nd:YAG laser source and the associated optical parametric generator	41

LIST OF FIGURES - continued

Figure		*Page*
10.	Experimental setup used for performing high-speed testing of BOSS devices	43
11.	Optical delay lines used to demonstrate the pulse-width agility, and the high-repetition-rate capability of BOSS devices	45
12.	Schematic diagram of the pulse-switch-out (PSO) generator which relies on two BOSS devices to generate as power	47
13.	Stripline configuration of the pulse-switch-out generator	49
14.	Effect of neutron irradiation on the opening transient of BOSS devices for several neutron fluences and non-irradiated material	53
15.	Current waveform generated by a Group-VI device which was only illuminated by a 4.5-mJ 1-μm laser pulse	56
16.	Effect of 15-minute thermal anneals on the photoconductivity response of a BOSS device irradiated at a fluence of 5.33×10^{15} cm^{-2}. Annealing temperature starting from the bottom: 110, 207, 225, and 268° C	58
17.	Demonstration of electrical-pulse-width agility, by varying the time delay between the turn-on and turn-off laser pulses, for an applied voltage of 3.7 kV	61
18.	Demonstration of the minimum electrical pulse width by showing the effect of bringing the turn-on and turn-off laser pulses too close together	63
19.	Demonstration of a 1-GHz (thick line) and a 290-MHz (thin line) repetition rate within a two-pulse burst at an applied voltage of 16 kV	66
20.	Fourier spectra for the waveforms illustrated in Fig. 19: a 3.4-ns laser pulse separation (thin line); and a 1-ns laser pulse separation (thick line)	67

LIST OF FIGURES - continued

Figure		*Page*
21.	Demonstration of two bipolar pulses produced by a PSO generator for a 500-ps (thick line) and a 2-ns (thin line) delay between the 1-μm laser pulses	69
22.	Fourier spectra of the two waveforms shown in Fig. 21	71
23.	Simulated current response showing the effect of reducing the time delay between the turn-on and turn-off laser pulses	79
24.	Simulated temporal variation of free carriers, and bound electrons in the Cu_B, EL2, and RC levels for a laser-pulse separation of 1.5 ns	80
25.	Temporal variations of free and trapped charges for a 400-ps separation between laser pulses	83
26.	Temporal variations of free and trapped charges for a 115-ps separation between laser pulses	84
27.	Simulation of the effect of increasing the peak photon flux of the turn-off laser (Ψ_{lo}) for a given time separation between the turn-on and turn-off laser pulses (Δt)	89
28.	Simulation of an enhanced opening effect resulting from increasing the pulse width (σ) and peak photon flux (Ψ_{lo}) of the turn-off laser pulse	90
29.	Simulation of changes in the electron occupation of the Cu_B level resulting from doubling the pulse width (σ) and the peak photon flux (Ψ_{lo}) of the turn-off laser	92
30.	Simulation of a 290-MHz repetition rate within a two-pulse burst using two pulses from the 1-μm laser	94
31.	Temporal variation of the free charges and deep-level electron occupations for a device, with an RC density of $4x10^{16}$ cm^{-3}, which exhibited a self-opening effect as shown in Fig. 30	95

LIST OF FIGURES - concluded

Figure *Page*

32. Simulation of the time dependence of the free charges and the deep-level electron occupations for a device that opens without the turn-off laser 98

33. Simulated repetitive operation of a BOSS device using the same material and laser parameters that were used to generate the dashed line in Fig. 23 and the deep-level results illustrated in Fig. 25 99

34. Simulation of the temporal response of the free charges and deep-level occupations for the first three switching transients shown in Fig. 33 100

A-1. Potential output of a PSO generator constructed by replicating data similar to that shown in Fig. 21 for a laser pulse separation of 500 ps 120

A-2. Power spectrum of the single monocycle, for a repetition rate of 1 kHz, that was used to create the four-pulse burst shown in Fig. A-1 121

A-3. Power spectrum of the waveform shown in Fig. A-1 for a 1-kHz burst-repetition rate 122

A-4. Potential output of a PSO generator constructed by replicating data similar to that shown in Fig. 21 for a laser pulse separation of 2.0 ns 124

A-5. Power spectrum of the waveform shown in Fig. A-4 for a 1-kHz burst-repetition rate 125

CHAPTER I

INTRODUCTION

In recent years there has been considerable interest in the development of high-speed, high-power photoconductive switches for use in direct DC, or quasi-DC, to RF conversion. The applications for this type of technology are primarily in the area of ultra-wide-band (UWB) radar, impulse radar, biological-effects testing, and high-speed diagnostics. These applications require that the switching speeds be as fast as possible so that the generated electrical pulses contain the highest possible frequency components.

The use of a photoconductor as a high-speed switch was first demonstrated by Auston in 1975 [1]. In Auston's experiments, a micro-stripline was manufactured on a high-resistivity silicon substrate with the bottom metalized to form a ground plane. A photoconductor was integrated by simply making a small gap between two conductors on the top of the stripline. A frequency-doubled, mode-locked Nd:glass laser (λ= 0.53 μm) was used to create an electron-hole plasma near the surface of the crystal between the two conductors. This served to close the switch and launch a current pulse to the load which was connected between the top conductor of the stripline and the ground plane. Because of the relatively long lifetime of the carriers in silicon (~20 μs), the switch remained closed after the laser pulse was terminated. In order to terminate the load current, the 1.06-μm

fundamental of the Nd:glass laser was used to short the stripline to ground at the location of the photoconductor. The short occurred because the penetration depth of the fundamental wavelength exceeded the thickness of the silicon substrate. The reported rise and fall times were approximately 10 ps and 15 ps, respectively, and were determined by the rise times of the laser pulses. Although this switch generated very short electrical pulses, it was not a true *opening switch.* Auston simply used the second laser pulse to divert (or crowbar) the current to ground. Therefore, the switch will conduct for microseconds, or as long as the source can supply the current . Thus, this switch concept is limited to relatively low-power and low-repetition-rate applications.

Photoconductive switches made from semi-insulating (SI) gallium arsenide (GaAs) were first proposed by Lee in 1977 for use as both closing and opening high-power switches [2]. This type of switch can be considered a light-sustained bulk photoconductive switch which requires light to sustain the photoconductivity in the presence of electron-hole recombination processes. The closing phase of this type of switch is normally achieved by exciting electrons from the valence band into the conduction band using a laser with a photon energy greater than that of the semiconductor's bandgap energy. Therefore, electron-hole pairs are only created in a relatively thin region below the surface of the semiconductor. Since the closing phase relies on photon absorption, which has been measured to be less than a 0.6 ps process [3], the temporal shape of the rise time of the switch conductance is primarily dominated by the shape of the laser pulse. This switching process has been labeled the *linear mode* of operation and is characterized by one electron-hole pair being produced

by each photon absorbed. Therefore, the switch conductance is approximately linearly proportional to the absorbed photon flux in the semiconductor material.

In most cases, the lifetimes of electron-hole pairs in SI materials range from tens of picoseconds to tens of nanoseconds [4]. If the lifetime of the photo-generated carriers in the bulk material is shorter than the fall time of the laser pulse, the switch conductance will basically follow the temporal shape of the laser intensity. The lifetime of the carriers in the bulk SI materials depends on both direct and indirect electron-hole recombination, as well as electron and hole trapping in deep traps within the bandgap of the semiconductor. Therefore, the conditions under which the material is processed, or grown, has a drastic effect on the opening phase of the switching cycle of a linear photoconductive switch. Generally, a relatively large optical energy density, on the order of mJ/cm^2, is required for a suitably low on-state impedance in the linear mode.

A third type of photoconductive switching mechanism in SI-GaAs material has recently been investigated. This nonlinear mechanism, called the *lock-on mode*, was found to occur when linear-mode III-V devices were operated at average electric fields that were greater than about 10 kV/cm [5]. In the lock-on mode, the switch fails to open following the termination of the laser pulse. Instead, a condition of persistent conductivity occurs that is characterized by a fixed voltage drop, or average electric field, across the device. In GaAs devices that have not been intentionally irradiated by high-energy particles, or doped with certain impurities, the lock-on electric field ranges from about 3.5 kV/cm to 9.5 kV/cm [6]. This lock-on field appears to be independent of the initial voltage applied to the switch as

well as the circuit load line, or current through the switch. Lock-on has also been seen in GaAs devices that were switched by a high-energy electron beam [7,8].

As the applied voltage across the device is increased, the required optical energy to initiate the lock-on mechanism is reduced. This ability to *trigger* the closing of a switch in the lock-on mode has been associated with a *gain* mechanism which is related to the ratio charge carriers created to the number of photons actually absorbed. This gain increases as the applied electric field is increased. For example, at 40 to 60 kV/cm across a GaAs switch, an optical energy density of only a few nJ/cm^2 was sufficient to trigger the device to close [9]. Both photoluminescence and electro-absorption images have shown that current filaments are formed in the bulk region while operating in the lock-on mode [10-12]. The fact that the lock-on mode is synonymous with filamentary conduction may limit the usefulness of this type of switching for long-lifetime applications at high power due to the resulting damage in the semiconductor material. Also, since filamentation is a breakdown mechanism, the resulting statistical variation in the switch closing time relative to the optical trigger pulse (or *jitter*) is in excess of that possible with linear switches. Jitter is particularly important if many photoconductive switches will be driving a phased-array antenna.

I.A The BOSS Switch Concept

A new type of photoconductive switch, which is called the Bistable (or Bulk) Optically controlled Semiconductor Switch (BOSS), was proposed by Schoenbach, et.al. in 1988 [13]. This concept relies on persistent photoconductivity, which can be considered a gain mode, followed by photo-induced quenching to provide both switch closing and opening, respectively. The SI-GaAs material used in this switch is manufactured by the

controlled electrical compensation of silicon-doped GaAs with copper (GaAs:Si:Cu). Copper forms two dominant deep acceptor levels in GaAs, at 0.14 eV (Cu_A) and 0.44 eV (Cu_B) above the valence band, and silicon is a shallow donor at 5.8 meV below the conduction band [14,15]. The Cu_B level is the copper level of interest for this switching concept. The various energy levels of interest within the bandgap of GaAs:Si:Cu, at 25° C, is shown in Fig. 1. Also included in Fig. 1 are one deep donor level (EL2) which is native to GaAs, and one recombination center (RC). The RC level will be addressed in greater detail in later chapters.

The photoionization cross section of holes (10^{16} cm^2) and electrons (10^{17} cm^2) for the Cu_B level were measured by Kullendorf, et.al. [16]. In addition, the capture cross sections for holes and electrons in the Cu_B center are $3x10^{-14}$ cm^2 and $8x10^{-21}$ cm^2, respectively [17]. The large ratio of the hole to electron capture cross sections make the Cu_B center a very strong hole trap. When the proper amount of copper is diffused into the GaAs:Si material to result in semi-insulating behavior, the electron Fermi level will be above the Cu_B level. Therefore, the Cu_B center will be, at least, partially full of electrons under the conditions of thermodynamic equilibrium. This fact, as well as the large ratio of capture cross sections, allow the BOSS switch concept to be realized.

In order to explain the BOSS concept, I consider the commonly used switch geometry that is shown in Fig. 2(a). It is comprised of a bulk piece of semi-insulating material with two electrical contacts, for connection to the external electrical circuit, manufactured on the same side of the substrate. The third port of the device is the optical illumination that activates the switch. As discussed in the following, one wavelength is used to turn the switch

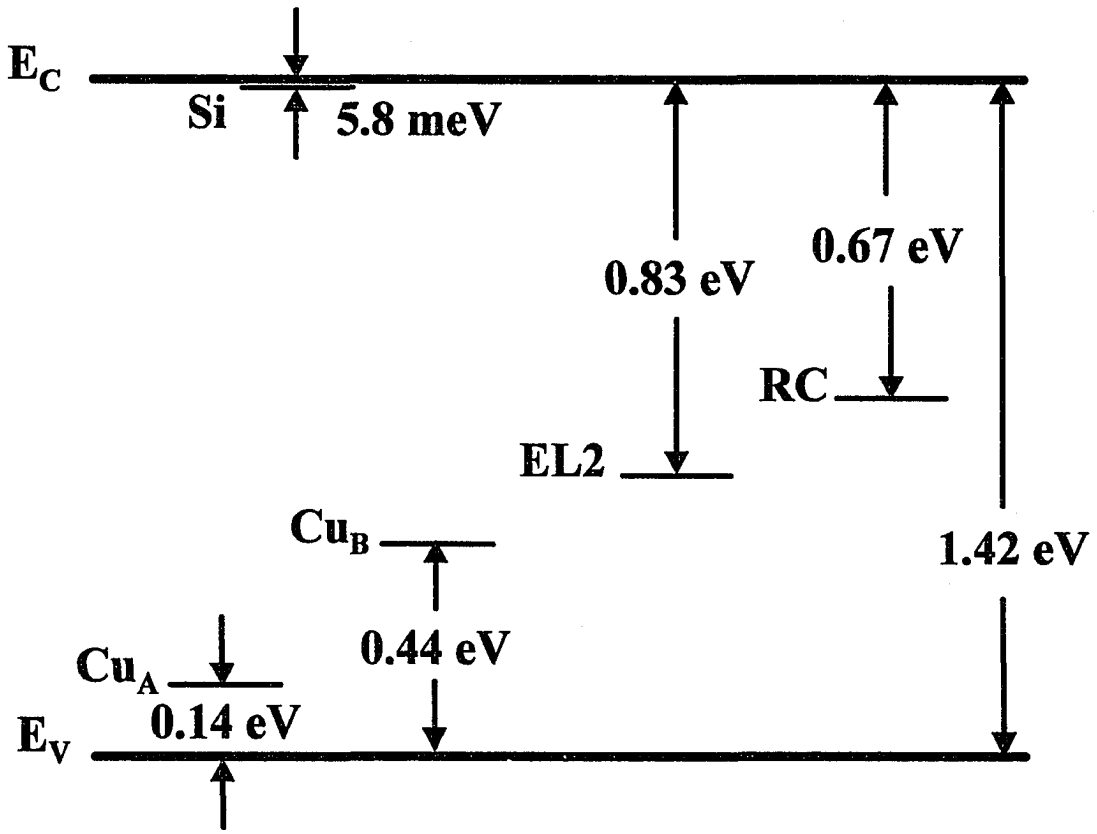

Figure 1 Energy-level diagram showing the dominant impurity levels of the semiconductor material used in the BOSS switch (GaAs:Si:Cu).

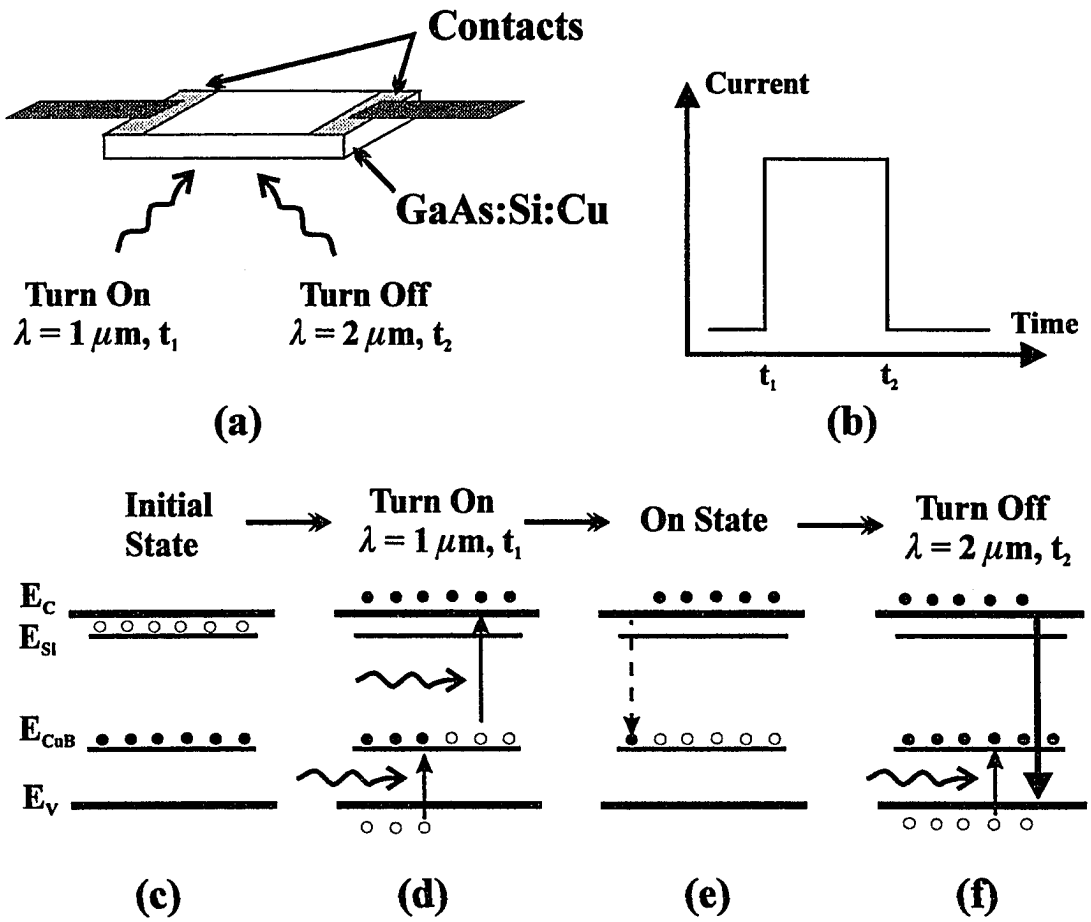

Figure 2 The basic geometry of the BOSS switch (a); the resulting current delivered to the load during the BOSS switching cycle (b); the initial high-resistivity state of the material prior to the first laser pulse (c); the optical excitation of electrons from the Cu_B center to the conduction band (d); the slow decay of electrons during the on state (e); and the fast photo-induced quenching of the photoconductivity.

on (λ=1.06 μm) and another wavelength is used to turn the switch off (λ=2.13 μm), thus generating a temporal current profile as shown in Fig. 2(b).

Figure 2 (c) illustrates the ideal case of all the thermally ionized electrons from the silicon level being trapped in the Cu_B center. This would result in an electrically compensated, high-resistivity material and represents the state of the BOSS switch when the voltage is first applied. At a time t_1, the switch is illuminated by a laser pulse with a photon energy sufficient to elevate electrons from the Cu_B center to the conduction band (i.e., with the fundamental wavelength of a Nd:YAG laser, λ=1.06 μm)[Fig. 2 (d)]. At the same time, holes are generated in the valence band through photo-ionization of empty Cu_B levels. As the laser pulse is terminated, there is a period of fast electron-hole recombination through the RC center. However, due to the large cross section of Cu_B for hole trapping, a sufficient density of holes are re-trapped to allow a large free-electron density to remain in the conduction band. Therefore, current is permitted to flow through the external circuit [Fig. 2 (b)]. Because the electron capture cross section of Cu_B is much smaller than the hole capture cross section, the electrons in the conduction band will remain for a relatively long period of time after the first laser pulse is terminated [Fig. 2 (e)]. The long lifetime of these electrons in the conduction band make GaAs:Si:Cu a high-gain photoconductor.

The current through the switch can be terminated by illuminating the GaAs crystal, at a time t_2, with photons of an energy that is less than the Cu_B-to-conduction-band transition, but greater than the valence-band-to-Cu_B transition (0.44 eV < $h\nu$ < 1 eV). These photons will elevate electrons back into the Cu_B level, leaving behind holes in the valence band which can then recombine with the free electrons in the conduction band, thus leading to the

opening of the BOSS switch on a nanosecond time scale [Fig. 2 (f)]. In the ideal case, the second laser pulse would reset the bulk material back to its condition prior to the first laser pulse. Therefore, the BOSS switch has the potential for very high repetition-rate operation.

I.B Historical Background

Copper-doped GaAs has been investigated for some time, however, not as a substrate material for a closing and opening photoconductive switch. Seminal work was performed by Blanc, et.al. [14] who studied the conductivity of GaAs:Si:Cu under low intensity conditions and at varying temperatures for the purpose of determining deep level parameters. They also showed that the material exhibited infrared quenching of the photocurrent at photon energies in the range of 0.4 eV < $h\nu$ < 1.1 eV, which was attributed to deep copper centers. Lyubchenko, et.al. showed in 1968 that the optimum photon energy for quenching the photocurrent in GaAs:Si:Cu was between 0.5 eV and 0.6 eV [18]. This is very convenient since the photon energy of the wavelength-doubled Nd:YAG laser is 0.58 eV. Therefore, one Nd:YAG laser, with a wavelength doubler, can be used for both closing and opening a BOSS device. Similar results were obtained in the early 1970's by Brodovoi and Kolesnik [19], and Brodovoi and Derikot [20].

Brodovoi and Derikot [20] also studied the effects of photoconductivity and photo-quenching in GaAs:Si:Cu at average electric fields of up to 35 kV/cm. They showed that after the voltage was applied, the current increased to a value that was limited by the circuit, following a time delay that was inversely proportional to the applied voltage. This low-resistivity state appears to be very similar to the lock-on mechanism. Similar results were obtained by Stoudt, et.al. [7] in SI-GaAs, and by Roush, et.al. [21] in GaAs:Si:Cu. Another

very interesting result shown by Brodovoi and Derikot [20] was that at 77 K, the low-resistivity state was retained for hours after the voltage pulse was removed. Furthermore, they showed that the material could be returned to a high-resistivity state by either heating it back up to room temperature, or by illuminating the crystal with infrared light with photon energy in the range of 0.2-0.7 eV. This indicates that the lock-on mechanism is related to trap-filling mechanisms as proposed by Brinkmann, et.al. [8].

The use of photo-induced quenching of photoconductivity in photoconductive switches, that can be opened and closed, on command, was initially demonstrated in copper-doped cadmium sulfide (CdS:Cu) by Germer, et.al. in 1988 [22], and Germer and Schoenbach in 1989 [23]. In their experiments, bulk CdS:Cu crystals were illuminated by a frequency-doubled Nd:YAG laser pulse (λ=532 nm) for turn on, and a fundamental Nd:YAG laser pulse for turning the switch off. Both laser pulses had a full-width-half-maximum (FWHM) of about 7 ns. The first laser pulse initiated long-lived photoconductivity lasting for several microseconds, while the second laser pulse successfully quenched the photoconductivity in about 250 ns [23]. According to the energy level diagram of CdS:Cu, the Nd:YAG fundamental wavelength corresponds to transitions from the valence band to deep-copper centers [24], much like the doubled Nd:YAG wavelength in GaAs:Si:Cu material.

The ability of the BOSS switch, made from GaAs:Si:Cu, to close and open has been demonstrated at relatively high power levels on the several-nanosecond time scale [25-28]. Recent experimental results have shown that the current through a BOSS switch could not be fully quenched by the application of a 140-ps (FWHM) 2.13-μm laser pulse [29]. A

numerical solution of the semiconductor rate equations for copper-doped GaAs showed that the primary cause for incomplete photo-quenching was that the concentration of the recombination centers (RC) was too low [30]. As stated above, the opening transient is the result of a two-step process. The second step is controlled by the electron-hole recombination lifetime which is dominated by the concentration of mid-gap RC's in the bulk material. A defect is considered a RC when the cross-sections for electron and hole capture are approximately equal. If there is an insufficient RC concentration, the holes that are generated by the 2.13-μm laser pulse will be re-trapped into the copper centers before they can recombine with electrons in the conduction band. This will result in the switch remaining closed after the second laser pulse.

I.C Overview

The work outlined below covers several areas involving the development of a high-speed, high-frequency, and high-power copper-doped GaAs photoconductive switch. In Chapter II, a rate-equation model will be introduced for the evaluation of the switching performance of BOSS devices. The computer code used for the evaluation of this model was originally developed by Dr. Ralf Peter Brinkmann while he was a visiting professor at ODU. This model has since been modified, with his permission, for the purpose of this discussion. In Chapter III, the various processing steps for the manufacture of BOSS devices are discussed. Since the GaAs:Si:Cu material was shown to be deficient in its RC density, fast-neutron irradiation was chosen as a means to produce higher concentrations of recombination centers [30]. Basic material characterization techniques will also be discussed in Chapter III. In Chapter IV, the experimental apparatus that are used to investigate the switching

performance of neutron-irradiated BOSS devices are discussed. In Chapter V, the results of various switching experiments are presented. These experiments will show the effects of varying the fast-neutron dose on the performance of BOSS devices. In Chapter VI, the experimental results are discussed within the context of the rate-equation model. Finally, in Chapter VII, the important conclusions of this work will be summarized, and the applicability of this technology to UWB applications will be addressed.

CHAPTER II

DEVICE MODELING

This chapter contains a discussion of the model which was used to determine the subnanosecond response of a BOSS switch. The model is zero-dimensional, which means that the continuity equations for electrons and holes are reduced to rate equations. These assumptions are valid in the bulk region away from the contacts where the electric field can change rapidly. This is a reasonable approach since the samples that were considered in this analysis were fitted with injecting contacts, made from a forward biased p^+-i-n^+ structure, which reduce the fields at the contacts considerably. The rate equations consider only the localized concentration of free and trapped charges, therefore, they are only valid under the conditions of low-carrier injection and moderate electric fields. The primary purpose for evaluating these rate equations is to gain some insight into the dynamics of the GaAs:Si:Cu deep-level system, and in particular, to understand the effects of increasing the recombination center density through neutron irradiation. Much of this chapter is taken from a paper written by Stoudt, et.al. [31].

II.A. The Semiconductor Rate Equations

The transient development of the electron density in the conduction band (n), the hole density in the valence band (p), and the relative occupation numbers ($0 \le r_i \le 1$) of the various

deep levels with a given density N_i is given by the following set of rate equations

$$\begin{aligned} \frac{dn}{dt} &= \dot{n}_{cv} + \sum_i N_i \dot{r}_{ci}, \\ \frac{dp}{dt} &= \dot{n}_{cv} + \sum_i N_i \dot{r}_{vi}, \\ \frac{dr_i}{dt} &= \dot{r}_{vi} - \dot{r}_{ci}. \end{aligned} \tag{1}$$

The terms containing $\dot{r}_{ci}$ and $\dot{r}_{vi}$ on the right hand side of Eqn. 1 denote the reaction rates corresponding to the transition of electrons between the deep levels and the conduction band and valence band, respectively. Band-to-band transitions ($\dot{n}_{cv}$) which consist of direct recombination, thermal emission, and a contribution from the action of two-photon excitation induced by the shorter wavelength laser are given by

$$\dot{n}_{cv} = k_d(n_i^2 - np) + \beta \frac{h\nu}{2} \Psi_{hi}^2, \tag{2}$$

where k_d is the direct-recombination coefficient, β is the constant for two-photon processes, $h\upsilon$ is the photon energy (1.165 eV), n_i is the intrinsic carrier concentration, and Ψ_{hi} is the short-wavelength-laser photon flux. The equations describing transitions to and from the deep levels can be expressed as

$$\dot{r}_{ci} = k_{ci}\left[\frac{1 - r_{i,eq}}{r_{i,eq}} n_{eq} r_i - (1 - r_i)n\right] + [\sigma_{ci}^{o}(h\nu_{lo})\Psi_{lo} + \sigma_{ci}^{o}(h\nu_{hi})\Psi_{hi}]\, r_i, \tag{3}$$

$$\dot{r}_{vi} = k_{vi}\left[\frac{r_{i,eq}}{1 - r_{i,eq}} p_{eq}(1 - r_i) - r_i p\right] + [\sigma_{vi}^{o}(h\nu_{lo})\Psi_{lo} + \sigma_{vi}^{o}(h\nu_{hi})\Psi_{hi}](1 - r_i), \tag{4}$$

where the photoionization cross sections for electrons (σ_{ci}^{o}) and holes (σ_{vi}^{o}) in the "i^{th}" deep

level are assumed to be independent of the photon energy, but are set equal to zero if the photon energy is too small to induce a particular transition. The first term in Eqns. 3 and 4 describes the processes of trapping and thermal emission, governed by the rate constants k_{ci} and k_{vi} (which are products of the corresponding cross sections σ_{ci} and σ_{vi}, respectively, and the thermal velocity v_{th}). The second term in Eqns. 3 and 4 describes the effects of stimulated emission due to the external laser irradiation. The "hi" subscript is associated with the high-frequency laser, and the "lo" subscript is affiliated with the low-frequency laser. The "eq" subscript in the equations is used to indicate the equilibrium values which are calculated once the Fermi level (E_F) is uniquely resolved by solving the Fermi-Dirac probability functions. These probability functions are given by

$$N_C \exp\left(-\frac{E_c - E_F}{kT}\right) + \sum_i \frac{N_{A,i}}{1 + 2\exp\left(\frac{E_{A,i} - E_F}{kT}\right)} = N_v \exp\left(\frac{E_V - E_F}{kT}\right) + \sum_i \frac{N_{D,i}}{1 + 2\exp\left(\frac{E_F - E_{D,i}}{kT}\right)}, \tag{5}$$

where the "A" subscripts are associated with deep acceptor levels and the "D" subscripts are associated with deep donor levels.

The rate equation model includes two copper levels (Cu_B & Cu_A) which act as deep acceptors, one deep donor level (EL2) which is native to GaAs, and one recombination center (RC) that is assumed to correspond to the defects created by the neutron irradiation [32]. Table 1 lists the various parameters used in the model for the different deep levels. The total

concentrations of the impurity levels, and their location within the bandgap, are presented in Table 2. The concentration of the RC level was varied from $4x10^{15}$ cm^{-3} to $1x10^{16}$ cm^{-3} in the initial analysis to simulate the effect of increasing the neutron irradiation from zero fluence, or as processed GaAs:Si:Cu material, to $1.95x10^{15}$ cm^{-2}, respectively [41].

Because the rate equations are zero dimensional, they do not contain any of the circuit parameters in which the BOSS devices are embedded. To facilitate comparison with the experimental results, the values of the calculated electron and hole concentrations are used to determine the overall switch conductivity (σ) from the following relation

$$\sigma(t) = q\left(n(t)\mu_n + p(t)\mu_p\right)\,[\Omega - cm]^{-1}, \qquad (6)$$

where μ_n (=2900 cm^2/V-s) and μ_p (=400 cm^2/V-s) are the assumed low-field electron and hole mobilities. Once the switch conductivity is determined, we calculate the switch resistance using a length of 0.5 cm and a cross-sectional area of 0.05 cm^2. The switch resistance is then placed into a 100-Ω load line, with an applied voltage of 50 V, to simulate the initial experiments.

II.B. Initial Numerical Results

In this section, the initial numerical results that were obtained with the rate-equation model are discussed. The results of the simulations are shown in Fig. 3 where the switch current is plotted as a function of time for seven different RC concentrations. One laser pulse with a photon energy of 1.165 eV (λ=1.064 μm) and a peak photon flux of $1.6x10^{26}$ $cm^{-2}s^{-1}$ (29.9 MW/cm^2) is used to turn on the switch and a second laser pulse with a photon energy of 0.5825 eV (λ=2.128 μm) and a peak photon flux of $1.6x10^{26}$ $cm^{-2}s^{-1}$ (14.9 MW/cm^2) is

Table 1. Deep-level parameters used in the simulation.

Parameters	Values	References
σ_n (Cu_B)	$8x10^{-21}$ cm^2	[33]
σ_p (Cu_B)	$3x10^{-14}$ cm^2	[33]
σ_n^o (Cu_B)	10^{-17} cm^2	[34]
σ_p^o (Cu_B)	10^{-16} cm^2	[34]
σ_n (RC)	10^{-13} cm^2	[35]
σ_p (RC)	10^{-13} cm^2	[35]
σ_n^o (RC)	10^{-16} cm^2	[*]
σ_p^o (RC)	10^{-16} cm^2	[*]
σ_n (EL2)	$4x10^{-16}$ cm^2	[36]
σ_p (EL2)	$2x10^{-18}$ cm^2	[36]
σ_n^o (EL2)	$8x10^{-17}$ cm^2	[37]
σ_p^o (EL2)	$3x10^{-17}$ cm^2	[37]
σ_n (Cu_A)	$8x10^{-21}$ cm^2	[*]
σ_p (Cu_A)	$3x10^{-14}$ cm^2	[*]
σ_n^o (Cu_A)	10^{-17} cm^2	[*]
σ_p^o (Cu_A)	10^{-16} cm^2	[*]
β	26 cm/GW	[38]
k_d	$7x10^{-10}$ cm^3s^{-1}	[39]

* These values are not known and are assumed as reasonable.

Table 2. Deep-level concentrations and energy levels.

Name	Energy	Concentration	References
Cu_A	E_v+0.14 eV	$6.0x10^{15}$ cm^{-3}	[40]
Cu_B	E_v+0.44 eV	$2.5x10^{16}$ cm^{-3}	[40]
EL2	E_v+0.59 eV	$5.0x10^{15}$ cm^{-3}	[25]
RC	E_v+0.75 eV	$4.0x10^{15}$ to $1.0x10^{16}$ cm^{-3}	[41]

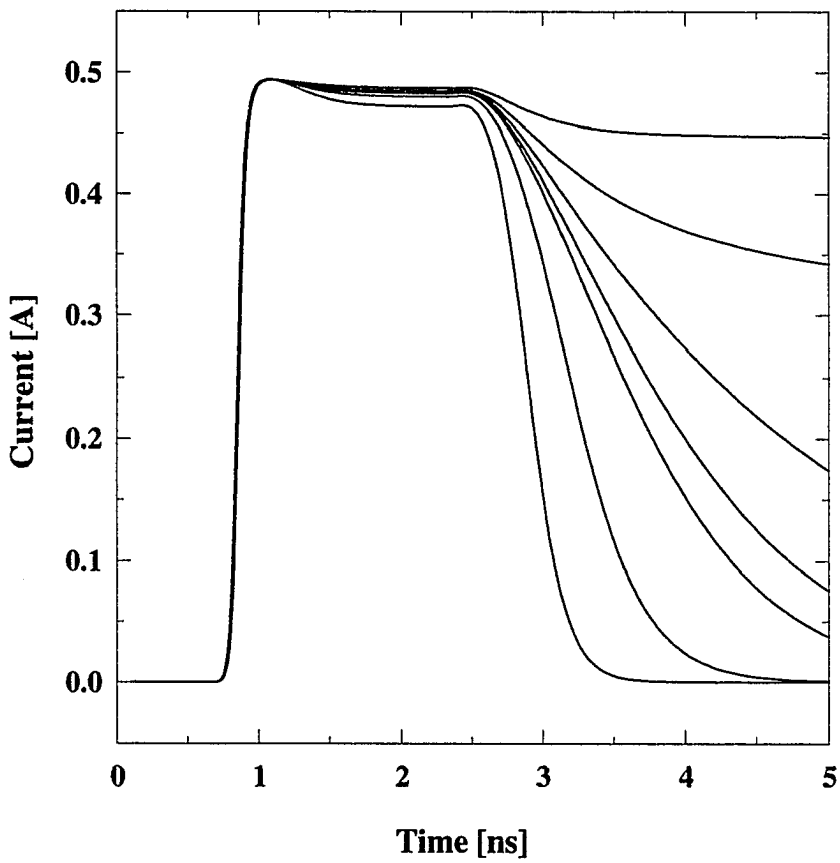

Figure 3 Simulated current response of a BOSS switch with the density of recombination centers as a variable parameter. N_{RC}[x10^{15} cm^{-3}]; (from the top) 4, 5, 5.5, 5.8, 6, 7, 10.

used to turn the switch off. The temporal shape of the laser pulse is assumed to be Gaussian with the standard deviation set equal to 70 ps in the simulation. The center of the turn-on laser pulse is at 1 ns, and the center of the turn-off laser pulse is at 2.5 ns. Figure 3 clearly shows that by increasing the RC concentration by a factor of 2.5, the ability of the BOSS switch to respond to the 2-μm 140-ps laser pulse is dramatically improved. When the RC density is $4x10^{15}$ cm^{-3}, the switch current is only reduced a small amount by the turn-off laser pulse. This current response is in good agreement, as will be shown in a later chapter, with the experimental results for a BOSS device that has not been irradiated by neutrons. The on-state of the switch was not adversely effected until the RC concentration was increased to $1.0x10^{16}$ cm^{-3} as indicated by a reduction in the on-state current. A higher on-state resistance would probably be more apparent if the electron and hole mobilities were adjusted for the increase in ionized impurity scattering.

In order to further explore the effect of enhancing the RC density on the BOSS switching cycle, the time variation of the free carriers and the changes in the Cu_B occupation will be examined. Temporal variations of the free electron and hole concentrations, as well as the bound electron concentration of the Cu_B level are shown in Fig. 4 for an RC concentration of $6.0x10^{15}$ cm^{-3}. For comparison, the temporal variation of the free charge carriers and bound electrons in Cu_B are shown in Fig. 5 for a RC concentration of $4.0x10^{15}$ cm^{-3}. As mentioned previously, the current waveform in Fig. 3, that is associated with the RC density used for Fig. 5 ($4.0x10^{15}$ cm^{-3}), is similar to the experimental current waveform of a non-irradiated BOSS device. As shown in Figs. 4 and 5, the turn-on laser generates both electrons and holes while the turn-off laser can only generate holes. The rapid fall in the

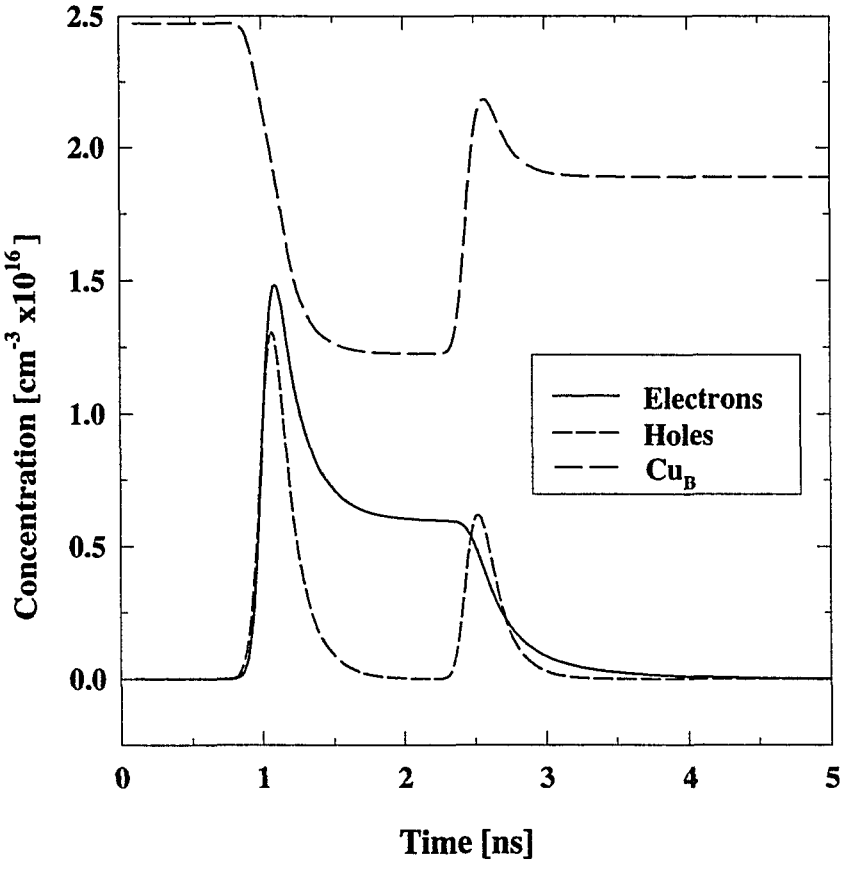

Figure 4 Simulated temporal variation of free carriers, and bound electrons at the Cu_B level for $N_{RC} = 6.0 \times 10^{15}$ cm^{-3}.

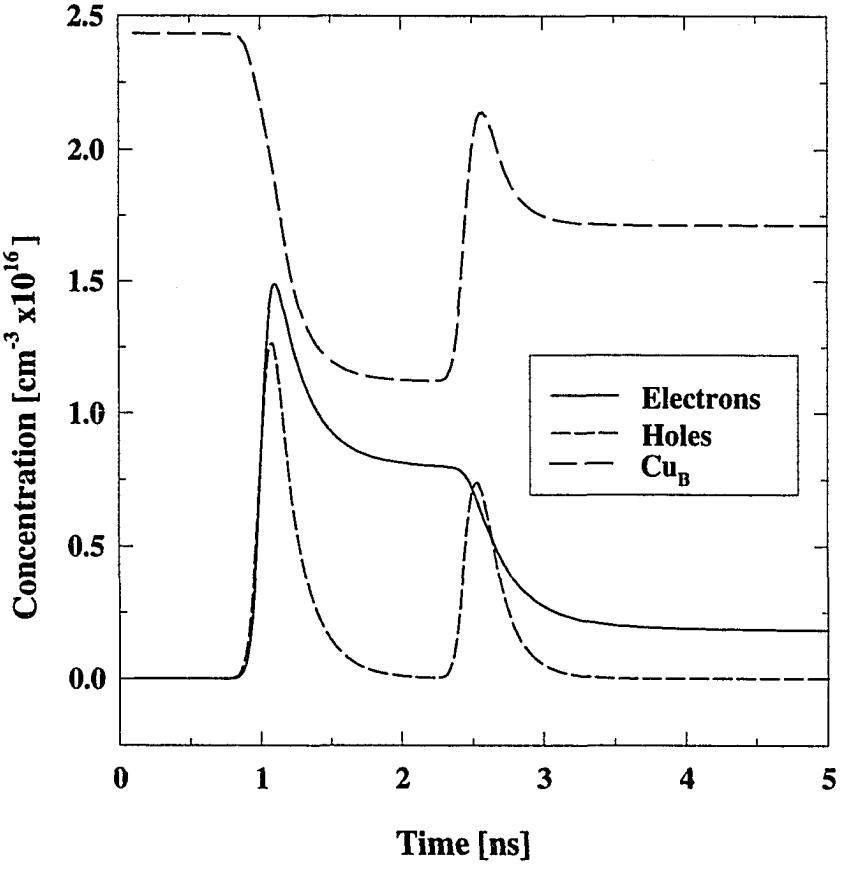

Figure 5 Simulated temporal variation of free carriers, and bound electrons at the Cu_B level for $N_{RC} = 4.0 \times 10^{15}$ cm^{-3}.

electron concentration after the turn-on laser pulse is primarily the result of electron-hole recombination through the RC's. As the RC concentration is increased, the time constant for recombination approaches that for hole capture into the Cu_B center. As this occurs, the on-state conductivity is reduced because electrons in the conduction band will recombine with holes in the valence band before those holes can be trapped into the Cu_B center. This result is shown in Figs. 4 and 5 where the material with a lower RC concentration has a higher on-state electron concentration. This process also reduces the number of holes that are trapped in the Cu_B center which, in turn, reduces the available sites to receive electrons from the valence band during the turn-off laser pulse.

The benefits of an increased RC concentration are shown to occur during the turn-off transient of the switch. First, the final electron occupation of the Cu_B center is examined. The lower RC concentration, used in Fig. 5, resulted in a final Cu_B electron occupation of about $1.7x10^{16}$ cm^{-3}, while the higher RC concentration, used in Fig. 4, resulted in a final Cu_B electron occupation of about $1.9x10^{16}$ cm^{-3}. Therefore, a lower RC concentration allowed more holes to be re-trapped into the Cu_B center. This has the effect of keeping more electrons in the conduction band which reduces the final off-state resistance of the switch. Even when there is a high RC concentration, as shown in Fig. 4, the final electron occupation of Cu_B is much less than what it was prior to the switching cycle because some electrons are trapped in both EL2 and the RC. For the waveforms shown in Fig. 4, the occupation of the RC starts at about $3x10^{12}$ cm^{-3} before the first laser pulse and ends up at about $5x10^{15}$ cm^{-3} after the second laser pulse has terminated. This effect occurs because the holes which are trapped in Cu_B are not available for recombination with the electrons in the RC. Eventually,

in a time less than about 1 ms, thermal emission and re-trapping processes will cause the system to return to the equilibrium state prior to the first laser pulse.

II.C. Effect of the Circuit

It is important to understand the effect of the circuit load line on the temporal variation of the switch current. In Figs. 4 and 5, large changes in the free-electron and free-hole concentrations are observed following the termination of the first laser pulse. However, these large variations have little or no effect on the observed current through the switch. This is a direct effect of the circuit load line. Changes in the switch conductivity are only seen in the switch current when the resulting switch resistance is within one or two orders of magnitude of the load line resistance.

When a particular time constant, for example recombination time, is obtained from the fall time of the material conductivity following the turn-off laser pulse, the actual fall time (90-10%) of the switch current may be three or four times longer than this time constant. To illustrate that this is an effect of the circuit load line an example will be given for the case of a 100-Ω load line, a 50-V bias voltage V_B, and a minimum on-state switch resistance $R_{sw}(t)$ of 1 Ω. For this case, the maximum switch current $i(t)$ would be 495 mA. Inserting these parameters into the load-line equation (Eqn. 7), allows the switch resistances

$$R_{sw}(t) = \frac{V_B - 100\,i(t)}{i(t)} \tag{7}$$

to be found at the 90% current value, and the 10% current value, 12 Ω and 910 Ω, respectively. Therefore, an 80% change in the switch current required a factor of about 76 change in the switch resistance, which is inversely related to the conductivity of the material.

To continue the example, a recombination-time constant of 100 ps is assumed. With this time constant, the time necessary to change the switch resistance from 12 Ω to 910 Ω can be calculated. The result of this calculation yields a time of 433 ps for the current to fall from 90% to 10% of its peak value. Therefore, even if a recombination time of 100 ps is obtained through neutron irradiation, a BOSS switch would still not open in under several hundred picoseconds.

II.D. Summary

A basic rate-equation model that is used to simulate the operation of BOSS devices, and to illustrate the effects of increasing the RC density, has been presented. The time variations of the free charge carriers, and the electron occupation of Cu_B, illustrated the effects of increasing the RC density from 4.0×10^{15} cm^{-3} to 6.0×10^{15} cm^{-3}. The free carrier concentrations are used to calculate a time-dependent conductivity which is then converted to a switch resistance, and is inserted into a 100-Ω load line for comparison to the experiments.

The numerical solutions of the rate equations demonstrated that the primary cause for incomplete photo-quenching, on a subnanosecond time scale, was that the concentration of the recombination centers was too low [30]. The opening phase of the BOSS switch is a two-step process. The second step is controlled by the RC density in the material. If there is an insufficient RC concentration, the holes generated by the turn-off laser pulse will be re-trapped into the copper centers before they can recombine with electrons in the conduction band. Therefore, the switch will remain closed after the turn-off laser pulse. The next chapter describes the method used to generate the proper RC concentration in GaAs:Si:Cu.

CHAPTER III

SAMPLE PREPARATION AND CHARACTERIZATION

The GaAs:Si:Cu material used in BOSS devices is not commercially available. Therefore, it is necessary to perform a thermal diffusion process to introduce the deep copper centers into the material. However, the GaAs:Si:Cu material produced by this thermal diffusion process contained an insufficient number of recombination centers to allow the BOSS switch to open in the subnanosecond regime [29,30]. Therefore, it became necessary to create a higher RC density in the GaAs crystal to allow the evaluation of a subnanosecond BOSS switch. Fast-neutron irradiation was chosen to introduce these RC energy levels in the bulk material. In the following sections, a brief introduction to neutron irradiation will be given, and a discussion of its effects on the steady-state electrical properties of copper-doped GaAs will be presented.

III.A Fast-Neutron Irradiation

The effects of neutron irradiation on semiconducting materials have been studied for many years [42]. A more recent effort has concentrated on the reduction of the minority-carrier lifetime in GaAs through fast-neutron irradiation [43]. This later work indicated that the crystal damage created by neutron irradiation could be used for the purpose of RC enhancement in a BOSS device.

The effect of a neutron on the target material depends on its initial kinetic energy (KE). In this respect two energy regimes are of special interest: *fast neutrons* (KE ≥ MeV) and *thermal neutrons* (meV ≤ KE ≤ 10's keV). One effect of thermal neutron irradiation is the production of impurity atoms resulting from an inelastic collision between the neutron and the target nucleus. This process is called transmutation doping. For GaAs it has been observed that Ga and As atoms which have captured a thermal neutron, subsequently decay through β emission into an atom of Ge and Se respectively, both of which act as donor impurities [44]. In order to minimize the creation of additional impurities in the BOSS material, the thermal neutron flux was reduced as much as possible.

The unit for describing the intensity of neutron radiation is *flux* in units of neutrons/cm^2-s. The time integral of the flux, called the *fluence*, has the units of neutrons/cm^2 and is designated by the symbol Φ. Fluence is the common term used in radiation effects work to describe neutron exposure. Another important characteristic of radiation is the energy spectrum. One neutron source used in our work was Sandia National Laboratory's SPR-III bare core reactor, and the other source was their annular core research reactor (ACRR). Special precautions were taken to insured that the sample temperature did not rise above 100° C during the time that the samples were being exposed. The energy spectrum for both of these sources is peaked at about 1 MeV, however, the ACRR source has a somewhat higher concentration of thermal-neutrons [45]. A boron shield was used during the irradiations to absorb thermal neutrons below 10 keV.

The interaction of fast neutrons with GaAs, and most other target materials, is dominated by elastic nuclear scattering. The total scattering cross section σ is so small, of

the order of 10^{-24} to 10^{-23} cm^2, that the mean free path λ_p in GaAs with a solid-state density ρ of $4.42x10^{22}$ cm^{-3} [46] becomes, according to the classical kinetic theory of gases

$$\lambda_p = \frac{1}{\rho \sigma} \approx 2.3 \rightarrow 23 \ cm. \qquad (8)$$

This means that fast neutrons will suffer at most one collision in the sample before emerging [47]. This one collision will result in the displacement of either a Ga, As, or impurity atom from its initial site with a recoil energy large enough to initiate a displacement cascade. The primary knock-on atom can have sufficient energy to create literally hundreds of defects in the crystal. These defects have been shown to behave as recombination centers in GaAs:Si:Cu material [30].

III.B Sample Preparation

In this section we will outline how the copper-doped GaAs samples were prepared. It has been know for some time that low resistivity, silicon-doped (n-type) GaAs can be made semi-insulating by the introduction of copper acceptor levels through a thermal-diffusion process [14]. The samples used in this investigation were taken from two-inch diameter n-type GaAs crystals grown using the horizontal Bridgman technique [48]. The material was originally doped with a silicon concentration of ~$1\text{-}2x10^{16}$ cm^{-3} which yielded a resistivity of about $7x10^{-2}$ Ω-cm.

The samples were sealed in evacuated (~10^{-6} torr) electronic-grade quartz ampoules (diam.=1.2 cm, length=15 cm) which were also loaded with solid sources of pure arsenic and pure copper. It was recently demonstrated by Thomas and Lakdawala [49], that GaAs:Si:Cu material annealed in such a sealed quartz ampoule had a higher concentration of Cu_B than

Cu_A. This is a desirable effect since Cu_B is the level required for the BOSS switching cycle, while Cu_A is viewed more as a parasitic level. An arsenic overpressure is provided to minimize the decomposition of the GaAs during the high-temperature anneal. After being sealed, the ampoules were then placed in a three-zone tube furnace and annealed at 575±2° C for 6 hours. This diffusion temperature corresponds to a solid solubility of copper in GaAs of ~$2x10^{16}$ cm^{-3} [50]. After the diffusion, the ampoules were opened and the samples were polished on both sides to a mirror finish. An analysis of the electrical-compensation curves for this material indicated that it was slightly p-type [40]. Dark current-voltage (I-V) characteristics of samples, that had not been irradiated with fast neutrons, yielded resistivities on the order of $1x10^5$ Ω-cm. This resulted in an increase of the material resistivity by about six orders of magnitude through the electrical-compensation process.

The electrical contacts that were used in this investigation resulted in the formation of a p^+-i-n^+ structure with a contact separation of 5 mm, and with the *i* region corresponding to the SI-GaAs material. The n-type contact metalization was manufactured by RF sputtering a 1000-Å Au:Ge (88%:12%) layer, a 250-Å nickel layer, and an additional 4000-Å Au:Ge layer to reduce the sheet resistance. The p-type contact was manufactured by sputtering 5000 Å of Au:Zn (85 %: 15 %). The contacts were then annealed at 420° C for 10 minutes in N_2 at atmospheric pressure. This annealing temperature was chosen because it is above the eutectic temperature of the gold alloys. Therefore, when the sample is allowed to cool, a Ge-doped n^+ region will be under the n-type contact [51], and a Zn-doped p^+ region will be under the p-type contact. The p-type behavior of the Zn-based contact was verified by depositing Au:Zn on an n-type substrate, and measuring the resulting p-n junction characteristics.

Table 3. Group designations and fluences of BOSS devices being investigated.

Group Designation	Neutron Fluence [cm^{-2}]	Neutron Source
I	$1.95x10^{15}$	SPR-III
II	$7.93x10^{14}$	SPR-III
III	$3.84x10^{14}$	SPR-III
IV	$1.62x10^{14}$	SPR-III
V	$5.33x10^{15}$	ACRR
VI	$1.78x10^{16}$	ACRR
VII	$2.45x10^{15}$	SPR-III
VIII	$3.93x10^{15}$	SPR-III
IX	$2.00x10^{15}$	SPR-III
X	$2.45x10^{15}$	SPR-III

Thus far BOSS devices have been irradiated at a total of ten different neutron fluences as outlined in Table 3. Devices in Groups I through IV were irradiated in SNL's SPR-III reactor prior to the fabrication of the electrical contacts. The rest of the groups of devices were irradiated after to contacts were fabricated and annealed. Groups V and VI were irradiated in the ACRR source because the cost of obtaining such a high neutron fluence in the SPR-III reactor was prohibitive. BOSS devices in Groups I through VI were fitted with 1-cm wide contacts, while the devices in Groups VII through X were fitted with 5-mm wide contacts. All of the devices had contact separations of 5 mm, and substrate thicknesses of about 0.5 mm.

III.C Sample Characterization

In order to initially characterize the effect of neutron irradiation on the BOSS material, four neutron fluences were used: 1.95×10^{15} cm^{-2} for Group I; 7.93×10^{14} cm^{-2} for Group II; 3.84×10^{14} cm^{-2} for Group III; and 1.62×10^{14} cm^{-2} for group IV. The fluence values are given relative to 1-MeV GaAs-equivalent damage [52]. Following the irradiation, the sample's radioactivity was allowed to decay, for approximately one month, until it was below the background level.

III.C.1. Majority-Carrier Mobility

In order to determine the effect of the neutron fluence on the electron mobility, Hall devices were manufactured out of the n-type GaAs:Si substrate and included in the four groups of devices. The Hall samples were 1 cm x 1 cm in size and were fitted with n-type contacts in the four corners. The Hall mobility results are shown in Fig. 6 where the non-irradiated material had a mobility of 4660 cm^2/V sec. At the highest fluence of 1.95×10^{15}

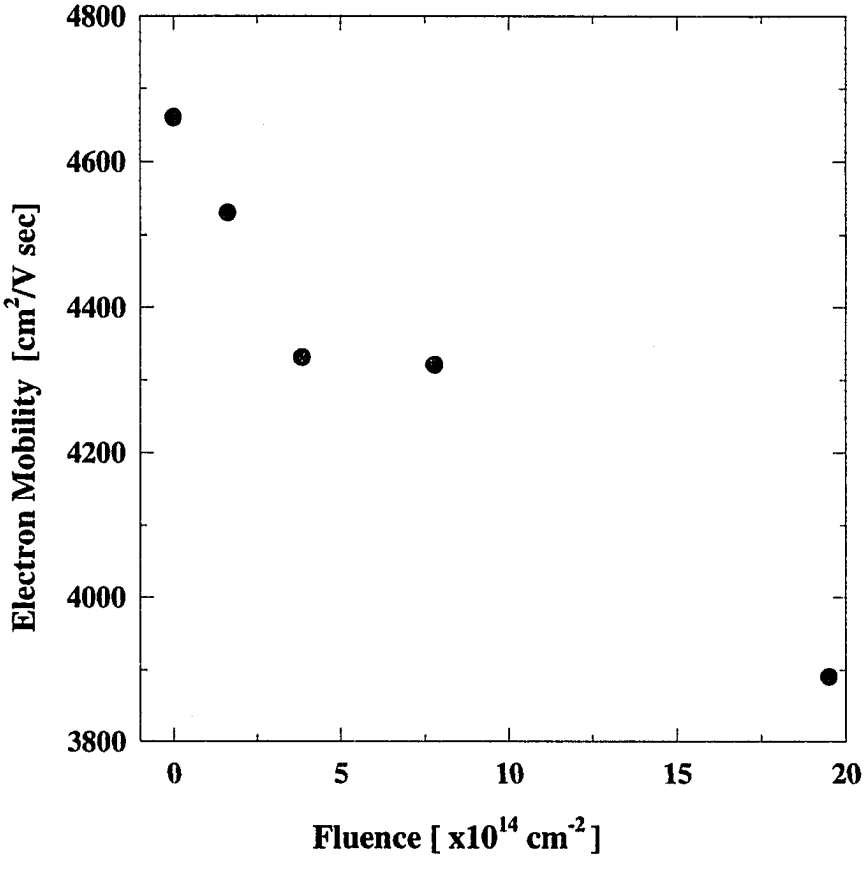

Figure 6 The effect of fast-neutron irradiation on the majority-carrier mobility in n-type gallium arsenide.

cm^{-2} (Group I) the mobility decrease by about 17% to 3890 cm^2/V sec. This effect is primarily the result of increased ionized impurity scattering and causes an increase of the on-state resistance of the BOSS device since the electrons are the majority carriers during this phase of the BOSS switching cycle. The reduction in the hole mobility has a negligible effect on the operation of a BOSS device.

Charged impurities have a larger scattering cross section than neutral ones, therefore, the change in mobility tends to be dominated by the introduction of ionized impurities (i.e., acceptors in n-type GaAs). For small changes in the Fermi level

$$\frac{1}{\mu} = \frac{1}{\mu_{LO}} + \frac{1}{\mu_{IO}} + K_{\mu}\Phi, \tag{9}$$

where μ_{LO} and μ_{IO} are the non-irradiated lattice and impurity scattering mobilities and K_{μ} is the mobility-damage constant [53]. When the inverse of the electron mobility is plotted as a function of neutron fluence, a linear curve fit to the data yields a mobility-damage constant of $2.04\pm0.24\times10^{-20}$ V-sec. The units of K_{μ} are found by $(cm^2/Vs)^{-1}$ /fluence(cm^{-2}) = V-sec. This result is in fairly close agreement with that of Kalma et al. [54], who reported a mobility-damage constant of 10^{-19} V-sec/electron for 1-MeV electron irradiations.

III.C.2. Majority-Carrier Concentration

Hall measurements yield the concentration of majority carriers as well as their mobility. If the radiation produces acceptor-like defects with energy levels below the Fermi level in n-type GaAs, the defects will capture free electrons and decrease the majority-carrier concentration. Although most complex radiation effects also include donor states, these states will not contribute many electrons unless they are close to the conduction band. A

relatively straight line, with a negative slope, is usually found when the free-electron concentration is plotted as a function of the neutron fluence. For small changes in the Fermi level, the electron density n after a radiation fluence Φ can be written as

$$n = n_o - K_n \Phi, \qquad (10)$$

where n_0 is the non-irradiated free-electron concentration, and K_n is the carrier-removal rate for electrons for the given Fermi level, temperature, and irradiation composition [55]. The units of K_n are cm^{-3}/fluence(cm^{-2})=cm^{-1}. A linear fit to the electron concentration data yielded a carrier-removal rate of 7.44±0.88 cm^{-1}. This value is in good agreement with D. Lang [56], who published carrier-removal rates in the range from 5 to 14 cm^{-1} for fission-neutron irradiations, which have an energy peak at about 1 MeV, in III-V materials.

III.C.3 DC I-V Characteristics

The dc I-V characteristics of the samples in Groups I through III are shown in Fig. 7. The sample in Group IV was damaged and could not be tested. The data in Fig. 7 indicate an increase in the switch resistance from about 1.3 MΩ for the non-irradiated devices to about 35 MΩ for the devices irradiated with the highest fluence. This increase in resistance is due to both a reduction of the electron mobility and a shift of the Fermi level towards the middle of the bandgap. The fact that the switch resistance increased by a factor of 27 while the electron mobility was only reduced by 17% is a clear indication that the dominant mechanism for the increased resistance is the movement of the Fermi level towards the middle of the bandgap.

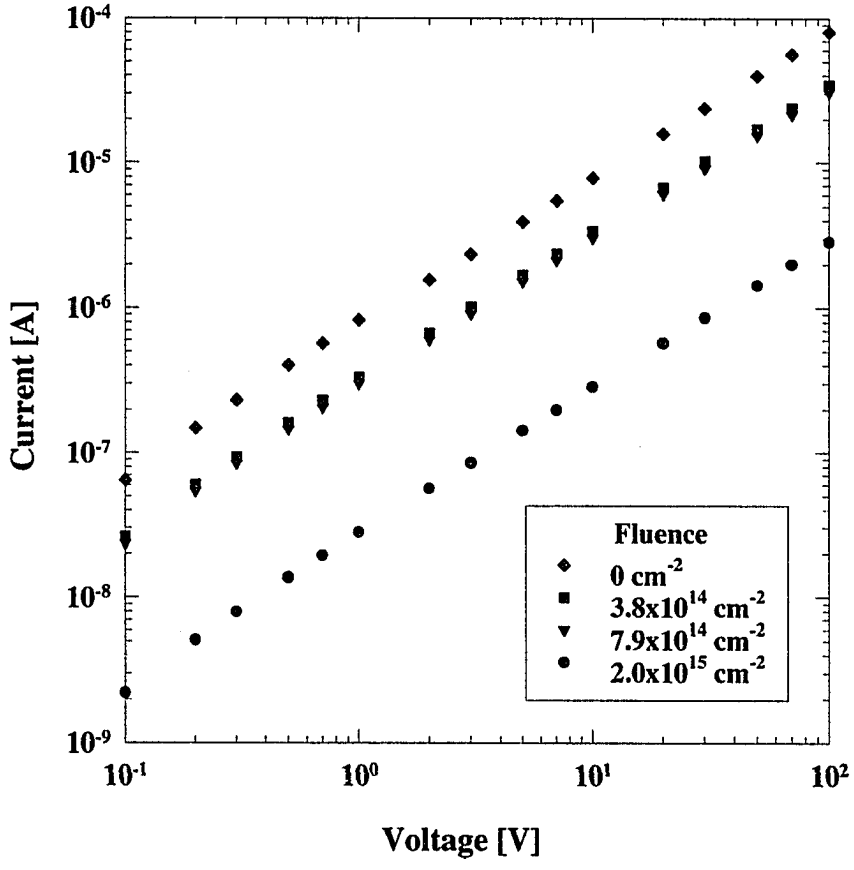

Figure 7 Effect of neutron irradiation on the dc I-V characteristics of copper-doped GaAs material. (◆: Non-irradiated; ■: Group III; ▼: Group II; ●: Group I)

The photoconductive switching results from the first SPR-III neutron run (Groups I - IV) indicated that a higher neutron fluence was necessary to achieve the desired opening performance. Therefore, a second set of BOSS devices were irradiated in the ACRR source. Two groups of samples were irradiated at the ACRR: 5.33×10^{15} cm^{-2} for Group V; and 1.78×10^{16} cm^{-2} for Group VI. The dc I-V characteristics of these devices indicated a dark resistance of 80 MΩ for Group V samples, and about 90 MΩ for Group VI samples. Unfortunately, these two fluences created too many RC's in the material. However, some of these devices were used to demonstrate the effect of thermal anneals on the damage created by the neutrons.

A third neutron run was made to the SPR-III reactor to try to bracket the desired neutron fluence. For this run, two sets of BOSS devices were neutron irradiated at two different fluences. The lower fluence was measured at 2.45×10^{15} cm^{-2} (Group VII) while the higher fluence was measured at 3.93×10^{15} cm^{-2} (Group VIII) 1-MeV-GaAs Equivalent damage. The sample temperature was held below about 70°C during both irradiations. Following the irradiation, the sample's radioactivity was allowed to decay, for approximately one month, until it was below the background level. The dc I-V characteristics of devices in both of these groups, both before and after the neutron irradiation, are shown in Fig. 8. The resistance of the device irradiated at the lower fluence increased from about 3.2 MΩ to about 55 MΩ while the resistance of the device irradiated at the higher fluence increased from about 4.3 MΩ to about 270 MΩ. These I-V characteristics indicate a substantial increase in the switch resistance (about a factor of 63!) resulting from an increase in the neutron fluence.

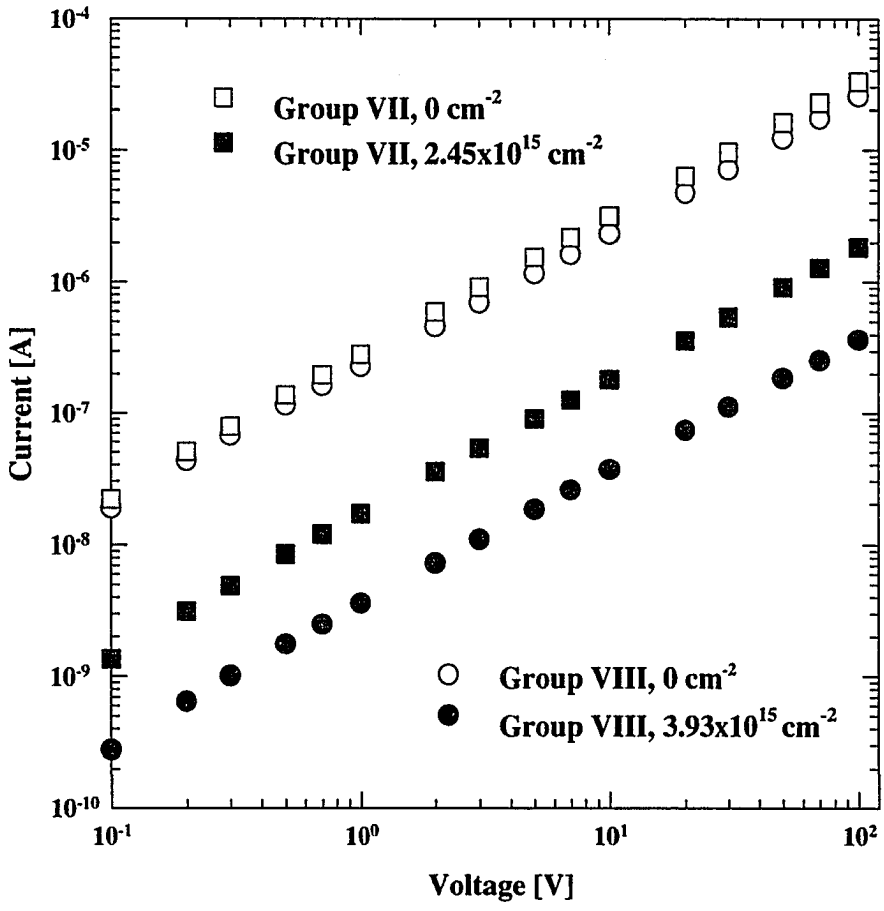

Figure 8 The dc I-V characteristics of devices from the third neutron-irradiation run. Open symbols indicate prior to irradiation, and closed symbols indicate after the irradiation.

Photoconductive switching results from the devices, whose characteristics are shown in Fig. 8, indicated that the Group VII fluence of 2.45×10^{15} cm^{-2} was the correct value to permit subnanosecond BOSS switching. Therefore, a fourth set of devices were sent to SNL for neutron irradiation in the SPR-III reactor. Two fluences were chosen for this run, the lower fluence was 2.00×10^{15} cm^{-2} (Group IX), and the higher fluence was 2.45×10^{15} cm^{-2}.

Two improvements were made to the processing of the bulk material for the devices in Groups IX and X. A non-contact, laminar-flow polisher was brought on line, which used a 0.5% solution of bromine in methanol, to create a very smooth finish on the GaAs surface [57]. The way that the contacts were delineated was changed from using a mechanical shadow mask to using photolithography. These improvements resulted in a much cleaner contact edge which should yield better switching results when the BOSS devices are operated at high power.

III.D. Summary

The method used for producing high-resistivity GaAs by electrically compensating shallow silicon donors with deep copper acceptors has been presented. There is evidence in the work done by Mil'vidskii [58], and by Thomas and Lakdawala [49, 59], that there is a variation in the copper compensation at different depths from the surface of the GaAs samples. However, is was demonstrated by Thomas and Lakdawala [59], that by performing the thermal diffusion process in a sealed ampoule with separate solid sources of arsenic and copper, the copper-concentration gradients can be minimized. This is precisely the thermal diffusion process used in this investigation.

Basic steady-state device characterization has been used for the neutron-irradiated GaAs devices. In particular, the mobility damage constant and the carrier removal rate were measured for n-type GaAs material exposed to Group I through Group IV neutron fluences. An increase in the resistivity of copper-doped GaAs material, as a result of neutron irradiation, was measured over a wide range of voltages. This increase was shown to primarily be the result of a shift in the Fermi level towards the middle of the bandgap, rather than a reduction of the electron mobility. In particular, for Group I devices, the electron mobility decreased by only 17% while the switch resistance increased by a factor of 27. Even though the GaAs:Si:Cu material was initially p-type, the hole mobility is not expected to decrease a sufficient amount to account for the large increase in the switch resistance.

The actual deep level parameters of the defects created by neutron irradiation are not available. A substantial amount of work has been performed by Goltzene, et.al. [60-62], using electron paramagnetic resonance (EPR) spectroscopy techniques. However, defects associated with recombination centers in neutron-irradiated GaAs are not presently understood. This does not preclude the use of neutron-irradiated GaAs:Si:Cu in subnanosecond BOSS devices.

CHAPTER IV

EXPERIMENTAL SETUP

In order to demonstrate the feasibility of the BOSS concept at high power in the subnanosecond time regime, an experimental apparatus has been constructed with a suitable bandwidth and voltage hold-off so as not to limit the operation of the device under test (DUT). This chapter will briefly describe the important components of the experimental apparatus used to make these photoconductive switching measurements. The discussion will cover the two-wavelength laser source, the circuit configurations used for generating both single-polarity or *video* pulses, as well as single-sinusoidal or *monocycle* pulses, the bandwidth of the diagnostics used to make the measurements, as well as the electrical circuit used to bias the DUT at voltages of about 20 kV.

IV.A. Two-Wavelength Laser Source

If it is desired to test the closing and opening time of a BOSS in times less than about three nanoseconds, the laser system used to generate the turn-on and turn-off laser pulses will need to be mode locked. It is extremely difficult to control the arrival time of two mode-locked laser pulses, with more than several hundred picoseconds of accuracy, if they are generated by two distinct laser sources. This is because the jitter in the high-voltage Q-switch circuitry, or in the apparatus used to mode lock the lasers, usually cannot be made

better than about one nanosecond. The jitter problem was alleviated in these experiments by using a single laser source, manufactured by Continuum, Inc., that is capable of producing both the turn-on and the turn-off laser pulses. Therefore, a simple optical delay line could be used to control when the switch was turned on and turn off. The system used was a 10-Hz, flash-lamp pumped, passive/active mode-locked Nd:YAG laser that is capable of generating a 150-mJ pulse with a FWHM of about 140 ps (see Fig. 9). The beam profile is basically Gaussian with an area of about 3 cm^2. Therefore, the peak laser power of this system is about 1 GW.

After the second-stage amplifier, the laser pulse went through a beam splitter and was then directed into an optical parametric generator (OPG) that was used to wavelength double the fundamental of the Nd:YAG laser [see e.g. a review by Byer [63]]. The OPG consists of three 2-cm long Potassium Titanyl Phosphate (KTP) crystals that are cut for Type-II phase matching (54°) so that normal incidence resulted in degenerate parametric conversion. In other words, a single 1.06-μm photon, from the pump beam, would be converted into two collinear 2.1-μm photons which comprise the signal and idler beams. The first KTP crystal constitutes the OPG while the second two KTP crystals, which are pumped by a second 1.06-μm beam, act as single-pass optical parametric amplifiers. The output of the OPG contains both the fundamental and the down converted photons. Dichroic mirrors, with optical coatings to pass the fundamental wavelength and turn the 2.1-μm wavelength, are used to separate the two beams. The final energy in the 2.1-μm beam is specified at a FWHM of between 120 and 140 ps and contains about 5 mJ in a cross-sectional area of about 0.28 cm^2. The initial experiments used the 1.06-μm beam that was split off prior to the OPG as the

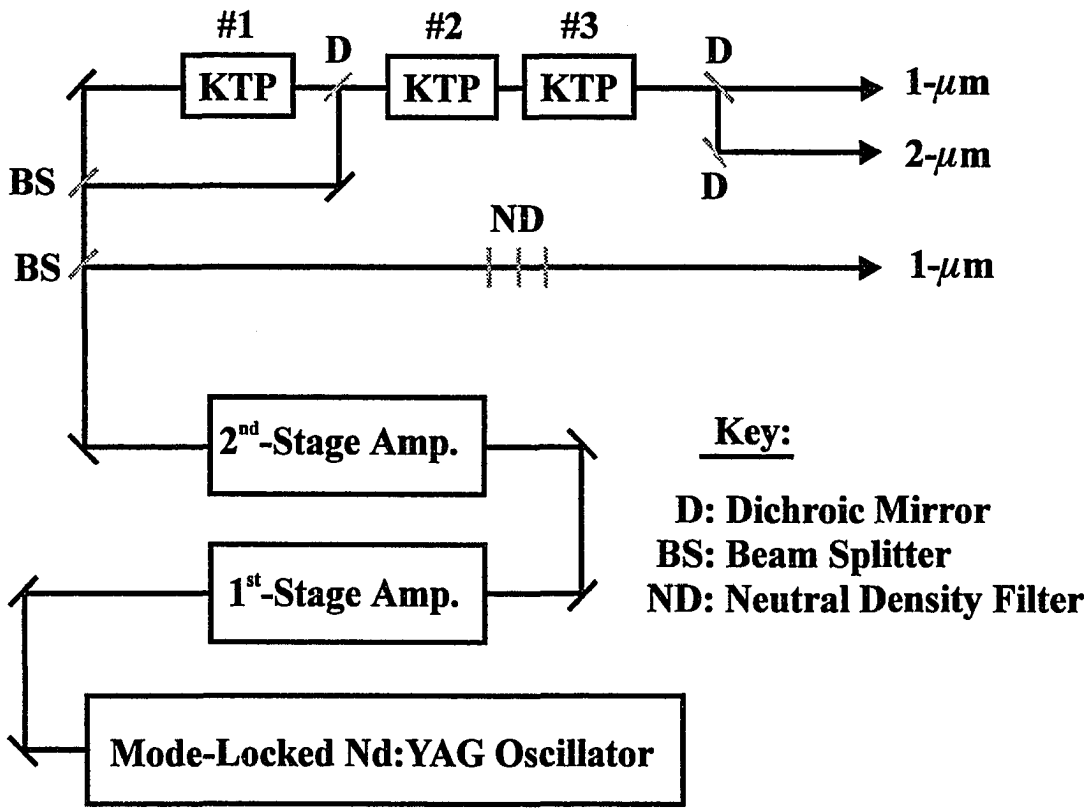

Figure 9 Schematic diagram of the flash-lamp pumped Nd:YAG laser source and the associated optical parametric generator.

turn-on laser pulse. The energy of this pulse was reduced by stacking volume-absorbing neutral-density filters in the beam path. Later experiments used the two beams out of the OPG for both the turn-on and the turn-off laser pulse.

One drawback of the passive/active mode-locking scheme was that the saturable laser dye used in the passive mode locking caused a timing jitter in the output of the laser that was on the order of microseconds. To alleviate this problem, a photo-diode was used to detect when the single pulse was switched out of the oscillator cavity. This was done by using a pulse-height discriminator to discriminate between the pre-pulses in the cavity to about forty round-trip times (7 ns) prior to the main pulse. The delay time of this trigger pulse could be adjusted to a maximum of about 300 ns. Therefore, a 300-ns window was available to pulse-charge the micro stripline that housed the BOSS device.

IV.B. Video-Pulse Circuit Configuration

Photoconductivity measurements, using a single-polarity bias voltage, were performed to evaluate the operation of the neutron irradiated BOSS devices at high voltages and high repetition rates. In these experiments, the BOSS switches were embedded in a 50-Ω transmission line (two-way transit time = 3 ns) that was pulse charged with roughly a 40-ns FWHM voltage pulse. The bias-voltage pulse was generated by two KN22 Krytron switches, that were connected in series to increase their voltage-handling capability, which discharged a 4 nF capacitor through a parallel combination of a 50-Ω resistor and the 50-Ω stripline as shown in Fig. 10. The duration of the bias-voltage pulse was controlled by the length of an RG-8 coaxial cable that was connected between the 50-Ω resistor in the voltage-modulator circuit and the SMA connector on the stripline. For these experiments, the 40-ns

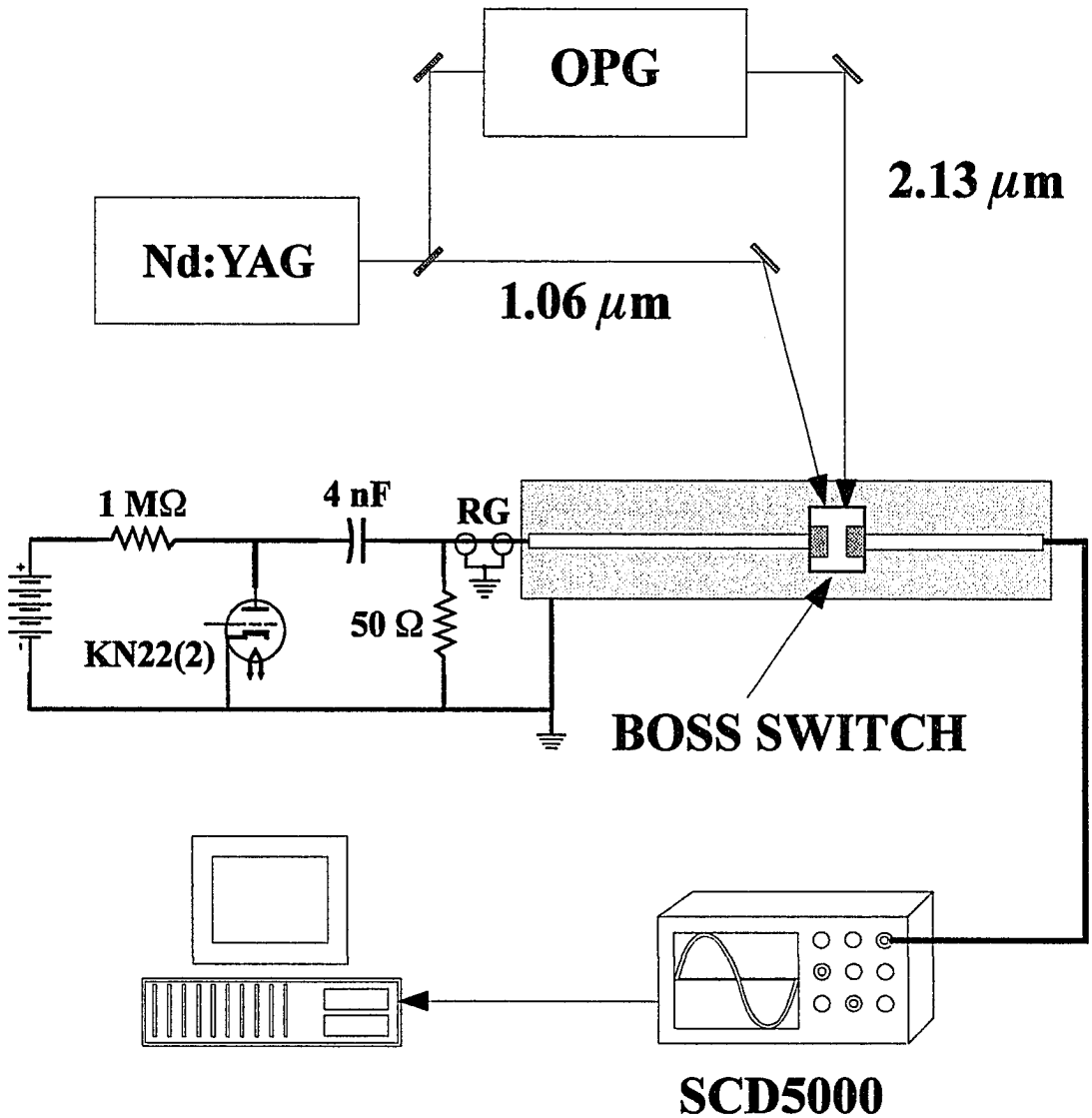

Figure 10 Experimental setup used for performing high-speed and high-power testing of BOSS devices.

pulse width corresponded to the round-trip time in the RG-8 coaxial cable. Voltage multiplication occurred at the end of the stripline were the DUT was located because it was effectively an open circuit. In an ideal situation, the voltage would be expected to double at the location of the BOSS switch. The measured multiplication value was about 1.8. The actual switch bias voltage was measured by a resistive voltage-divider located on the stripline. The maximum voltage applied to the BOSS devices was about 18 kV.

The current through the device was measured by a 50-Ω current-viewing resistor (CVR) placed after the switch in the 50-Ω line. The CVR was manufactured by Barth, Inc. (Model 2237-HFNFP) and can handle up to a 10 kV voltage pulse for a duration of up to 400 ns. The rise time of the CVR was specified to be <50 ps. The current waveform was recorded by a Tektronix SCD5000 digitizer with a 3.0 GHz analog/digital bandwidth which corresponded to a minimum rise time of 120 ps. Therefore, the overall bandwidth of the experiment was limited to 3.0 GHz.

It was not possible to operate the laser system at repetition rates above 10 Hz. Therefore, a special optical delay line was set up which divided the 1-μm and 2-μm laser pulses into two pulses, each with one half of the total energy. The experimental arrangement of the delay line is shown in Fig. 11. Both the 1-μm and the 2-μm wavelengths were taken out of the OPG. Dichroic mirrors were used to separate the two wavelengths, and 50:50 beam splitters were used to make the second set of laser pulses. Optical rails were fitted with 180° turning prisms, with anti-reflection coatings to minimize the optical losses, which allowed the laser-pulse separation to be easily adjusted. The setup shown in Fig. 11 could be configured either to create a single switching event with a variable delay between the turn-

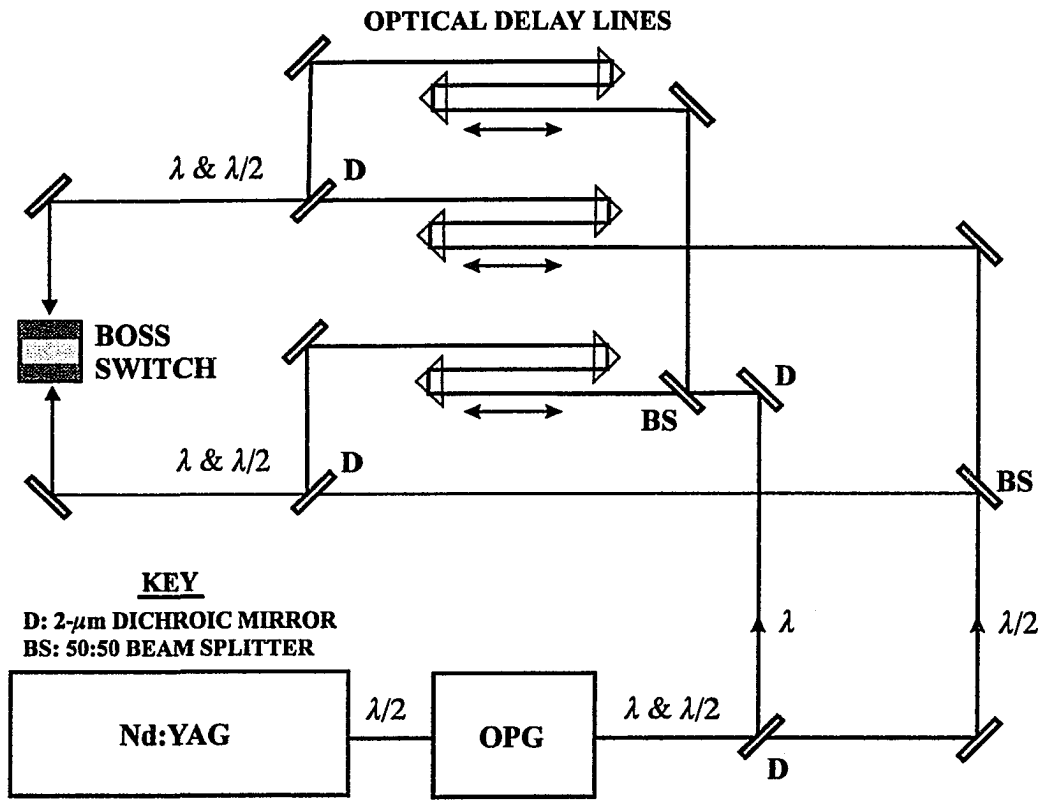

Figure 11 Optical delay lines used to demonstrate the pulse-width agility, and the high-repetition-rate capability of BOSS devices.

on and turn-off laser pulses, or to create a two-pulse burst by repetitively switching a single BOSS device. In the second case, a BOSS device could be switched at repetition rates as high as 1 GHz within the two-pulse burst. BOSS devices could only be tested at high repetition rates in a burst mode due to limitations in the laser system.

IV.C. Monocycle Circuit Configuration

One potential application for the BOSS technology is for it to be incorporated into a wide-band, frequency-agile source that can *radiate* the RF energy with a broadband antenna. In order to maximize the radiative efficiency of the source, it is necessary to produce ac power which reduces the dc component of the waveform. This is important since the dc component cannot be radiated out of an antenna. The ability of the BOSS switch to open, as well as close, in the subnanosecond regime allows a new type of RF source to be developed that is capable of generating repetitive high-power microwave cycles of varying duration, depending on the relative delay between the turn-on and turn-off laser pulses.

A source configuration that is capable of generating ac power with real-time frequency agility is shown in Fig. 12 and is called the pulse-switch-out (PSO) generator [64]. Positive and negative half-cycles are generated by first closing and opening each switch in succession. The frequency content in the generated RF pulses can be adjusted by either varying the time between the turn-on and turn-off of each switch, or by varying the time between the closure of each BOSS device while keeping the electrical pulse width the same. The second method results in a cross-over distortion which has a dramatic effect on the

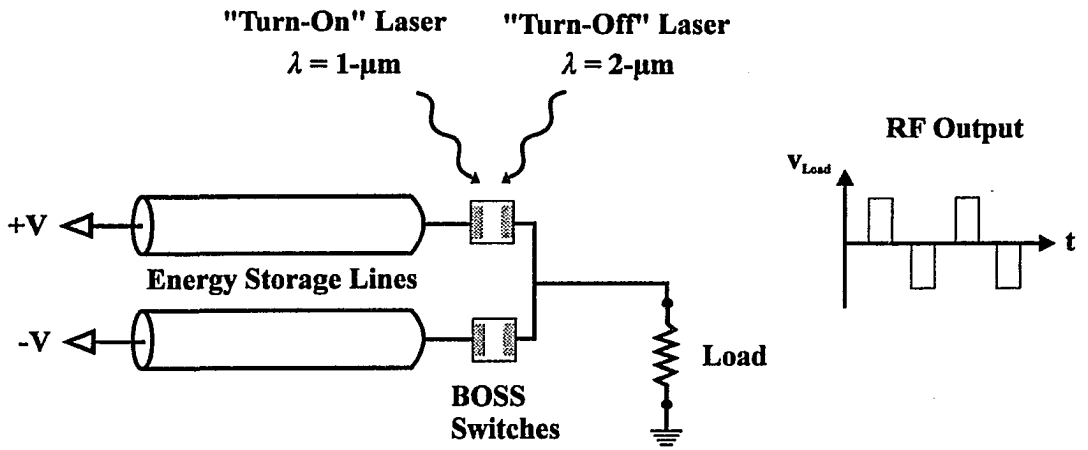

Figure 12 Schematic diagram of the pulse-switch-out (PSO) generator which relies on two BOSS devices to generate ac power.

generated frequency spectrum. Measured current waveforms and their associated frequency spectra will be shown in the following chapters.

The stripline configuration of the PSO source is shown in Fig. 13 where two BOSS switches are embedded in oppositely charged 50-Ω transmission lines. Both switches feed into a single 50-Ω transmission line that leads to a matched load consisting of the CVR discussed earlier. The two devices are connected at the same point on the stripline so that there will not be any current reflections off of the opened switch when the other switch is closed. It should be noted that when one of the BOSS devices is closed, the potential across the other device is doubled, assuming that both devices were biased at equal values with opposite polarities. Therefore, the switches in the PSO configuration must be able to withstand voltages that are twice as high as the charge voltage on the switch. This problem does not limit the operating voltage as much as it appears since each BOSS device is only closed for less than one or two nanoseconds. The circuit shown in Fig. 13 was also biased with a 40-ns voltage pulse. However, the output of the Krytron circuit had to be divided between the positive and negative striplines. Therefore, the maximum voltage that could be applied to each device was about 10 kV.

The optical delay lines illustrated in Fig. 11 can also be used to control both BOSS devices in the PSO configuration. The outputs of both delay lines are simply used to control each switch separately. With this setup, the second switch can be closed at any time relative to the first switch. This includes closing the second switch *before* the first switch is opened, a situation that will be discussed in the following chapters.

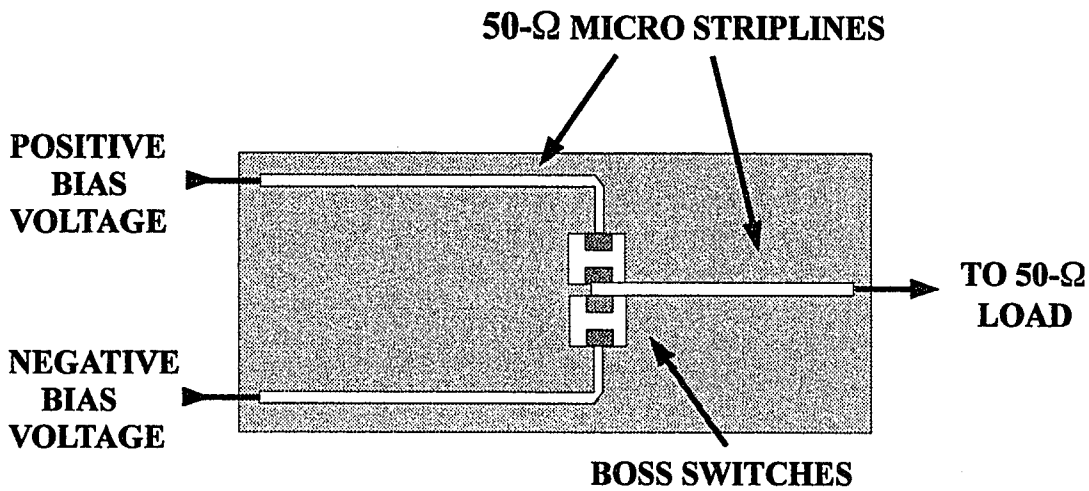

Figure 13 Stripline configuration of the pulse-switch-out generator.

IV.D. Summary

The experimental apparatus used to measure the photoconductive response of BOSS devices to subnanosecond laser pulses have been presented. A unique two-photon laser source has been described which can generate both the turn-on and the turn-off laser pulses without any time jitter between them. This feature is particularly important when more than one BOSS device is to be operated. The electrical circuit that was used to pulse-bias the BOSS devices has been explained, as was the high-bandwidth diagnostics used to measure the generated current waveforms. Two stripline configurations were presented, one capable of demonstrating the repetition-rate capability of BOSS devices, and the other which illustrates the use of two BOSS devices to create ac power. Experimental results demonstrating the high-power, the high-repetition-rate, and the variable-pulse-width capability of BOSS devices will be presented in the next chapter.

CHAPTER V

EXPERIMENTAL RESULTS

The photoconductive properties of BOSS devices that were exposed to various levels of fast-neutron irradiation were measured. The labels given to the DUT's correspond to the group designations listed in Table 3 on page 29. The experimental results will be discussed further, within the context of the numerical simulation, in Chap. VI.

In Chap. IV, two different experimental setups were described. The experiments that were conducted to characterize the effect of increasing the neutron fluence were done with a single-polarity bias voltage using the setup shown in Fig. 10. The DUT's in this setup could either be dc biased at low voltages, or pulse charged at high voltages, as shown in the figure. Experiments were also performed on devices in the circuit configuration shown in Fig. 13. These experiments were used to demonstrate the ability of BOSS devices to generate high-frequency ac power that can be radiated from an antenna.

The experimental results cover a wide range of neutron fluences. The effect of low and excessively high fluence levels on the switch behavior will be discussed. It happens that this outline basically follows the chronological order in which the devices were prepared for testing. The first section will describe the results obtained on devices in Groups I through III. Recall that the device from Group IV was damaged and could not be tested. The second

section will discuss results obtained from the devices in Groups V and VI which were irradiated in the ACRR reactor. These results will show that the neutron fluences used were too high, and that the damage created by neutron irradiation can be removed by thermally annealing the devices. The third section will describe the results obtained with devices in Groups VII and VIII. Devices in this section have shown the most positive results that have been measured to date. Devices in Groups IX and X were basically manufactured to provide a larger number of devices that performed in a similar manner to those in Groups I and VII, respectively.

V.A. Effects of a Low Neutron Fluence

Photoconductivity measurements were performed to evaluate the operation of the neutron-irradiated BOSS devices in Group I (1.95×10^{15} cm^{-2}), Group II (7.93×10^{14} cm^{-2}), and Group III (3.84×10^{14} cm^{-2}), all of which were irradiated in the SPR-III reactor. The photoconductivity response of a similar device, that had not been irradiated, was also measured. The incident pulse energy for the 1-μm laser was 2.1 mJ while the incident pulse energy for the 2-μm laser was 5.0 mJ. The results of four different measurements are superimposed on top of each other as shown in Fig. 14. The measured rise time of the current is roughly the same for each waveform in Fig. 14, and is equal to about 120 ps. This rise time is basically limited by the SCD5000 digitizer which has a analog/digital bandwidth of 3.0 GHz. The top waveform in Fig. 14 shows the response of the non-irradiated BOSS device. In this case there is only a small reduction of the switch current as a result of the 2-μm laser pulse. As mentioned previously, the waveform associated with the non-irradiated

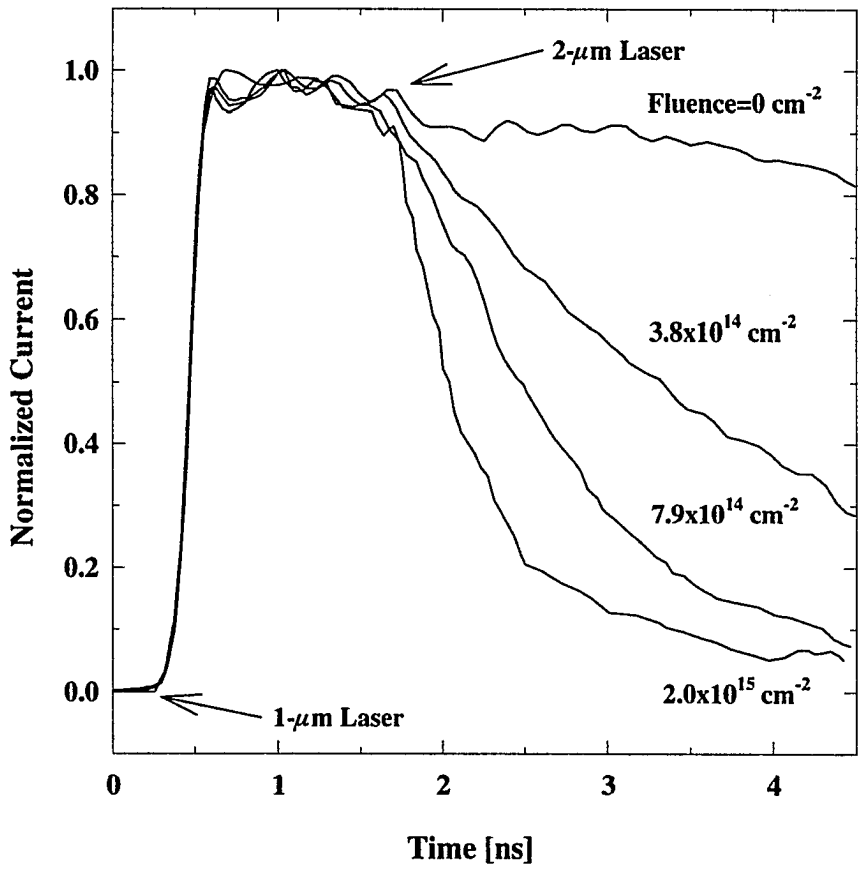

Figure 14 Effect of neutron irradiation on the opening transient of BOSS devices for several neutron fluences and non-irradiated material.

device closely approximates the simulated waveform, shown in Fig. 3, corresponding to a RC density of $4x10^{15}$ cm^{-3}.

As illustrated in Fig. 14, the ability of the 2-μm laser pulse to quench the current through a BOSS device was greatly improved as the neutron fluence was increased from $3.8x10^{14}$ cm^{-2} to $2.0x10^{15}$ cm^{-2}. These results strongly indicate that fast-neutron irradiation of GaAs:Si:Cu material creates defects which behave as recombination centers. They also substantiate the earlier findings that indicated the need to increase the RC density in order to allow the BOSS switch to be opened in the subnanosecond regime. For the device in Group I, a single exponential fit to the fall time of the switch conductivity, which was extracted from the circuit load line using Eqn. 7, yielded a recombination time constant of about 250 ps. A performance goal of a 100-ps recombination time constant was determined to be sufficient to allow the BOSS switch to be completely opened in the subnanosecond regime [see Sec. II.C]. Therefore, the results shown in Fig. 14 indicated that a higher neutron fluence would be required to meet this goal.

V.B. Effects of an Excessive Neutron Fluence

In order to further enhance the RC density in the GaAs:Si:Cu material, two higher neutron fluences were selected to try to obtain subnanosecond opening performance. Due to the relatively high neutron fluences required, SNL's ACRR was selected as the neutron source. Two groups of samples were irradiated at the ACRR: $5.33x10^{15}$ cm^{-2} for Group V; and $1.78x10^{16}$ cm^{-2} for Group VI, roughly an order of magnitude higher than for the previously discussed samples.

The setup used for the experiments is shown in Fig. 10. The results of experiments with Group VI samples were quite dramatic and showed that the switch would open immediately following the termination of the 1-μm laser pulse *without* needing the 2-μm laser pulse to quench the current. An example of a waveform measured for a Group-VI device is shown in Fig. 15. The inability of the switch to remain closed after the 1-μm laser pulse was terminated was an indication that the electrons that were elevated into the conduction band were recombining with holes in the valence band before those holes could be trapped in the Cu_B level. The applied voltage for this waveform was 6050 V which resulted in a peak current of 47 A with a FWHM of 260 ps. The fall time (90-10%) of the current was 340 ps, and an exponential fit to the fall time of the switch conductance yielded a time constant of 77 ps. The 1-μm laser energy used for these measurements was 4.5 mJ. Even though the laser-pulse energy was relatively high, the minimum switch on-state resistance was still 29 Ω. Therefore, while the peak power delivered to the 50-Ω load was 110 kW, the peak power dissipated in the switch was 64 kW. To seriously be considered as a high-power, high-repetition-rate switch, the minimum on-state resistance must be on the order of several ohms or less.

Photoconductivity experiments were also conducted on devices from Group V, where the fluence was about one third of that for Group VI. Results from devices in Group V also indicated that the RC density, and hence the neutron fluence, was still too high. The Group-V devices also exhibited the self-opening effect, although not with as short a fall time as was measured for the Group-VI devices. When it was determined that the RC density was too high, an experiment was designed to examine the effects of a moderately low thermal anneal

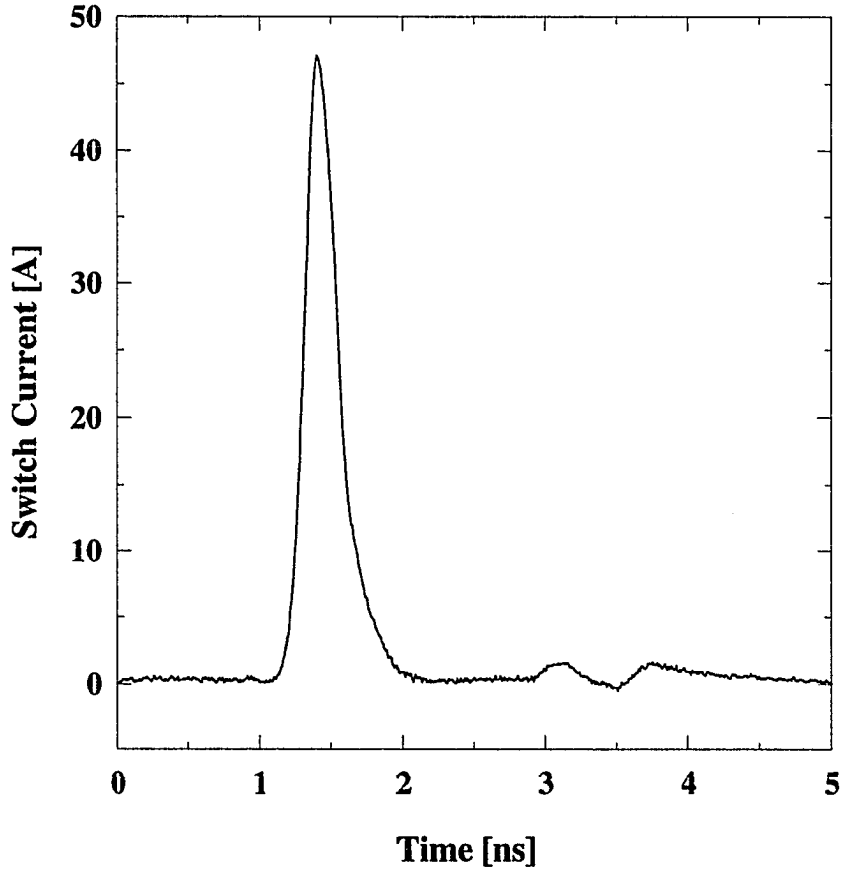

Figure 15 Current waveform generated by a Group-VI device which was only illuminated by a 4.5-mJ 1-μm laser pulse.

on the performance of irradiated BOSS devices. The results of the annealing experiments on the switches photoconductive response, for an applied dc bias voltage of 10 V, are shown in Fig. 16. The 1-μm laser energy used for these measurements was about 13 mJ and the 2-μm laser energy was 4 mJ. The time separation between the two laser pulses was about 1.5 ns. The bottom trace of Fig. 16 is the response of the switch after it was annealed at 110° C for about 15 minutes. The switch current rapidly decreases after the 1-μm laser pulse is terminated. The second hump in the switch current occurs following the arrival of the 2-μm laser pulse. The effect of the 2-μm laser pulse is noticeable because the increase in the switch conductance, due to hole current, is on the same order of magnitude as the residual switch conductance from the 1-μm laser pulse.

V.C. Effect of Annealing

To systematically remove some of the neutron-induced damage, one sample was annealed for 15 minutes at increasing temperatures of 207, 225, 247, and finally 268° C. Both dc I-V and photoconductivity measurements were made between each anneal. The anneals had a negligible effect on the dc I-V characteristics. However, the photoconductivity measurements, illustrated in Fig. 16, show a rapid increase in the current, after the termination of the 1-μm laser pulse, as the annealing temperature was increased. The amplitude of the increase in the switch current, resulting from hole production by the 2-μm laser pulse, becomes less significant as the on-state conductance of the switch is increased. A curve fit to the fall time of the switch conductance, which was extracted from the load line, indicated a recombination time of 180 ps after the 268° C anneal. Initial measurements

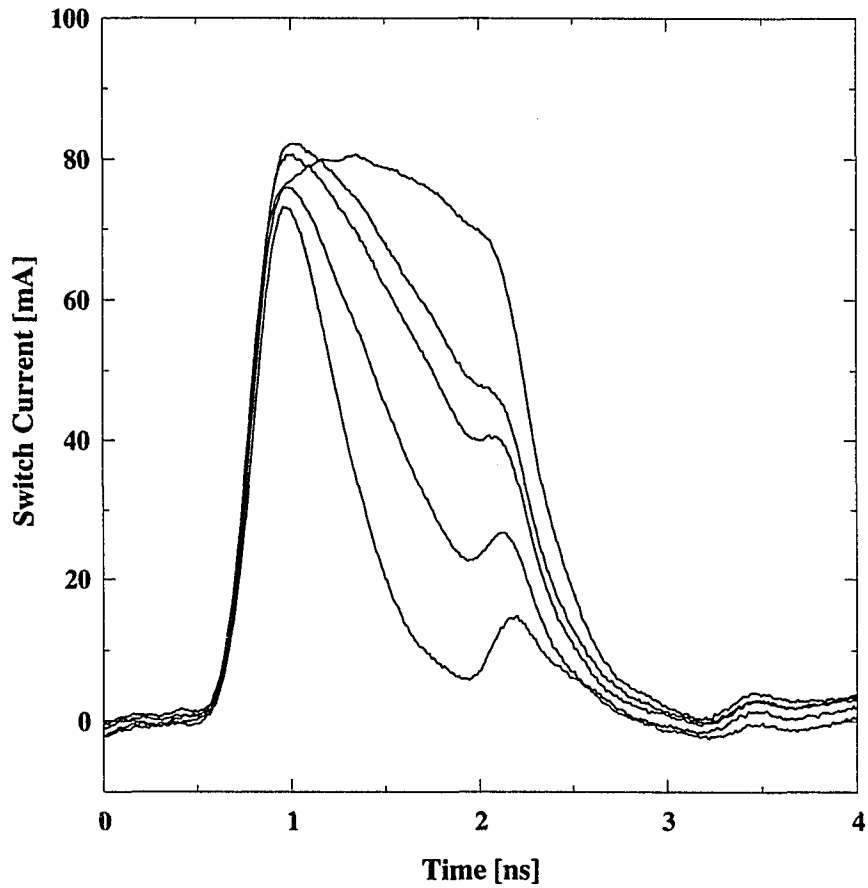

Figure 16 Effect of 15-minute thermal anneals on the photoconductivity response of a BOSS device irradiated at a fluence of 5.33×10^{15} cm^{-2}. Annealing temperature starting from the bottom: 110, 207, 225, 247, and 268° C.

indicate that the on-state of the switch is in the 20-Ω regime; still too high for any practical pulsed-power applications.

The strong effect that these low-temperature anneals had on the switching performance of BOSS devices indicates that the 420° C contact anneals on the samples in Groups I through IV, may have removed some of the radiation damage. Previously reported annealing studies of neutron-irradiated GaAs show one pronounced annealing step at about 225° C and a second, larger step starting at about 400° C [56]. Most of the explanations for the annealing mechanism in irradiated GaAs deal with the movement of Frenkel pairs, which are point defects consisting of an interstitial atom and a lattice-vacancy site [65]. Brailovskii et.al. [66] proposed that the room-temperature-stable point defects created in GaAs, as a result of high-energy-particle irradiation, become movable as the temperature is raised. At temperatures below about 300° C, the first annealing step, these mobile defects can agglomerate forming large defect clusters. The second annealing step, at roughly 400° C, would then be associated with the annealing of the defect clusters.

It has also been reported that almost all of the neutron-induced defects are annealed out at temperatures between 500° C and 600° C [67]. This was also seen in this work when neutron-irradiated, n-type GaAs was compensated with copper at a diffusion temperature of 575° C. Although the dark resistance of the sample was about 3 MΩ, the photoconductivity data indicated that there was no enhancement of the RC density over the non-irradiated material. Therefore, the neutron-induced defects were probably annealed out by the six-hour 575° C anneal.

V.D. Electrical Pulse-Width Agility

The experimental results on the Group-V and Group-VI devices indicated that the fluence levels used for these irradiations were too high. Despite the fact that some of the irradiation-induced damage could be removed by thermal annealing, the on-state resistance and the required 1-μm laser energy still made devices irradiated at these fluence levels impractical. Therefore, a third set of devices were sent to SNL's SPR-III reactor to fill the gap between the fluence levels of the Group-I and the Group-V devices.

Two different neutron fluences were selected for the third set of devices to be irradiated. The lower fluence was 2.45×10^{15} cm^{-2} (Group VII) and the higher fluence was 3.93×10^{15} cm^{-2} (Group VIII). Results obtained with Group-VII devices yielded satisfactory switching results and will be discussed in this section. Results obtained with Group-VIII devices indicated that this fluence was still too high. However, Group-VIII devices have successfully been switched at high repetition rates and will be discussed in the next section.

Switching results illustrating the photocurrent for a Group-VII device are shown in Fig. 17 for an applied voltage of 3.7 kV. The maximum voltage that was switched with this device was about 18 kV which was limited by the modulator used to bias the device. The switching behavior of this sample did not change as the applied voltage was increased. Figure 17 shows several current waveforms superimposed to demonstrate the ability to control the pulse width of the electrical pulse delivered to the 50-Ω CVR. The laser pulse energy for both the 1-μm and the 2-μm wavelengths was set at 4.5 mJ. The minimum switch resistance during the transient was measured to be ≤1 Ω. The minimum pulse width achieved with this device was measured to be about 650 ps FWHM. A curve fit to the switch

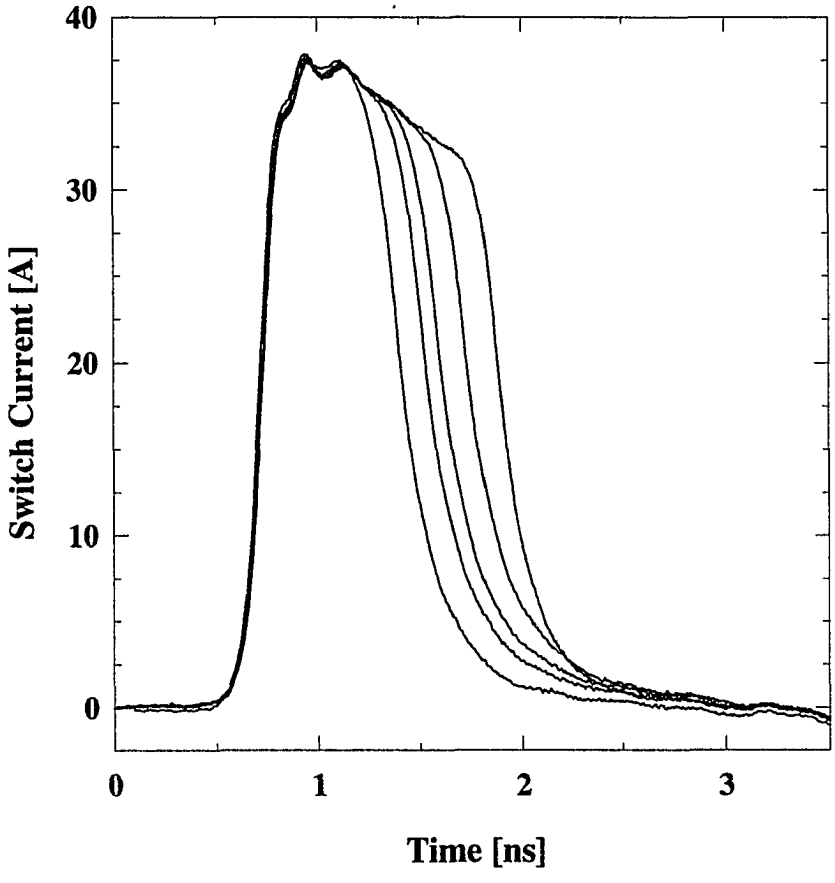

Figure 17 Demonstration of electrical-pulse-width agility, by varying the time delay between the turn-on and turn-off laser pulses, for an applied voltage of 3.7 kV.

conductance during the opening phase, after it was extracted from the circuit load line, indicated a recombination time constant of 100 ps. Therefore, the goal of obtaining a 100-ps time constant, in a device that requires the 2-μm laser pulse to open, has been met by devices irradiated with a neutron fluence of 2.45×10^{15} cm^{-3}.

Figure 17 illustrates that as the time between the two laser pulses is increased, the switch conductivity decreases with time prior to the turn-off laser pulse. This is a result of the enhanced RC density in the GaAs:Si:Cu material. The effect of a decreasing switch conductance prior to the turn-off laser pulse will ultimately limit the switch *on-time* of neutron-irradiated BOSS devices. It should be noted that BOSS devices that were not irradiated with neutrons had demonstrated on-state times of several hundred nanoseconds [28]. Therefore, there is a trade-off between the maximum time that the switch will remain closed after the 1-μm laser pulse, and the RC density in the material.

One of the goals of this research was to determine the minimum electrical pulse width that could be generated by a BOSS device, while still maintaining the ability to vary the pulse width by adjusting the time delay between the turn-on and turn-off laser pulses. Figure 18 illustrates the effect of further *reducing* the time between the two laser pulses from the minimum time separation shown in Fig. 17. As shown in Fig. 18, when the time between laser pulses is too short, the 2-μm laser pulse is no longer able to completely quench the photocurrent. The dashed line in Fig. 18 shows the smallest pulse width illustrated in Fig. 17. The time-delay reduction between waveforms in Fig. 18 is roughly 100 ps. Eventually, when the two laser pulses are roughly coincident, the switch will behave as if there was no 2-μm laser pulse at all. The primary reason why the switch will not open properly when the

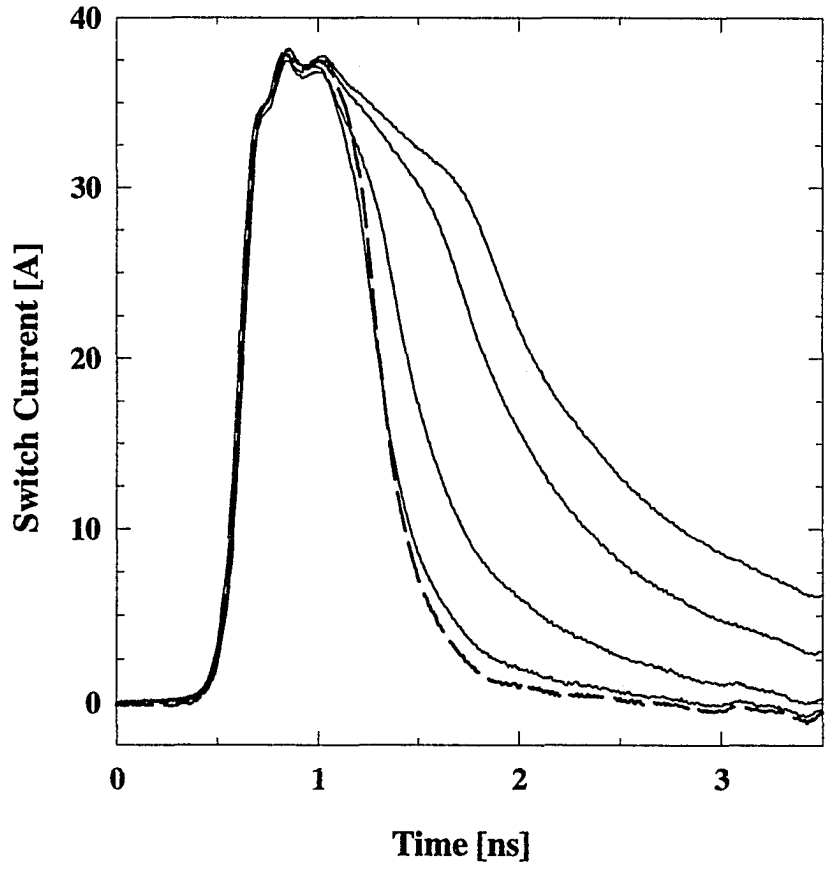

Figure 18 Demonstration of the minimum electrical pulse width by showing the effect of bringing the turn-on and turn-off laser pulses too close together.

laser pulses are too close together is that it takes a certain amount of time for the electron-hole plasma generated by the 1-μm laser pulse to recombine. This, coupled with the fact that the dominant copper center (Cu_B) requires a certain amount of time to fill with a sufficient quantity of holes to permit complete photo-quenching, sets a lower limit on the time between the turn-on and turn-off laser pulses. These effects will be discussed in more detail in Chapter VI with the help of a rate-equation model.

V.E. High-Repetition-Rate Capability

As mentioned earlier, photoconductive switching experiments on Group-VIII devices indicated that they had an excessive RC density. However, as discussed in Sec. V.B, a benefit can be derived if the RC density is made high enough to cause the switch to open without the need of the turn-off laser pulse. This effect is shown in Fig. 19 where two 1-μm laser pulses, with a variable time separation, were used to *close* a Group-VIII device at high repetition rates. This experiment was designed to evaluate the repetition-rate capability of the Group-VIII devices, in addition to their photoconductive response. The applied voltage for the waveforms shown in Fig. 19 was about 16 kV. The minimum on-state resistance of the switch was measured to be roughly 20 Ω. The FWHM of both current pulses was about 340 ps. The time separation between the two laser pulses was varied from about 3.5 ns, corresponding to a repetition rate of roughly 285 MHz, down to less than 1 ns, corresponding to a repetition rate of greater than 1 GHz. These repetition rates are basically five orders of magnitude higher than any other type of high-power photoconductive switch. The experiments were performed at a maximum applied voltage of 18 kV, yielding and average electric field of 36 kV/cm. It is important to note that there was no indication of the device

collapsing into a filamentary-current mode of conduction, or "lock-on," at any point in the switching cycle. This is significant since almost all previously reported photoconductive switching experiments on non-neutron-irradiated GaAs, including those performed on GaAs:Si:Cu material, exhibited a transition into filamentary conduction at average electric fields of $\geq$10 kV/cm [68]. It has been reported by Loubriel, et. al. [69], however, that chrome-doped GaAs switches, that were irradiated at a neutron fluence of $5x10^{15}$ cm^{-2}, did not transition into a filamentary conduction mode until the applied average electric field was greater than 62 kV/cm. This electric field would correspond to an operating voltage of roughly 30 kV for the 5-mm gap BOSS devices that have been discussed in this chapter.

Since one of the potential applications of a BOSS device is in an impulse or ultra-wide-band (UWB) radar, the Fourier spectra of the waveforms in Fig. 19 were examined, as was the effect of varying the pulse separation on the frequency content. The results of performing a 4096-point fast-Fourier transform (FFT) on the data in Fig. 19 are shown in Fig. 20. To provide a higher spectral resolution, the time-domain data was *padded* with zeros, resulting in a total time window of 40 ns. Zero padding is frequently used in Fourier-transform analysis to increase the spectral resolution of the resulting FFT. The spectral resolution is basically given by two times the inverse of the total time window that is being analyzed. If the length of the time window is doubled, then the resulting frequency step will be smaller by a factor of two. Therefore, the 40-ns time window resulted in a frequency step of 50 MHz for the real-frequency components.

Figure 20 shows significant frequency content up to about 3 GHz which was the bandwidth limit of the SCD5000 digitizer. The result of adjusting the delay between the two

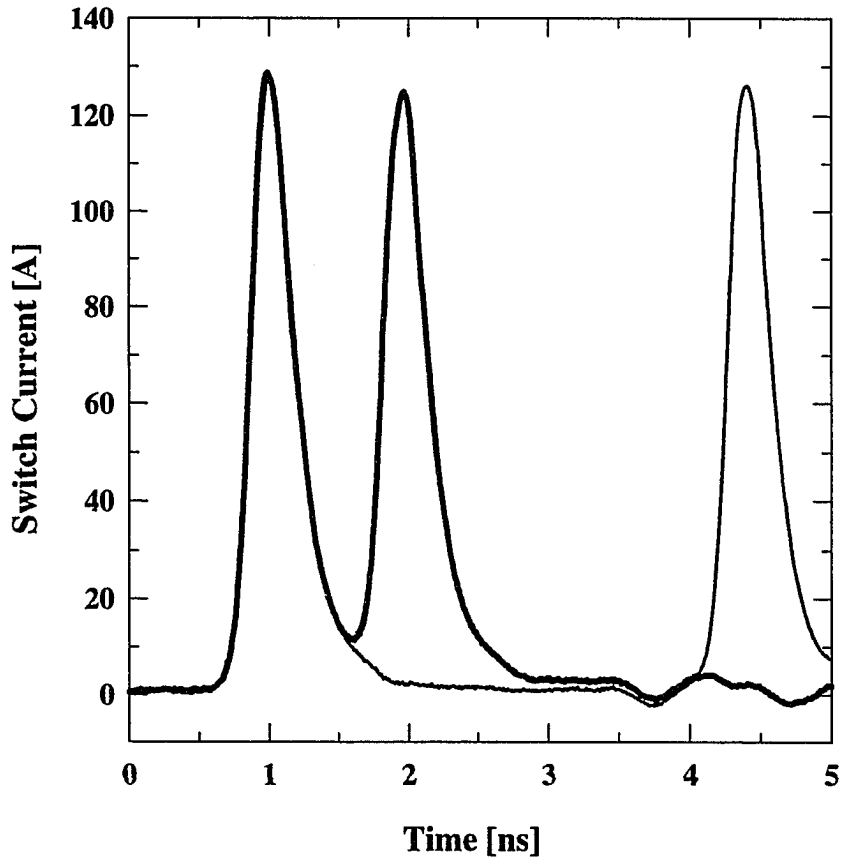

Figure 19 Demonstration of a 1-GHz (thick line) and a 290-MHz (thin line) repetition rate within a two-pulse burst at an applied voltage of 16 kV.

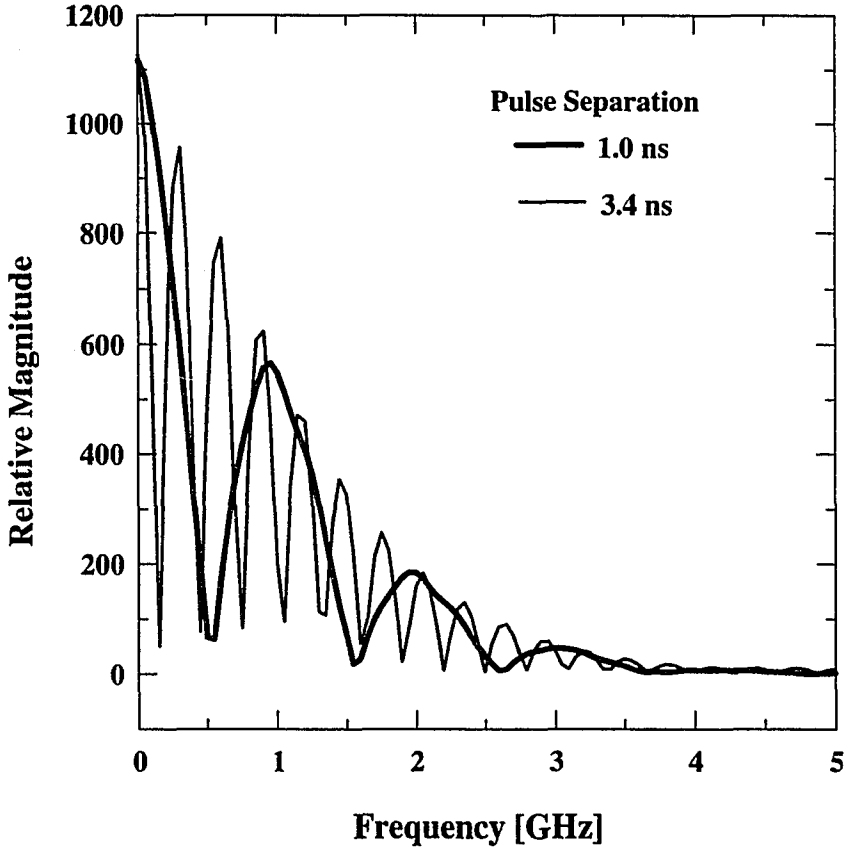

Figure 20 Fourier spectra for the waveforms illustrated in Fig. 19: a 3.4-ns laser pulse separation (thin line); and a 1-ns laser pulse separation (thick line).

pulses can be seen as a change in the number, and location, of the *nulls* in the spectra. For example, by changing the time delay from 1 ns to 3.4 ns, the spectral peak at 1 GHz is changed to a null.

V.F. Monocycle RF Generation

Experiments were performed with two devices, from the Group-VIII fluence, embedded in the PSO circuit configuration shown in Fig. 13. These devices were biased with a 40-ns voltage pulse with a maximum amplitude of about 9.5 kV. Since these devices were self opening, only the 1-μm wavelength was used for the PSO demonstration.

The time-domain waveforms for a time delay between the 1-μm laser pulses of about 500 ps and about 2 ns are shown in Fig. 21. The time delay of about 500 ps resulted in the formation of a single RF cycle, or monocycle, with a duration of a little over 1 ns. There is a considerable amount of pulse sharpening of the positive half-cycle that occurs as a result of the second switch closing prior to the complete recovery of the first switch. This effect occurs because the opposite polarity of the charge voltage results in a cancellation of the voltage that is actually delivered to the CVR. The advantage of this mechanism is that slightly higher frequencies can be obtained. However, this voltage cancellation also reduces both the peak amplitude of the negative half-cycle as well as the total energy contained in the positive half-cycle. The peak amplitude imbalance can be corrected by biasing the second switch at a slightly higher negative voltage. When the laser time delay is increased to about 2 ns, the actual response of the first switch is measured, as shown in Fig. 21. For this case, the negative half-cycle is roughly the mirror image of the positive half-cycle. The remaining

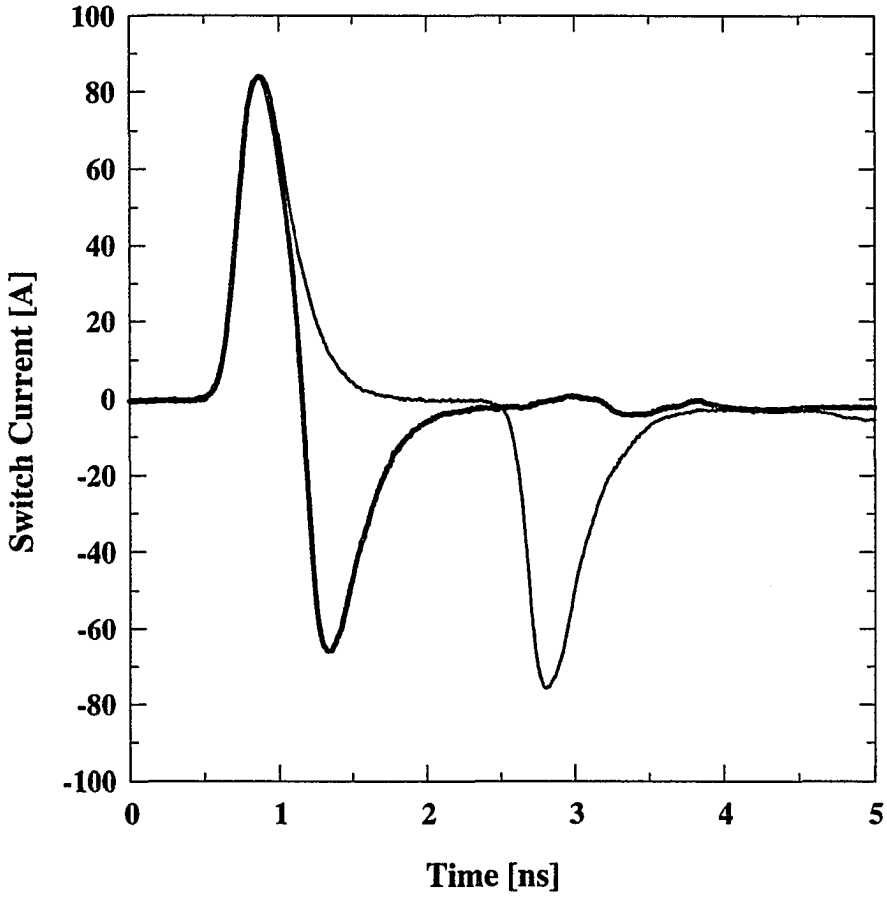

Figure 21 Demonstration of two bipolar pulses produced by a PSO generator for a 500-ps (thick line) and a 2-ns (thin line) delay between the 1-μm laser pulses.

differences in the peak amplitudes are the result of the bias-voltage modulator rather than the operation of the switches.

The ability to vary the time between the positive and negative half-cycles has a dramatic effect on the spectrum of the waveform. Several important characteristics of the Fourier spectra, obtained from the waveforms in Fig. 21, are illustrated in Fig. 22. First, unlike the spectra shown in Fig. 20, the spectra in Fig. 22 contain a significantly reduced dc component. As mentioned earlier, a reduction in the dc component will greatly increase the ability to radiate the pulse out of an antenna. Secondly, there is a drastic effect on the spectrum of the bipolar pulse when cross-over distortion is intentionally created. The spectrum associated with the undistorted monocycle (thick line) has a bandwidth of roughly 150%. In other words, dividing the FWHM of the spectrum, which is about 1.5 GHz, by the center frequency of the spectrum, which is about 1 GHz, yields a bandwidth of 1.5. Notice that it is difficult, if not impossible, to apply the same definition of spectral bandwidth to the case when there is a separation between the positive and negative half-cycles, as shown by the thin line in Fig. 22.

As was the case in Fig. 20, varying the time delay between the positive and negative half-cycles changes the number and location of the nulls in the spectrum. Also, since the energy in the pulse must be conserved, increasing the number of nulls, by increasing the time delay, results in a higher power-spectral density in the peaks of the spectrum. This is shown in Fig. 22 where the relative magnitude of the lower-frequency peaks, of the distorted waveform, are more than a factor of two greater than the peak of the spectrum associated with the monocycle. Note that a slight increase in the energy associated with the distorted

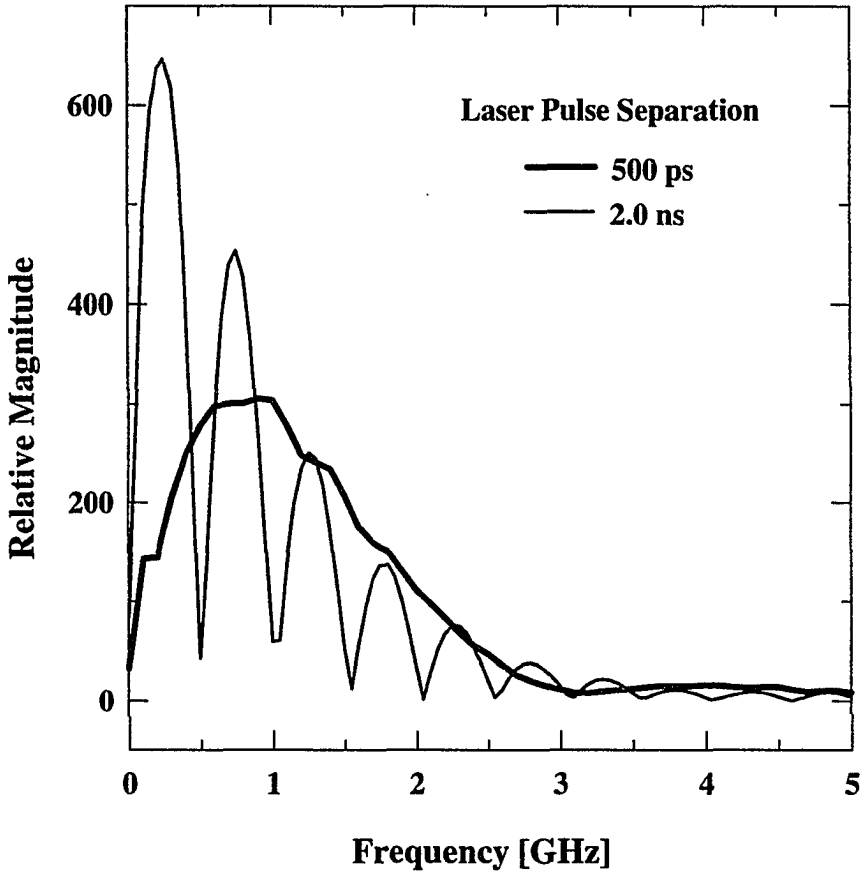

Figure 22 Fourier spectra of the two waveforms shown in Fig. 21.

waveform is expected due to the lack of cancellation of part of the positive half-cycle. The dominant mechanism for the increased lower frequency content is associated with a reduction of the *fundamental* frequency of the waveform. The fundamental frequency is basically a sine wave with its positive and negative peaks coincident with the positive and negative peaks of the distorted waveform. For example, in Fig. 21, the distorted waveform has a 2-ns separation between the positive and negative peaks. This separation would therefore result in a fundamental frequency of 250 MHz, which corresponds to the first peak in the spectrum as shown in Fig. 22.

The capability to change the generated spectrum by simply changing the optical delay between laser pulses could be very useful in UWB radar applications, particularly if certain frequency bands are to be avoided. Potential RF waveforms that could be radiated by a PSO generator are discussed in Appendix A.

V.G. Summary

Experimental results have been presented which demonstrate the speed and power capabilities of BOSS devices that have been irradiated with fast neutrons. Variable pulse-width agility was demonstrated by simply changing the optical delay between the turn-on and turn-off laser pulses. The minimum electrical pulse width that could be generated by reducing this time delay was also investigated. The effect of increasing the neutron fluence on the ability of BOSS devices to respond to the turn-off laser pulse was presented, as well as the ability of a BOSS devices to open, without the turn-off laser pulse, when the neutron fluence was too high. Data concerning the ability to remove the damage created by fast-neutron irradiation, through relatively low temperature thermal anneals, was also presented.

The operation of BOSS devices, that did not require the turn-off laser pulse to open, were demonstrated at up to a 1-GHz repetition rate, within a two pulse burst, at applied voltages as high as 18 kV. Two of these devices were also operated in a PSO configuration to demonstrate a frequency-agile RF source topology where the number an location of the nulls in the frequency spectrum could be adjusted by varying the time delay between the turn-on laser pulse of each switch. The data presented cover several parameters which are included in the rate-equation model introduced in Chap. II, including the time delay between the two laser pulses and the recombination center density. The next chapter will discuss these results within the context of the rate-equation model.

CHAPTER VI

DISCUSSION OF RESULTS

The purpose of this discussion is to gain insight into the underlying deep-level dynamics that occur during the various types of switching experiments. To accomplish this, the semiconductor rate equations that were introduced in Chapter II will be used extensively to illustrate the time dependence of the deep-level electron occupations during the various phases of the switching cycle. It will be shown that these numerical results are in good qualitative and quantitative agreement with the various experimental studies. This is a somewhat surprising result since many of the switching experiments were conducted at fairly high average electric fields. Thus the effects of current injection at the contacts, as well as the formation of spatial domains in the bulk material, appear to be of secondary importance during the experiments presented in Chapter V.

The discussion in this chapter will basically follow along with the order of the experiments presented in Chapter V. Somewhat detailed discussions of the basic BOSS switching cycle on the ten-nanosecond time scale, and some of the various deep-level effects, have been presented previously through the use of a simplified rate-equation model [70], and a steady-state analysis [71], and will therefore not be presented in this discussion. Instead, the emphasis will be placed on the performance of BOSS devices on the subnanosecond time

scale and at megawatt power levels. The primary physical parameters that will be adjusted for the purpose of this discussion are the recombination-center density, and the relative timing of the subnanosecond laser pulses used to illuminate the BOSS devices.

The discussion will begin by evaluating how well the deep-level parameters selected for the numerical simulations agree with those published in the literature. The most suspect parameter used in the simulation is the RC density and its relation to the associated neutron fluence. However, it will be shown that the parameters selected appear to be reasonable. Next, the minimum electrical-pulse-width limitations of the BOSS switch will be examined. The results of these simulations appear to be in very good agreement with the temporal response of the BOSS switch in the associated switching experiments. Next, the numerical simulation of the high-repetition-rate experiments presented in Chapter V will be evaluated along with a discussion of the switches potential for producing extended bursts of RF energy. Finally, some of the parameters that could ultimately limit the high-power operation of the BOSS switch will be qualitatively discussed. A quantitative discussion of the power limitations must be limited to a very restrictive experimental parameter space.

VI.A. Recombination-Center Density vs. Neutron Fluence

The calculated off-state resistances (see Chap. II), of the neutron irradiated samples, were within an order of magnitude above the measured resistances. For example, the theoretical results for an RC density of 7.0×10^{15} cm^{-3} yielded an initial off-state resistance of 43 MΩ. The current waveform, shown in Fig. 3, calculated with this RC density best approximates the falling edge of the experimental waveform, shown in Fig. 14, associated with the sample irradiated by a fluence of 2.0×10^{15} cm^{-2} which had an initial off-state

resistance of 35 MΩ. The calculated off-state resistance for an RC density of $4.0x10^{15}$ cm^{-3} was 9.9 MΩ which is still less than an order of magnitude above the 1.3 MΩ that was measured for the non-irradiated sample. Since the off-state resistance depends exponentially on the placement of the Fermi level within the bandgap, and since the location of the Fermi level depends on the various deep-level concentrations and exponentially on the deep-level energies, as shown in Eqn. 5, agreement within an order of magnitude is deemed sufficient. This is particularly true since a detailed deep-level analysis of the GaAs material used in this investigation was not available.

It can be determined if the RC densities used in the model are reasonable by matching the current fall times of the theoretically obtained curves with the experimental data. With this information the RC generation rate can be compared with other published generation rates. For the comparison of defect generation rates, the data that was used was published by Goltzene, et al. [41] in which semi-insulating GaAs was irradiated with fast neutrons and subsequently evaluated by electron paramagnetic resonance (EPR) spectroscopy. Here it is assumed that the 'defect' that they measure behaves as a recombination center. In their work, it was found that the defect density was roughly proportional to the neutron fluence with a constant of proportionality of about 13.6. In other words, a neutron fluence of $1x10^{15}$ cm^{-2} would yield a defect density of about $1.4x10^{16}$ cm^{-3}. The curve in Fig. 14 corresponding to a neutron fluence of $3.8x10^{14}$ cm^{-2} is best approximated by the theoretical curve corresponding to a RC density of $5.5x10^{15}$ cm^{-3} yielding a proportionality constant of 14.4. Similarly, the data corresponding to a neutron fluence of $7.9x10^{14}$ cm^{-2} is closely approximated by the theoretical curve for a RC density of $6.0x10^{15}$ cm^{-3} yielding a

proportionality constant of 7.6. In both of these cases the proportionality constant was within a factor of two of the 13.6 which was published by Goltzene [41]. Due to variations in the experimental parameters between the work presented here and that of Goltzene, such as neutron-source spectrum, GaAs substrate material, sample preparation, etc., it is difficult to get a true quantitative agreement. However, this analysis does indicate that the RC densities used in the model presented in Chapter II are reasonable.

VI.B. Analysis of the Minimum Electrical Pulse Width

The temporal variation of the free charge carriers and the electron occupation of the Cu_B and recombination centers were briefly discussed in Section II.B. It was later shown in section V.A, that the experimentally measured current response of BOSS devices, that had been irradiated at Group I through III fluences, appeared to fall within the numerical solutions that were obtained for RC densities between $4x10^{15}$ cm^{-3} and $1x10^{16}$ cm^{-3}. The primary result of the initial experiments was that a higher neutron fluence was needed to achieve the desired switching performance. After photoconductivity experiments on devices from Groups V and VI indicated that their neutron fluences were too high, it was determined that devices irradiated at a fluence of $2.45x10^{15}$ cm^{-2} (Group VII) produced suitable results as shown in Fig. 17. However, as the turn-on and turn-off laser pulses were brought closer together, the fall time of the switch current began to increase as shown in Fig. 18.

In this section the rate-equation model is used to analyze the time dependence of deep-level trapping effects, and how this time dependence ultimately limits the minimum time separation between the turn-on and turn-off laser pulses while, at the same time, minimizing the fall time of the switch current. The only parameter that was adjusted in the

numerical simulation, other than the relative timing of the laser pulses, was the RC density which was increased to $2x10^{16}$ cm^{-3} in order to produce numerical results that were similar to the experiment. It is interesting to note that when the Group VII fluence of $2.45x10^{15}$ cm^{-2} is compared to an RC density of $2x10^{16}$ cm^{-3}, the ratio yields a constant of 8.2 which is well within a factor of two to the 13.6 published by Goltzene, et.al. [41].

The results of the simulations of the effect of bringing the two laser pulses too close together are shown in Fig. 23, for an applied voltage of 3.7 kV, where the switch current is plotted as a function of time for six different time delays between laser pulses. The dashed line in Fig. 23 demonstrates the fastest fall time of the current for a 400-ps separation between the two laser pulses. The solid lines in Fig. 23, from left to right, show the effect of reducing the time delay to 200, 150, 135, 125, and 115 ps, respectively. The simulated results in Fig. 23 are in very good qualitative agreement with the experimental results shown in Fig. 18. The effects shown in Figs. 18 and 23 can be best understood by examining the time dependence of the free electrons and holes and the electron concentrations in the Cu_B, EL2, and RC deep levels. This time dependence is shown in Fig. 24 for the case of a 1.5-ns time separation between the two laser pulses. This increased time separation was chosen to illustrate how the various charges reach a quasi-equilibrium after the 1-μm as well as the 2-μm laser pulses. The effects of bringing the laser pulses closer together will then be examined.

The first thing to notice about Fig. 24 is that nearly equal concentrations of free electrons and holes are created during the turn-on laser pulse. This results from the fact the electron optical ionization cross-section for Cu_B is an order of magnitude larger than the hole

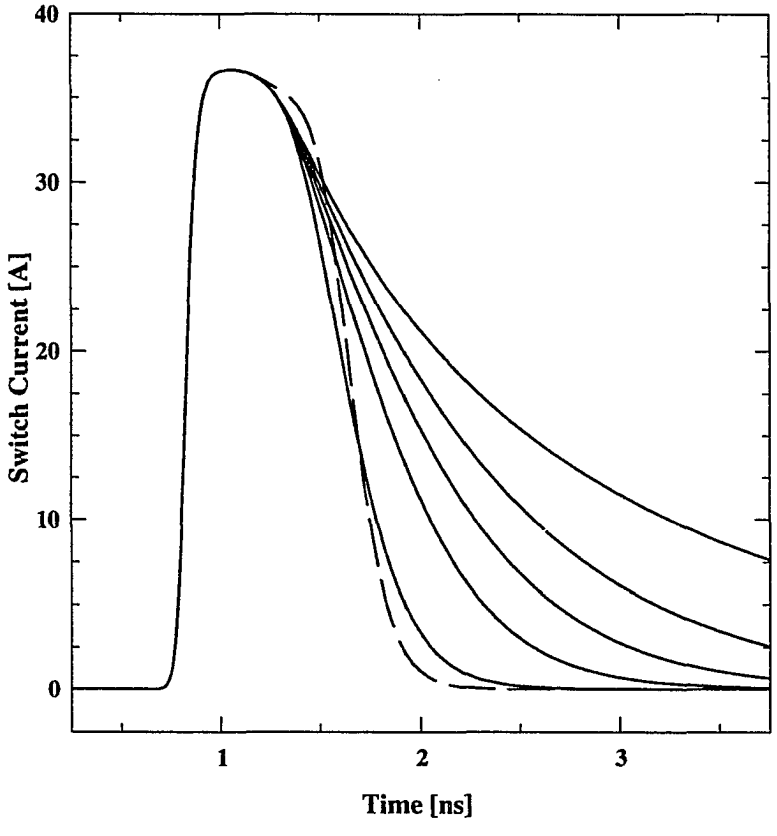

Figure 23 Simulated current response showing the effect of reducing the time delay between the turn-on and turn-off laser pulses.

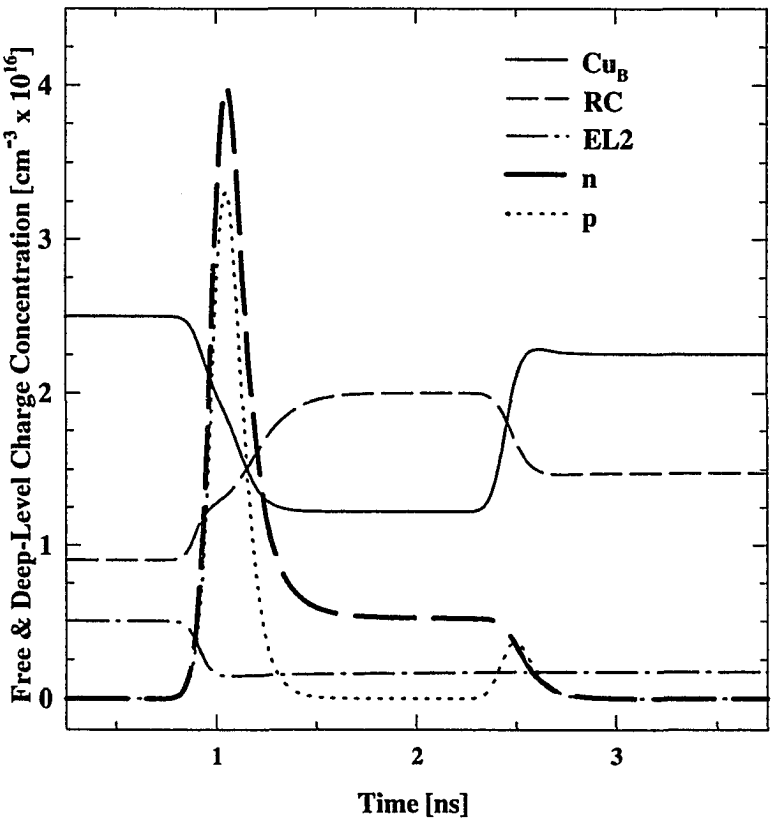

Figure 24 Simulated temporal variation of free carriers, and bound electrons in the Cu_B, EL2, and RC levels for a laser-pulse separation of 1.5 ns.

optical ionization cross-section. Therefore, electrons will be optically elevated from the valence band into the Cu_B center at the same time that electrons are being elevated from the Cu_B center into the conduction band. Recall that the 1-μm laser pulse does not have sufficient energy to directly excite electrons from the valence band into the conduction band. The primary reason why the peak electron concentration is higher than that of the holes is because some holes are trapped in the Cu_B center immediately after being created. The reduction in the EL2 electron occupation, as a result of optical excitation, appears to be countered by the increase in the RC occupation, as a result of electron trapping, during the turn-on laser pulse. Following the turn-on laser pulse, centered at 1 ns, most of the electrons and holes recombine. During this time, holes are also being trapped in the Cu_B level. After the hole concentration is depleted, the free-electron concentration appears to stabilize. At roughly the same time, the RC center is basically full of electrons ($2x10^{16}$ cm^{-3}) because there are no longer any holes in the valence band to stimulate recombination. Because the Cu_B center is filled will holes primarily by hole-trapping, as opposed to optical excitation, the electron concentration in Cu_B also stabilizes when the free-hole concentration is depleted.

The 2-μm laser, which irradiates the sample at 2.5 ns (Fig. 24), generates free holes by elevating electrons from the valence band into the Cu_B center. Therefore, an increase in the electron occupation of Cu_B is observed. There is insufficient energy in the 2-μm photons to alter the charge concentration in either EL2 or the RC by optical excitation. However, the creation of holes in the valence band opens a recombination channel for the electrons in the RC. Therefore, electrons in the conduction band are also able to recombine, resulting in a reduction of the switch conductivity. It should be noted that following the two laser pulses,

the deep level occupations are not exactly the same as they were prior to the switching event. The electron occupation of the RC center increased from about 45% up to 74% full, while the electron occupation of the Cu_B center decreased from roughly 100% down to about 90% full. This may have an adverse effect on the ability of the BOSS switch to operate at high repetition rates and will be studied in more detail in a later section.

The simulated temporal variations of the free and trapped charges are shown in Fig. 25 for a time separation between the two laser pulses of 400 ps. This data results in the temporal behavior of the current shown as the dashed line in Fig. 23. The final deep-level occupations in Fig. 25 are almost identical to those shown in Fig. 24. Even the Cu_B occupation just prior to the 2-μm laser pulse was only slightly higher in Fig. 25. Both the current waveform associated with Fig. 24 and that associated with Fig. 25 exhibited complete extinction of the current. Note that the fall time of the dashed line in Fig. 23 occurs in the time between 1.5 and 2.0 ns. During this time there does not appear to be a significant change in the various charge concentrations as illustrated in Fig. 25. The current change is substantial, while there is little change in the free and trapped charge concentrations, because of the influence of the circuit. The switch is imbedded in a 100-Ω load line. Therefore, the most noticeable current change occurs when the switch resistance increases from the 10-Ω to the 1000-Ω range. The effect of the load line was previously discussed in Section II.C. According to the numerical simulations, the switch conductivity is decreasing from the $1\text{-}\Omega^{-1}cm^{-1}$ to the $10^{-6}\text{-}\Omega^{-1}cm^{-1}$ range during the opening transient.

The case where the peaks of the two laser pulses are only separated by 115 ps, as shown in Fig. 26, will now be examined. The data in Fig. 26 corresponds to the solid line

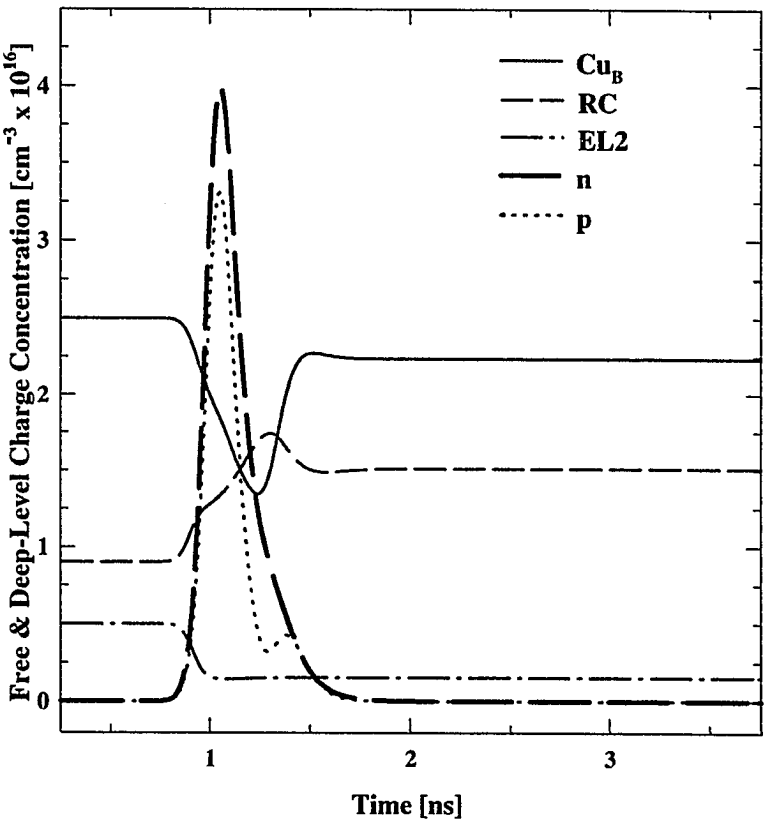

Figure 25 Temporal variations of free and trapped charges for a 400-ps separation between laser pulses.

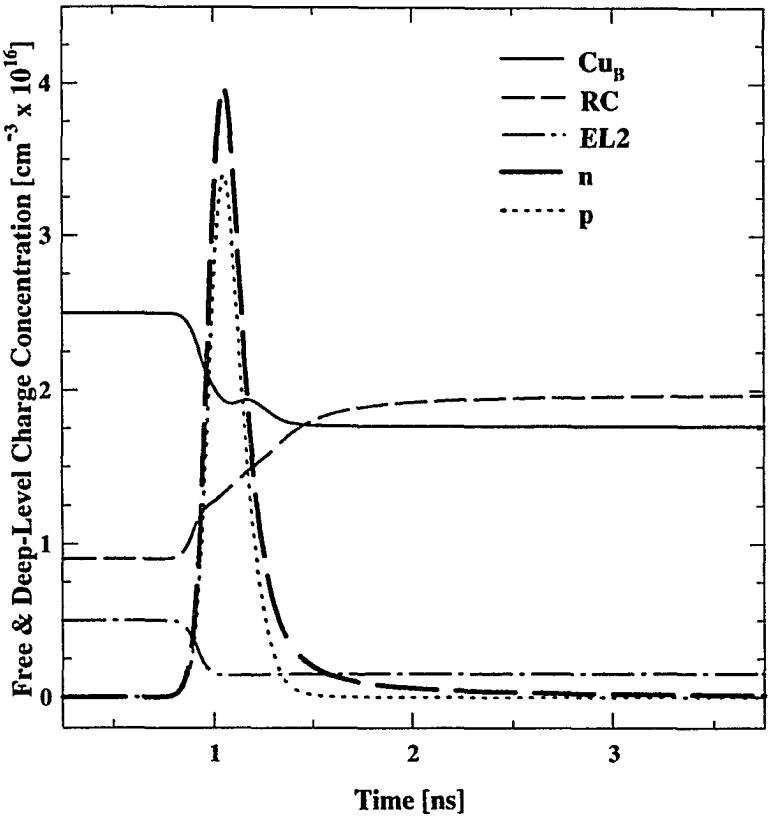

Figure 26 Temporal variations of free and trapped charges for a 115-ps separation between laser pulses.

in Fig. 23 that shows the weakest opening effect. In Fig. 26, the effect of the 2-μm laser pulse is seen only as a small perturbation of the electron occupation of the Cu_B level. The high free-hole concentration, generated by the first laser pulse, has not yet sufficiently decayed during the time between the two laser pulses. Therefore, the holes created by the turn-off laser pulse cause only a relatively slight increase in the total concentration of holes. Furthermore, the final Cu_B occupation in Fig. 26 is found to be a factor of 1.4 higher than the Cu_B occupation in Fig. 24 just after the 1-μm laser pulse. This is due to the fact that the 2-μm laser pulse elevates the electrons into the Cu_B center during the time that the free electrons and holes are still recombining. The result is that the final electron occupations of the Cu_B and RC levels are very different from those shown in Figs. 24 and 25. This difference in the deep-level occupations results in a much more gradual reduction of the electron concentration, as shown in Fig. 26, which ultimately causes the BOSS device to show a very weak or slow opening effect. As the time delay between the two laser pulses is further reduced, the switch will behave as if there was no turn-off laser pulse at all.

These results demonstrate an inherent limitation of the minimum electrical pulse width that can be generated by a BOSS switch that requires a 2-μm laser pulse to open. The minimum electrical pulse width that was experimentally measured for a device of this type was about 650 ps. The minimum electrical pulse width that was obtain from the numerical simulation was about 800 ps which is only about 23% higher than the experimental results. The exact value of the minimum electrical pulse width will, of course, depend on the exact experimental and material parameters used for the measurement. It is important to recognize that the temporal feature which appears to limit the minimum time delay between laser

pulses, and hence the minimum electrical pulse width, is that time when the free hole concentration becomes negligible. This is primarily because the holes created by the turn-off laser pulse must dominate the free-hole concentration if they are to have a substantial effect. Also, the recombination-center density must be sufficiently high to allow electron-hole recombination to dominate hole trapping back into the Cu_B center. On the other hand, if the RC density is too high, then the electrons and holes generated by the turn-on laser pulse will recombine before the free holes can be trapped in the Cu_B center, thus resulting in a high on-state resistance. Hence, a balance must be achieved to obtain the desired switching results over a limited parameter space.

For example, it was demonstrated in Fig. 17 that at an RC density that was high enough to allow the switch to be opened in less than 500 ps, the on-state resistance increased as a function of time between the two laser pulses. The reason for this can be determined by looking at the time dependence of the free-electron concentration, plotted in Fig. 25, during the on-state of the switch. It is obvious that, during the on-state, the free-electron concentration is still decreasing as a result of electron-hole recombination. Once again, it is the circuit that minimizes the effect of temporal variations of free carriers on the switch current, so long as the switch resistance is relatively low. The effect of these temporal variations will ultimately limit the maximum electrical pulse width that can be achieved with this device while maintaining a subnanosecond current fall-time.

VI.C. Variation of the Turn-Off-Laser Energy and Pulse Width

The opening time of the BOSS is dominated by two processes. One process is the electron-hole lifetime, while the other is the trapping of holes into the Cu_B level. The speed

by which electrons are removed from the conduction band depends on the concentration of free holes. Therefore, as the free-hole concentration is depleted through both electron-hole recombination and hole trapping into the Cu_B center, the free-electron concentration, and hence, the switch conductivity will decrease at a slower rate. Thus, it should be possible to increase the rate at which the electrons and holes recombine, through the recombination center, by increasing the pulse width of the 2-μm laser pulse. The result would be a higher electron concentration in the Cu_B center because the 2-μm laser pulse would be elevating electrons from the valence band for a longer period of time. This effect was investigated, with the help of the rate equation model, to determine if increasing the 2-μm laser pulse width, while maintaining the laser pulse energy constant, would reduce the minimum electrical pulse width by enhancing the turn-off effect.

The analysis considered the case shown as the dashed line in Fig. 23 where the turn-on and turn-off laser pulses were separated by 400 ps. The turn-on laser-pulse parameters remained constant at a peak photon flux of 3.2×10^{26} $cm^{-2}s^{-1}$, and a Gaussian standard deviation (σ) of 70 ps. The pulse width of the turn-off laser pulse was roughly doubled by increasing σ by a factor of two. When it was necessary to keep the energy contained in the pulse a constant, the peak photon flux was reduced by a factor of two. The results of this analysis did not indicated a decrease in the electrical pulse width. However, there was a decrease in the electrical pulse width when the peak photon flux was left at 1.6×10^{26} $cm^{-2}s^{-1}$, which basically amounted to doubling the energy contained in the turn-off laser pulse. The numerical results showed that it was an increase in the photon flux, or laser-pulse energy, rather than an increase in the laser pulse width, that resulted in a faster turn-off when the

laser pulses were close together. The effect of increasing the peak photon flux, on the switches ability to open, is shown in Fig. 27. The bold dashed line in Fig. 27 corresponds to the data illustrated as a dashed line in Fig. 23. The thin solid line in Fig. 27 corresponds to the solid line in Fig. 23 for a laser- pulse separation of 200 ps. The thin dashed line and the bold dash-dot line in Fig. 27 illustrates the effect of increasing the peak photon flux of the turn-off laser by a factor of two and three, respectively. These results show that the switch was able to open slightly faster when the turn-off laser-pulse energy was increased. Notice also that this effect appears to be saturating; as the photon flux is increased, the reduction of the current fall time decreases. Ultimately, the current fall time will be limited by the electron-hole lifetime.

An increase in the pulse width of the turn-off laser *did* have a substantial effect when the switch was opened following the depletion of the free-hole concentration that was generated by the turn-on laser pulse. For this analysis, the data shown in Fig. 3 that corresponds to an RC density of $6x10^{15}$ cm^{-3} will be compared to data generated by doubling the turn-off laser pulse width. The results of this analysis are shown in Fig. 28 where two cases were considered. First, the peak photon flux was reduced by a factor of two to maintain a constant energy in the laser pulse. Then, the peak photon flux was held constant, thereby doubling the energy contained in the pulse. The solid line in Fig. 28 corresponds to the data presented earlier in Fig. 3. The bold dashed line in Fig. 28 illustrates the effect of doubling the laser pulse width while keeping the energy in the pulse a constant. The dash-dot line in Fig. 28 shows the effect of doubling both the laser pulse width and the energy in the pulse. These variations of the laser-pulse parameters had a dramatic effect on the

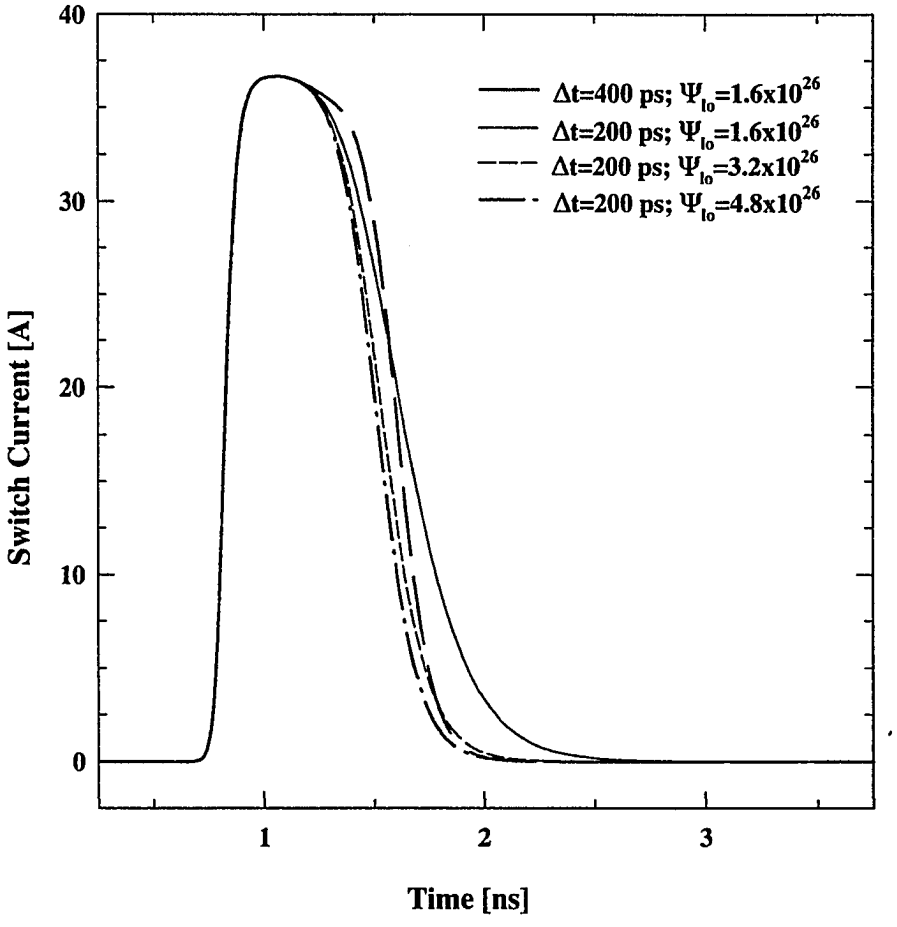

Figure 27 Simulation of the effect of increasing the peak photon flux of the turn-off laser (Ψ_{Io}) for a given time separation between the turn-on and turn-off laser pulses (Δt).

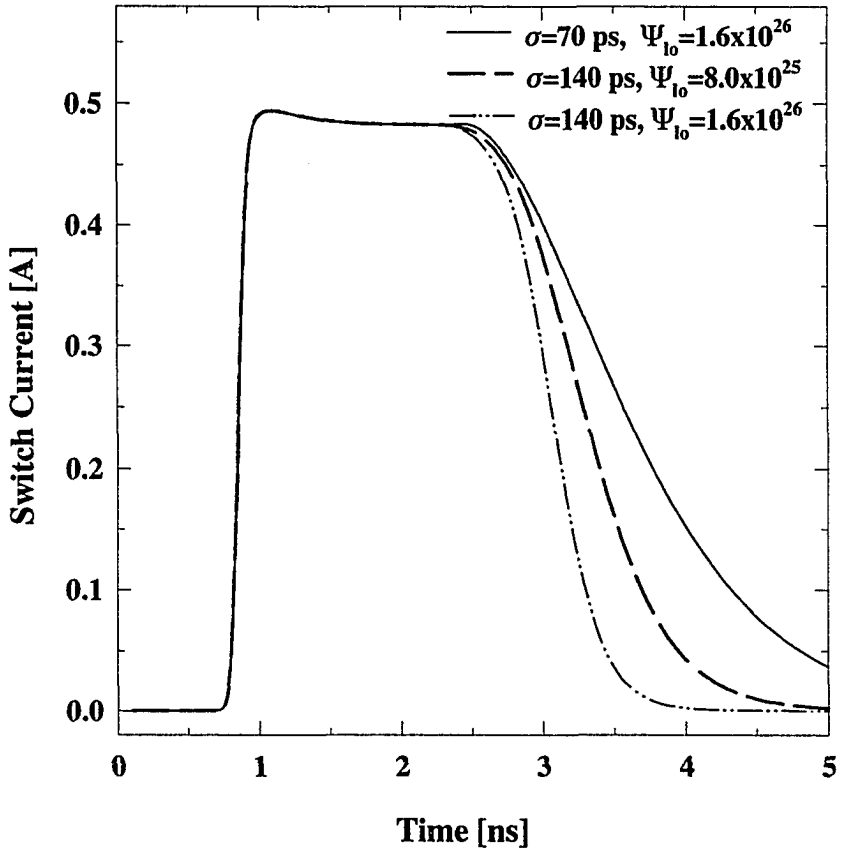

Figure 28 Simulation of an enhanced opening effect resulting from increasing the pulse width (σ) and peak photon flux (Ψ_{Io}) of the turn-off laser pulse.

switches ability to open. In fact, the fall-time of the current in Fig. 28, for the case when both the pulse width and energy are doubled, is very similar to that shown in Fig. 3 for the case of an RC density of $1x10^{16}$ cm^{-3}. Recall that there are several inherent advantages to having a lower RC density. For example, a lower on-state resistance is achieved due to a slower electron-hole recombination rate after the turn-on laser pulse. This is seen in Fig. 3 as a reduction in the on-state current when the RC density was increased to $1x10^{16}$ cm^{-3}. Also, a lower RC density would require a lower neutron fluence, thereby resulting in higher carrier mobilities in the material. The ideal situation would be to have a turn-off laser pulse that behaves similar to a square pulse with a fast rise-time, and a duration that was long enough to allow the switch to open in a time given by the recombination lifetime of the free carriers.

As mentioned earlier, an enhanced switch turn-off was expected because the longer pulse width should keep more electrons in the Cu_B center. To illustrate this thought further, the time dependence of the electron occupation of the Cu_B center is given in Fig. 29 for the three cases shown in Fig. 28. The larger laser pulse width necessarily means that the leading edge of the laser pulse occurs earlier in time (the peak of the laser pulse occurs at the same time for all three cases). This is seen in Fig. 29 as an earlier increase in the electron concentration of the Cu_B level when the standard deviation is 140 ps. The current illustrated in Fig. 28 does show an earlier start of the opening transient as a result of the wider pulse width. The overshoot in the Cu_B electron concentration is indicative of holes being trapped back into the Cu_B center after the turn-off laser pulse is terminated. However, as expected, the final Cu_B occupation is higher for both cases when the laser pulse width is doubled. This is because the second laser pulse elevates electrons into the Cu_B center for a longer period

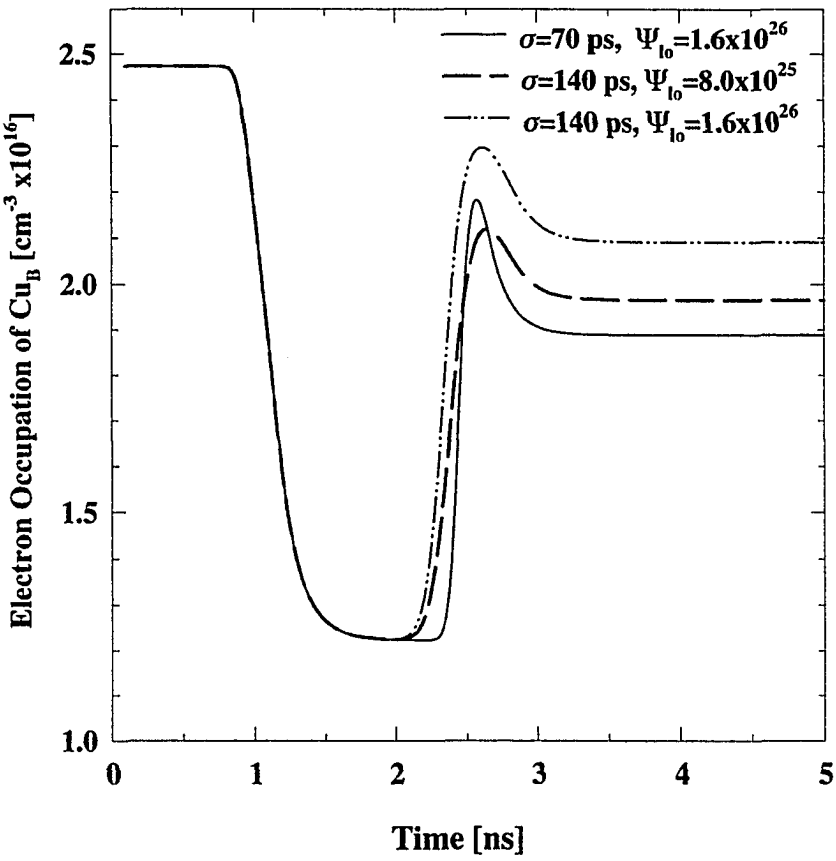

Figure 29 Simulation of changes in the electron occupation of the Cu_B level resulting from doubling the pulse width (σ) and the peak photon flux (Ψ_{Io}) of the turn-off laser.

of time, thereby reducing the net concentration of holes that are re-trapped by the Cu_B center. Therefore, more holes are available to recombine with electrons in the conduction band.

VI.D. High-Repetition-Rate Self-Opening Switches

One drawback of an increased RC concentration is that the on-state conductivity will be reduced because electrons in the conduction band will recombine with holes in the valence band before those holes can be trapped in the Cu_B center. This process reduces the number of holes that are trapped in the Cu_B center which, in turn, reduces the available sites to receive electrons from the valence band during the turn-off laser pulse. However, if the RC concentration in the bulk material is made high enough to cause the switch to open, on the desired time scale, without the need of the turn-off laser pulse, then high-repetition-rate operation with one laser wavelength is possible. This effect was shown in Fig. 19 where two 1-μm laser pulses were used to *close* a Group-VIII device at a high repetition rate. The reason why this device opened without the turn-off laser pulse was because it was irradiated at a higher neutron fluence than the Group-VII devices which required the turn-off laser to open the switch. Therefore, there was a higher RC density in the bulk material of the Group-VIII device. This effect was successfully simulated by the rate-equation model by reducing the peak photon flux of the turn-on laser to 8.0×10^{25} $cm^{-2}s^{-1}$, and by increasing the RC density from 2.0×10^{16} to 4.0×10^{16} cm^{-2}. The results of the simulation illustrating the switch current are shown in Fig. 30 while the time dependence of the free charges and the various deep-level electron occupations are shown in Fig. 31. Once again, the ratio of this higher RC density to the Group-VIII neutron fluence of 3.93×10^{15} cm^{-2} yields a constant of 10.2 which is good agreement with the value of 13.6 which was published by Goltzene, et.al. [41].

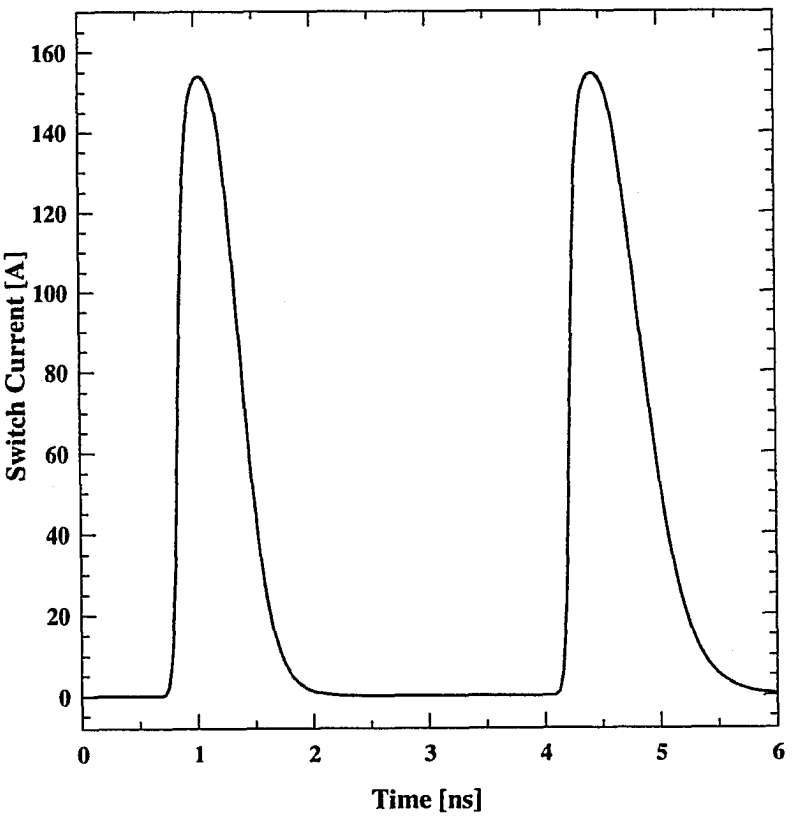

Figure 30 Simulation of a 290-MHz repetition rate within a two-pulse burst using two pulses from the 1-μm laser.

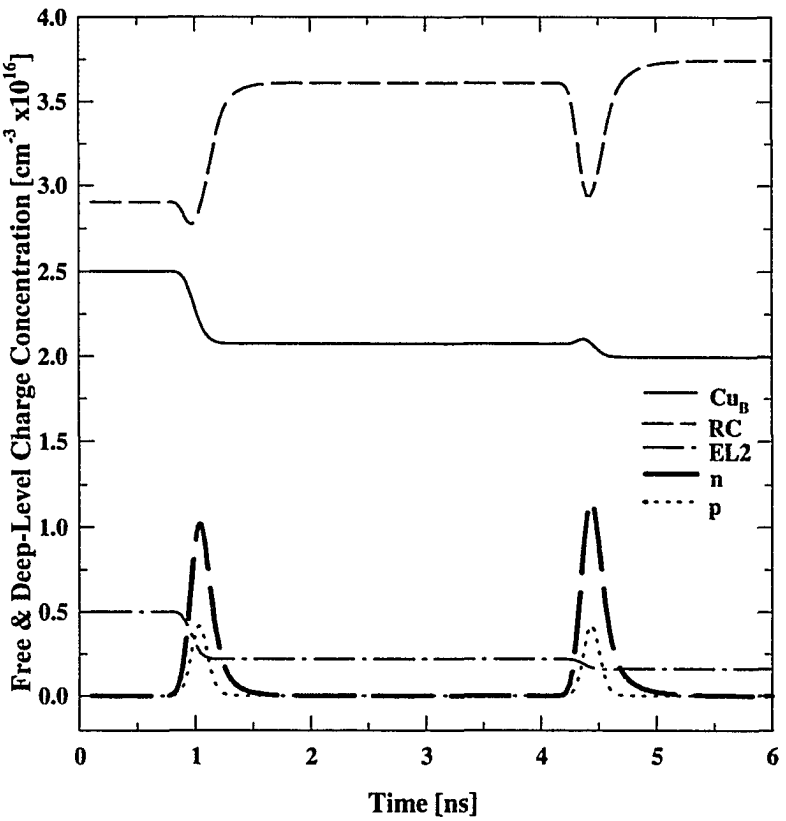

Figure 31 Temporal variation of the free charges and deep-level electron occupations for a device, with an RC density of $4x10^{16}$ cm^{-3}, which exhibited a self-opening effect as shown in Fig. 30.

The applied bias voltage used for the computed curve shown in Fig. 30 was 16 kV for comparison with Fig. 19. The simulated minimum resistance was about 4 Ω as opposed to the experimentally obtained value of about 20 Ω. A closer match could be obtained by reducing the 1-μm photon flux used in the simulation or by reducing the carrier mobilities. Note that the pulse width of the second current pulse in Fig. 30 is somewhat wider than the first. This is primarily the result of a slightly lower Cu_B occupation caused by the first switching transient as shown in Fig. 31.

A fundamental change in the switching action, from the first laser pulse to the second laser pulse, can be seen in Fig. 31. When the first laser pulse is incident on the switch, the Cu_B center is basically full while the recombination center is only about 71% full with an electron concentration of 2.85×10^{16} cm^{-3}. As previously demonstrated, the occupation of the Cu_B center is reduced, following the first turn-on laser pulse, as a result of optical excitation and hole trapping. After the free holes are depleted, the Cu_B occupation settles at about 2.1×10^{16} cm^{-3}, or 84% full of electrons. A dip in the RC occupation, resulting from optical excitation of electrons into the conduction band, is seen during the first laser pulse. The RC occupation then quickly rises to a constant value of about 3.6×10^{16} cm^{-3}, or 90% full.

The changes in the deep level occupations are quite different when the second turn-on laser pulse is incident on the switch. The Cu_B occupation actually shows a slight increase during the second laser pulse prior to settling down to an electron occupation of about 2.0×10^{16} cm^{-3}, or about 80% full. On the other hand, the RC occupation shows a strong dip from about 90% full to about 73% full. The electrons that were optically excited from the RC to the conduction band account for about 75% of the peak free-electron concentration

during the second laser pulse. After these electrons are elevated into the conduction band, most are quickly re-trapped back into the recombination center. The final RC occupation, after the second laser pulse, was about 3.75×10^{16} cm^{-3}, or about 94% full.

The changes in the final electron occupations of the Cu_B level and the recombination center appear to become smaller with each consecutive laser pulse. To investigate this effect further, a switching transient was simulated using four 1-μm laser pulses that were separated by 3.4 ns. The pulse width of the generated current pulse did not noticeably increase after the second laser pulse. The deep-level occupations, following each switching transient, basically saturated after the third laser pulse, as shown in Fig. 32. The final occupation of the recombination center was 3.78×10^{16} cm^{-3}, or about 95% full, and the final occupation of the Cu_B center was 1.98×10^{16} cm^{-3}, or 79% full. These results indicate that it should be possible to generate four-pulse bursts, similar to those shown in Figs. A-1 and A-4 in Appendix A, using BOSS devices irradiated at the Group-VIII fluence.

It was mentioned previously, in reference to Fig. 24, that the deep-level occupations were not the same as they were prior to the switching transient, and that this may have an adverse effect on the ability of a BOSS device to operate at high repetition rates. In order to investigate the ability of a BOSS device, that requires both a turn-on *and* a turn-off laser pulse to operate at high-repetition rates, a simulation was conducted using the same material and laser parameters that were used to generate the dashed line in Fig. 23. The only exception was that four switching transients, separated by 3.4 ns, were simulated instead of one. The switch-current results for this simulation are shown in Fig. 33, and the deep-level results are shown in Fig. 34. Only the first 9 ns of the simulation is shown in Fig. 34 so that

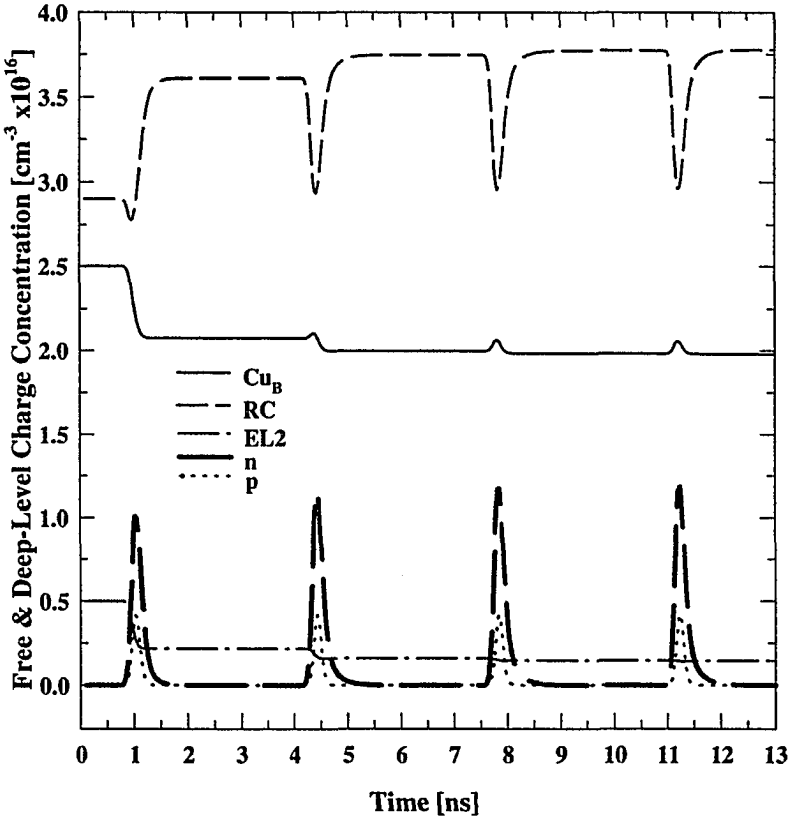

Figure 32 Simulation of the time dependence of the free charges and the deep-level electron occupations for a device that opens without the turn-off laser.

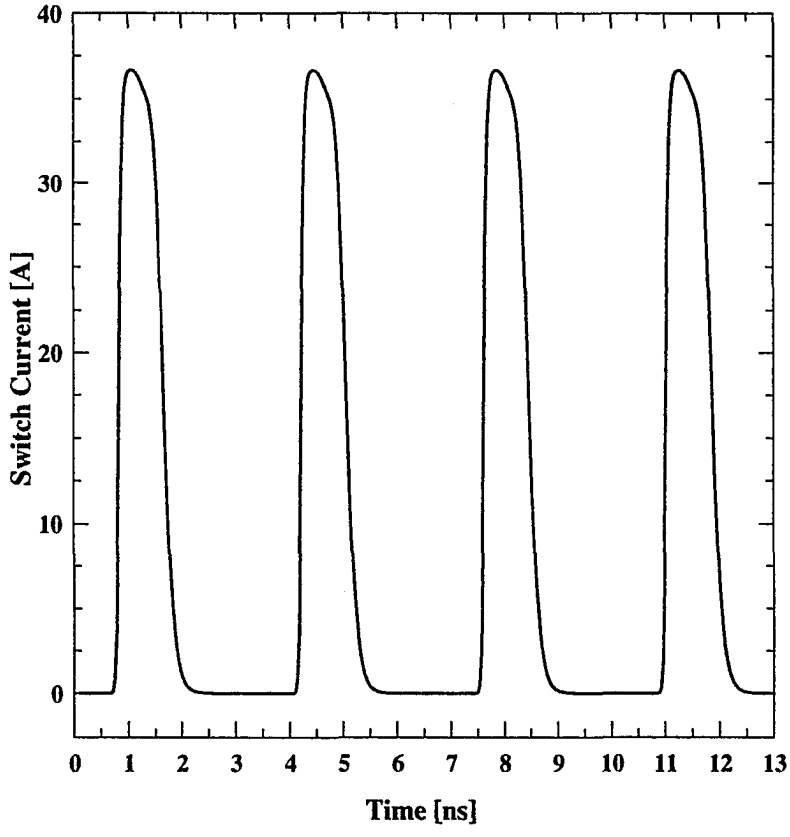

Figure 33 Simulated repetitive operation of a BOSS device using the same material and laser parameters that were used to generate the dashed line in Fig. 23 and the deep-level results illustrated in Fig. 25.

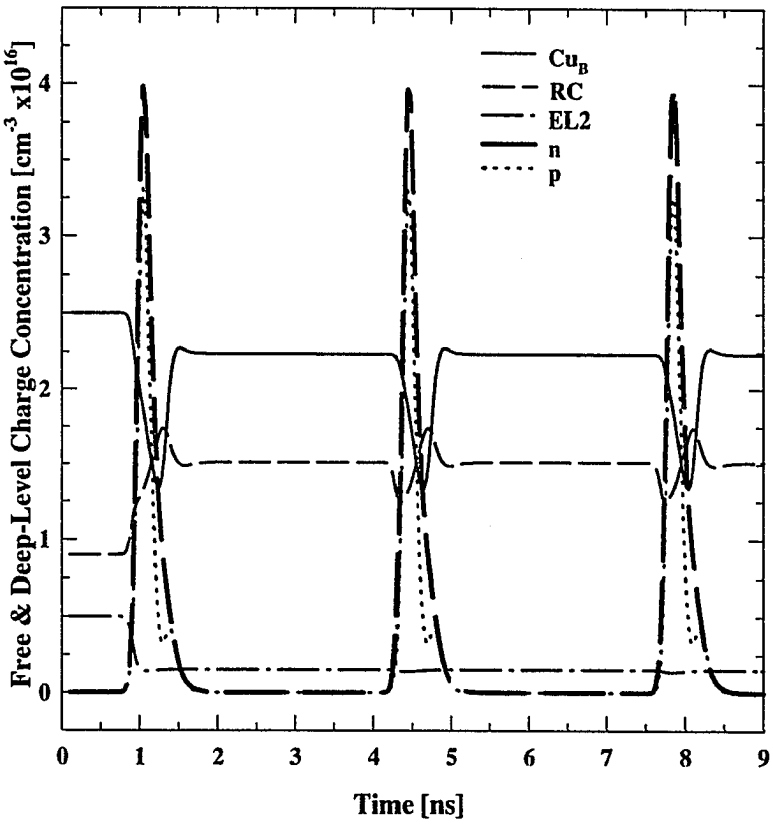

Figure 34 Simulation of the temporal response of the free charges and deep-level occupations for the first three switching transients shown in Fig. 33.

the time dependence of the various concentrations can be seen more clearly. The most important result is that the current pulse widths are the same for all four switching transients. The reason for this becomes clear when the time dependence of the deep-level occupations, shown in Fig. 34, are examined. The first switching transient, illustrated in Fig. 34, results in the same deep-level occupations, after the switch was opened, as those calculated for Fig. 25. The second, third, and fourth (not shown) switching transients, shown in Fig. 34, also result in the same deep-level occupations each time the switch is opened. That means that the turn-off laser pulse re-establishes the various deep-level parameters to the same occupations after each switching event. Unlike the results shown in Fig. 32, where several switching transients were required to saturate the changes in the deep-level occupations, the results in Fig. 34 indicate that only one switching event is required to establish the various deep-level occupations for the remaining switching events within the burst. Therefore, it appears that if the experimental results of a single switching transient are satisfactory, then it should be possible to repeat those results, at a very high repetition rate, simply by using identical laser parameters in each successive switching event. However, it is important to remember that the model used to obtain these results does not include thermal effects which could limit the repetitive operation of BOSS devices.

VI.E. High-Power Capability

The voltage and current limitations of the BOSS determine its applicability for high-power applications. One voltage limitation, particularly in lateral device geometries as shown in Fig. 2a, is surface-flash-over which is determined by the dielectric strength of the switch surface, the dielectric strength of the surrounding medium, and the contact geometry.

The empirical maximum average-electric-field limit is in the range of about 100 kV/cm in GaAs photoconductive switches [5,68]. An engineering safety factor of two brings the operating limit down to about 50 kV/cm for electrode gaps of greater than one millimeter. It should be pointed out that the results discussed in Refs. 5 & 68 were for different combinations of the bias-voltage duration, the dielectric medium in which the switch is immersed, and for various GaAs substrate materials. Therefore, this surface-flash-over limit should only be regarded as a rough estimate. Given that this is the case, the 5-mm gap devices discussed here should be able to operate at voltages as high as 25 kV without experiencing a surface flash-over. The dielectric medium used in this investigation was Fluorinert (FC-77), manufactured by 3M, which is useful for both its high-dielectric strength as well as its ability to act as a heat sink.

The initiation of current filaments in bulk photoconductors usually limits their maximum operating voltage at values lower than the surface-flash-over limit. Devices which rely on this filamentary current mode of operation are said to be operating in the "lock-on" mode [68]. This effect was found to be the result of a breakdown in the bulk semiconductor material while the conductivity of a photoconductive switch, operating in the linear mode, was being reduced through electron-hole recombination processes following the termination of the laser pulse. This breakdown mechanism occurred in non-irradiated GaAs devices when the average electric field reached about 10 kV/cm. As mentioned previously, neutron-irradiated BOSS devices have operated at average electric fields of 36 kV/cm without any indication of a transition into a filamentary conduction mode.

In order to give a qualitative explanation as to why neutron-irradiated BOSS devices are more resistant to filament formation, the theory associated with double-injection in semi-insulating materials will briefly be examined. This mechanism was first proposed by Lampert [72] and later modified by Ashley and Milnes [73]. At low voltages, most of the injected charges are trapped in the vicinity near the contacts while most of the switch remains free from excess charges and retains its initial low conductivity. As the voltage is increased, the injected charges are able to traverse deeper into the bulk region of the switch as the various deep-level traps are filled, and the value of the current increases. Eventually, as the voltage and current become large enough to allow the injected charge carriers to transit the electrode gap, the recombination centers become less significant than the injected carriers in determining the space charge, and thus, the current flow. At this point, the lifetime of the injected carriers becomes longer than the transit time and the space-charge limitations are relaxed. These effects result in the voltage decreasing as the current through the switch is increasing, thus the device enters a region of negative differential conductivity (NDC) [74]. Furthermore, it has been shown that the threshold voltage at which NDC is reached is proportional to the density of recombination centers in semiconductors doped with two deep-level traps [75]. The I-V characteristics of a device exhibiting double injection are of the current-controlled, or S-type, form. Such I-V characteristics have been theoretically predicted [76], and measured [77], in copper-doped GaAs material. Recently, a two-dimensional, time-dependent code was used to evaluate the effects of the switch geometry, the laser pulse distribution, negative differential resistance, and intrinsic impact ionization on the operation of a BOSS device [78].

Ridley has considered both current and voltage instabilities in semiconductors, and has postulated, based on minimum entropy production, that a device exhibiting a current-controlled NDC is unstable against the formation of a current filament [79]. This filament is expected to nucleate at some device inhomogeneity, is stationary, and grows in diameter as the current is increased. The exact type of inhomogeneity that results in the initiation of the filament is not known, however, it is expected to be the result of small doping variations in the vicinity of one of the contacts.

The fact that the threshold condition for current-controlled NDC is proportional to the RC density in the bulk material, and that this type of NDC normally yields filamentary conduction, gives an indication as to why neutron-irradiated BOSS devices have shown resistance to current filaments, or the "lock-on" effect.

Below electron drift-velocity saturation, the current that is controlled by a BOSS device, for a given applied voltage, is dictated by the circuit impedance. However, given that current filamentation and surface flash over can be avoided, the maximum current that can be delivered to the load will ultimately be limited by drift-velocity saturation. Drift-velocity saturation is electric-field dependent, and is known to occur in GaAs at average electric fields in excess of 3 kV/cm [80]. Therefore, for a given switch geometry, the voltage (V_m) at which velocity saturation occurs is a constant. Thus, for a given on-state resistance (R_s), the maximum current is determined by $I_m=V_m/R_s$. Since the power delivered to the load depends quadratically on the current, a factor of two reduction in the on-state resistance results in a factor of four increase in the maximum power. Since the excessively irradiated BOSS devices have an on-state impedance of 10 to 20 Ω, their power-handling capability will be

limited. However, the minimum on-state resistance of devices irradiated at a fluence of 2.45×10^{15} cm^{-2} (Group VII) was measured to be on the order of 1 Ω. Therefore, Group VII devices should be able deliver several hundred amperes to the load before drift-velocity saturation occurs.

VI.F. Summary

The experimental results presented in Chap. V have been evaluated, within the context of the rate-equation model, and were found to be in good agreement with the numerical simulation. The relation between the RC density and the fast-neutron fluence that was used in the simulation was in good agreement with the defect-generation rate published in the literature [41]. The minimum electrical pulse width that can be generated by a BOSS device, requiring both a turn-on and a turn-off laser pulse, was evaluated by examining the time dependence of the deep-level occupations following the turn-on laser pulse. It was determined that the minimum electrical pulse width was primarily dependent on the time necessary to allow the free-hole population to decay through hole trapping into Cu_B and through electron-hole recombination through the recombination centers. The minimum possible electrical pulse width was found to be in the range of 500 ps to less than one nanosecond, depending on the various deep-level and laser parameters. Pulse widths that were less than 400 ps were simulated by increasing the RC density to the point where the switch would self-open after the turn-on laser pulse.

The operation of devices that exhibited the self-opening effect, as well as those that required both laser pulses, were simulated at a 290-MHz repetition rate within a four-pulse burst. An examination of the time dependence of the free charges and the deep-level

occupations, for self-opening devices, indicated that several switching events were required before the occupation of the deep levels reached the same point after each switching transient. However, the deep-level occupations, in BOSS devices that required both laser pulses to operate, reached the same point after each switching event. These results indicate that it should be possible to operate BOSS devices at very high repetition rates within relatively short bursts. Continuous operation would probably not be possible due to excessive heating of the device.

Finally, a brief discussion of the apparent immunity of neutron-irradiated BOSS devices to transition into a filamentary mode of conduction was presented. If the transition into filamentary conduction, as implied by the double-injection model, is the result of a current-controlled NDC, than a higher RC density should result in a higher threshold voltage for the initiation of current filaments.

CHAPTER VII

CONCLUSIONS

The purpose of this study has been to examine the high-speed and high-power capabilities of the bistable optically controlled semiconductor switch (BOSS). The goal of this research was to demonstrate the operation of BOSS devices at multi-megawatt peak power levels, at subnanosecond closing and opening times, and at repetition rates of greater than 100 MHz. The motivation for this work has been the development of a frequency-agile high-power microwave (HPM) source for use in electronic counter measures (ECM) applications, as an ultra-wide-band (UWB) radar transmitter, and as a directed-energy weapon (DEW). If successful, this source may offer substantial benefits over other HPM sources that are currently being developed.

When this work began, the BOSS concept had been demonstrated at a peak power of less than one megawatt, and at electrical pulse widths of tens of nanoseconds or greater. The laser pulse widths that had previously been used to demonstrate these capabilities had a FWHM of several nanoseconds. In discussing the experimental work, the range of operation of the BOSS has been extended into the subnanosecond range. A mode-locked, flash-lamp pumped Nd:YAG laser, fitted with an optical parametric generator (OPG), was

obtained to facilitate testing of BOSS devices in the subnanosecond regime. The FWHM of both the turn-on and turn-off laser pulses generated by this laser system was about 140 ps.

In order to use the BOSS in the subnanosecond regime, the recombination time had to be reduced from nanoseconds to hundreds of picoseconds. The method that was used to generate the recombination centers was fast-neutron irradiation. The neutron fluence that created a sufficient number of recombination centers, to allow the switch to open in the subnanosecond regime, was 2.45×10^{15} cm^{-2}. If the neutron fluence was increased to 3.93×10^{15} cm^{-2}, the switch was found to open without requiring the turn-off laser pulse. The inability of the switch to remain closed after the turn-on laser pulse was terminated was an indication that the electrons that were elevated into the conduction band were recombining with holes in the valence band before those holes could be trapped in the Cu_B level. These results indicated that a balance had to be achieved between the hole trapping time of the Cu_B center, and the electron-hole recombination time, if the switch was to operate properly.

The power-handling capability, the pulse-width agility, the minimum current fall time, and the minimum electrical pulse width that could be generated by a subnanosecond BOSS device was studied experimentally and theoretically. Neutron-irradiated BOSS devices with gaps of 5 mm have been operated at voltages as high as 18 kV without any indication of a transition into a filamentary mode of conduction. These voltages resulted in peak powers as high as 3 MW being delivered to the 100-Ω load. The generated electrical pulse width was changed by varying the time between the turn-on and the turn-off laser pulse. A curve fit to the switch conductance during the opening phase, after it was extracted from the circuit load line, indicated an effective recombination time constant of 100 ps. The

current fall time associated with this time constant was about 400 ps. The minimum electrical pulse width that was experimentally measured for a device with a fluence of 2.45×10^{15} cm^{-2} was about 650 ps which was found to be in good agreement with the numerical simulation. These results indicate that the mechanism which limits the minimum time delay between laser pulses, and hence the minimum electrical pulse width, is the residual free-hole concentration after the turn-on laser pulse. This is primarily because the holes created by the turn-off laser pulse must dominate the free-hole concentration if they are to have a substantial effect.

Experiments were also performed with heavily neutron-irradiated devices which exhibited the self-opening effect. This effect was also simulated by the model for the case that the RC density was increased by a factor of two. The electrical pulse widths that were experimentally generated by these devices were about 340 ps FWHM. The devices were operated at repetition rates has high as 1 GHz, within a two-pulse burst, and at voltages as high as 18 kV.

Four-pulse bursts were simulated with the rate equation model to investigate the number of pulses necessary to reach the same deep-level occupations following each switching event. For devices which exhibited the self-opening effect, it took three or four switching transients before the deep-level occupations stabilized. It was also found that, after the first laser pulse, the conduction electrons were primarily obtained by elevating electrons from the RC center into the conduction band.

Four-pulse bursts were also simulated in devices that required both a turn-on and a turn-off laser pulse. Unlike the self-opening devices, the deep-level occupations in these

devices were reset to the same point following each turn-off laser pulse. It therefore seems possible that these devices would successfully operate at very high repetition rates when a suitable laser system is developed to produce the desired laser pulses.

Based on the capabilities of the subnanosecond BOSS, a device was developed which allows the generation high-power, frequency-agile RF waveforms. The HPM-source concept that was demonstrated, for the first time, is called the pulse-switch-out generator (PSO). Two switches, each embedded in an oppositely charged transmission line, were used to demonstrate the PSO source. Positive and negative half-cycles were then generated by first closing and opening each switch in succession. The frequency content in the generated pulse was then adjusted by varying the timing between the closure of each device. The Fourier spectra of the generated waveforms demonstrated that the ability to vary the time between closing each switch allowed the number and location of the nulls in the spectrum to be changed. Furthermore, when four-pulse bursts were replicated from the experimental data, the power in each one of the spectral peaks was shown to increase by at least a factor of 16 over the peak power in the single cycles. The ability to increase the power spectral density in certain parts of the spectrum, while minimizing the spectral content in other parts of the spectrum, may produce substantial benefits in electronic counter measures (ECM), ultra-wide-band (UWB), and directed-energy weapons (DEW) applications.

The operating speed and the power-handling capability of BOSS devices have now been increased to the point that a BOSS-based, high-power, frequency-agile RF source could be realized. However, it is still necessary to demonstrate the ability of a BOSS device to operate at high repetition rates for extended periods of time. With the appropriate laser, it

should be possible to build an RF source that could radiate a peak power of roughly one megawatt with frequency content between 100 MHz and 2 GHz.

LIST OF REFERENCES

[1] D.H. Auston, "Picosecond optoelectronic switching and gating in silicon," *Appl. Phys. Lett.*, Vol. 26, pp. 101-103, 1975.

[2] C.H. Lee, "Picosecond optoelectronic switching in GaAs," *Appl. Phys. Lett.*, Vol. 30, pp. 84-86, 1977.

[3] D. Grischkowsky, C.-C. Chi, I.N. Duling III, W.J. Gallagher, N.H. Halas, J.M. Halbout, and M.B. Ketchen, "Photoconductive generation of subpicosecond electrical pulses and thier measurement applications," *Picosecond Electronics and Optoelectronics II, Springer Series in Electronics and Photonics, Vol. 24*, F.J. Leonberger, C.H. Lee, F. Capasso, H. Morkoc, Eds., Berlin: Springer-Verlag, 1987, pp. 11-17.

[4] G. Mourou, W.H. Knox, and S. Williamson, "High-power picosecond switchin in bulk semiconductors," *Picosecond Optoelectronic Devices*, C.H. Lee, Ed., New York: Academic Press, 1984, pp. 219-248.

[5] G.M. Loubriel, M.W. O'Malley, and F.J. Zutavern, "Toward pulsed power uses for photoconductive semiconductor switches: Closing switches," *Proc. 6th IEEE Pulsed Power Conf.*, Arlington, VA, 1987, pp. 145-148.

[6] F.J. Zutavern, G.M. Loubriel, M.W. O'Malley, L.P. Shanwald, W.D. Helgerson, D.L. McLaughlin, and B.B. McKenzie, "Photoconductive semiconductor switch experiments for pulsed power applications," *IEEE Trans. on Electron Devices*, Vol. ED-37, pp. 2472-2477, 1990.

[7] D.C. Stoudt, K.H. Schoenbach, R.P. Brinkmann, V.K. Lakdawala, and G.A. Gerdin, "The recovery behavior of semi-insulating GaAs in electron-beam-controlled switches," *IEEE Trans. on Electron Devices*, Vol. ED-37, pp. 2478-2485, 1990.

[8] R.P. Brinkmann, K.H. Schoenbach, D.C. Stoudt, V.K. Lakdawala, G.A. Gerdin, and M.K. Kennedy, "The lock-on effect in electron-beam-controlled gallium arsenide switches," *IEEE Trans. on Electron Devices*, ED-38, pp. 701-705, 1991.

[9] M.D. Pocha, R.L. Druce, and W.W. Hofer, "High voltage, subnanosecond photoconductive switching," *UCRL 53868-89*, available from the National Technical Information Service, US Department of Commerce, 5285 Port Royal Road, Springfield, VA 22161.

[10] G.M. Loubriel, F.J. Zutavern, H.P. Hjalmarson, R.R. Gallegos, W.D. Helgeson, and M.W. O'Malley, "Measurement of the velocity of current filaments in optically triggered, high gain GaAs switches," *Appl. Phys. Lett.*, Vol. 64, pp. 3323-3325, 1994.

[11] R.A. Falk, J.C. Adams, and G.L. Bohnhoff-Hlavlacek, "Optical probe techniques for avalanching photoconductors," Proc. 8th IEEE Pulsed Power Conf., San Diego, CA, 1991, pp. 29-36.

[12] K.H. Schoenbach, J.S. Kenney, A. Koenig, B.J. Ocampo, R.F.K. Germer, and H.J. Schulz, "Electric field measurements in photoconductive GaAs switches," *Proc. 8th IEEE Pulsed Power Conf.*, San Diego, CA, 1991, pp. 105-108.

[13] K.H. Schoenbach, V.K. Lakdawala, R. Germer, and S.T. Ko, "An optically controlled closing and opening semiconductor switch," *J. Appl. Phys.*, Vol. 63, pp. 2460-2463, 1988.

[14] J. Blanc, R.H. Bube, and H.E. MacDonald, "Properties of high-resistivity gallium arsenide compensated with diffused copper," *J. Appl. Phys.*, Vol. 32, pp. 1666-1679. 1961.

[15] S.M. Sze and J.C. Irvin, "Resistivity, mobility, and impurity levels in GaAs, Ge, and Si at 300 K," *Solid State Electron.*, Vol. 11, pp. 599-604, 1968.

[16] N. Kullendorff, L. Jansson, and L.A. Ledebo, "Copper-related deep level defects in III-V semiconductors," *J. Appl. Phys.*, Vol. 54, pp. 3203-3212, 1983.

[17] D.V. Lang and R.A. Logan, "A study of deep levels in GaAs by capacitance spectroscopy," *J. Electronic Materials*, Vol. 4, pp. 1053-1066, 1975.

[18] A.V. Lyubchenko, M.K. Sheinkman, V.A. Brodovoi, and N.M. Krolevets, "Determination of the parameters of recombination centers in copper-doped gallium arsenide," *Fiz. Tekh. Poluprov.*, Vol. 2, pp. 492-500, 1968 [*Sov. Phys. - Semicond.*, Vol. 2, pp. 406-412, 1968].

[19] V.A. Brodovoi and N.I. Kolesnik, "Photoconductivity of Cu-doped GaAs in strong electric fields," *Fiz. Tekh. Poluprov.*, Vol. 4, pp. 2059-2063, 1970 [*Sov. Phys. - Semicond.*, Vol. 4, pp. 1770-1774, 1971].

[20] V.A. Brodovoi and N.Z. Derikot, "Properties of GaAs:Cu in strong electric fields," *Fiz. Tekh. Poluprov.*, Vol. 6, pp. 276-280, 1971 [*Sov. Phys. - Semicond.*, Vol. 6, pp. 237-240, 1972.

[21] R.A. Roush, K.H. Schoenbach, and R.P. Brinkmann, "Bistable behavior of the dark current in copper-doped semi-insulating gallium arsenide," *J. Appl. Phys.*, Vol. 71, pp. 4354-4360, 1992.

[22] R.K.F. Germer, K.H. Schoenbach, and S.G.E. Pronko, "A bulk optically controlled semiconductor swtich," *J. Appl. Phys.*, Vol. 64, pp. 913-917, 1988.

[23] R.K.F. Germer and K.H. Schoenbach, "Stimulated switch-off and repetitive switching of a bistable optically controlled semiconductor switch," *J. Phys. D: Appl. Phys.*, Vol. 22, pp. 398-403, 1989.

[24] O. Madelung, Ed., *Landolt-Börnstein, Group III: Crystal and Solid State Physics, 17b*, New York: Springer-Verlag, 1982, p. 417.

[25] S.T. Ko, V.K. Lakdawala, K.H. Schoenbach, and M.S. Mazzola, "Influence of copper doping on the performance of optically controlled GaAs switches," *J. Appl. Phys.*, Vol. 67, pp. 1124-1126, 1990.

[26] M.S. Mazzola, K.H. Schoenbach, V.K. Lakdawala, and S.T. Ko, "Nanosecond optical quenching of photoconductivity in a bulk GaAs switch," *Appl. Phys. Lett.*, Vol. 55, pp. 2102-2104, 1989.

[27] D.C. Stoudt, M.S. Mazzola, and S.F. Griffiths, "Characterization and switching study of an optically controlled GaAs switch," *Proc. SPIE, Vol. 1378, Optically Activated Switching*, 1990, pp. 280-285.

[28] D.C. Stoudt, R.A. Roush, M.S. Mazzola, and S.F. Griffiths, "Investigation of a laser-controlled, copper-doped GaAs closing and opening switch for pulsed power applications," *Proc. 8th IEEE Pulsed Power Conf.*, San Diego, CA, 1991, pp. 41-45.

[29] M.S. Mazzola, R.A. Roush, S.F. Griffiths, D.C. Stoudt, and D.H. Keil, "Subnanosecond performance of the BOSS GaAs opening switch," *Proc. 20th Power Mod. Symp.*, Myrtle Beach, SC, 1992, pp. 266-270.

[30] D.C. Stoudt, R.P. Brinkmann, and R.A. Roush, "Subnanosecond high-power performance of a bistable optically controlled GaAs switch," *Int. Symp. GaAs and Related Compounds, Inst. Phys. Conf. Ser. No. 136: Chapter 5*, Freiberg, Germany, 1993, pp. 325-330.

[31] D.C. Stoudt, R.P. Brinkmann, R.A. Roush, M.S. Mazzola, F.J. Zutavern, and G.M. Loubriel, "Effects of 1-MeV neutron irradiation on the operation of a bistable optically controlled semiconductor switch (BOSS)," *IEEE Trans. Electron Dev.*, Vol. 41, pp. 913-919, 1994.

[32] M. Parenteau and C. Carlone, "Damage coefficient associated with free exciton lifetime in GaAs irradiated with neutrons and electrons," *J. Appl. Phys.*, Vol. 71, pp. 3747-3753, 1992.

[33] D.V. Lang and R.A. Logan, "A study of deep levels in GaAs by capacitance spectroscopy," *J. Electronic Mater.*, Vol. 4, pp. 1053-1066, 1975.

[34] N. Kullendorf, L. Jansson, and L-A. Ledebo, "Copper-related deep level defects in III-V semiconductors," *J. Appl. Phys.*, Vol. 54, pp. 3203-3212, 1983.

[35] J.S. Weiner and P.Y. Yu," Free carrier lifetime in semi-insulating GaAs from time-resolved band-to-band photoluminescence," *J. Appl. Phys.*, Vol. 55, pp. 3889-3891, 1984.

[36] A. Mitonneau, A. Mircea, G.M. Martin, and D. Pons, "Electron and hole capture cross section at deep centers in gallium arsenide," *Rev. Phys. Appl. (France)*, Vol. 14, pp. 853-861, 1979.

[37] G.M. Martin, "Optical assesment at the main electron trap in bulk semi-insulating GaAs," *Appl. Phys. Lett.*, Vol. 39, pp. 747-748, 1981.

[38] T.F. Boggess, A.L. Smirl, S.C. Moss, I.W. Boyd, and E.W. Vanstryland, "Optical limiting in GaAs," *IEEE J. Quant. Elect.*, Vol. QE-21, pp. 488494, 1985.

[39] Y.P. Varshni, "Band to band radiative recombination in group IV, VI, and III-V semiconductors (I)," *Phys. Stat. Sol.*, Vol. 19, pp. 459-514, 1967.

[40] R.A. Roush, D.C. Stoudt, and M.S. Mazzola, "Compensation of shallow silicon donors by deep copper acceptors in gallium arsenide," *Appl. Phys. Lett.*, Vol. 62, pp. 2670-2672, 1993.

[41] A. Goltzene, B. Meyer, C. Schwab, S.G. Greenbaum, R.J. Wagner, and T.A. Kennedy, "Electron paramagnetic resonance spectroscopy of fast neutron-generated defects in GaAs," *J. Appl. Phys.*, Vol. 56, pp. 3394-3398, 1984.

[42] V.S. Vavilov, *Effects of Radiation on Semiconductors* (Translation by the Consultants Bureau Enterprises, Inc. New York), 1963.

[43] C.L. Wang, M.D. Pocha, and J.D. Morse, "Neutron-treated, ultrafast, photoconductor detectors," *Appl. Phys. Lett.*, Vol. 54, pp. 1451-1453, 1989.

[44] L. Borghi, P.De. Stefano, and P. Mascheretti, "Photoconductivity of neutron-irradiate gallium arsenide," *J. Appl. Phys.*, Vol. 41, pp. 4665-4668, 1970.

[45] P.J. Griffin, J.G. Kelly, and D.W. Vehar, "Updated neutron spectrum characterization of SNL baseline reactor environments, Vol. 1: Characterization," Sandia Report, SAND93-2554, UC-713, 1994.

[46] S.M. Sze, *Physics of Semiconductor Devices*, 2nd ed., New York: John Wiley & Sons, 1981, p. 850.

[47] Chr. Lehmann, *Interaction of radiation with solids and elementary defect production*, Amsterdam: Nort-Holland Pub. Co., 1977, p. 150.

[48] Crystal numbers 1488 and 508. Grown by Bertram Laboratories, Somerville, NJ 08876.

[49] L.M. Thomas and V.K. Lakdawala, "Study of diffusion of copper in silicon doped gallium arsenide using photoinduced current transient spectroscopy for deep level characterization," *Defect and Diffusion Forum*, Vol. 95-98, pp. 931-936, 1993.

[50] R.N. Hall and J.H. Racette, "Diffusion and solubility of copper in extrinsic and intrinsic germanium, silicon, and gallium arsenide," *J. Appl. Phys.*, Vol. 35, pp. 379-397, 1964.

[51] N. Braslau, "Alloyed ohmic contacts to GaAs," *J. Vac. Sci. Technol.*, Vol. 19, pp. 803-807, 1981.

[52] Private communication with Patrick J. Griffin, SNL, Radiation Effects and Reactor Design Division. See also P.J. Griffin, J.G. Kelly, T.F. Luera, A.L. Barry, and M.S. Lazo, *IEEE Trans. Nuclear Science*, vol. 38, no. 6, p. 1216, 1991.

[53] V.A.J. van Lint, T.M. Flanagan, R.E. Leadon, J.A. Naber, and V.C. Rogers, *Mechanisms of Radiation Effects in Electronic Materials, Vol. 1*, New York: John Wiley & Sons, 1980, p. 270.

[54] A.H. Kalma, R.A. Berger, and R.A. Cesena, *Radiation Damage and Defects in Semiconductors*, University of Reading, Inst. Phys. Conf. Ser. 16, London and Bristol, 1973, pp. 364-370.

[55] J.G. Williams, J.U. Patel, A.M. Ougouag, and S.-Y. Yang, "Carrier removal and changes in electrical properties of neutron irradiated GaAs," *J. Appl. Phys.*, Vol. 70, pp. 4931-4937, 1991.

[56] D.V. Lang, "Review of Radiation-Induced Defects in III-V Compounds," *Inst. Phys. Conf. Ser., No. 31*, pp. 70-94, 1977.

[57] N.A. Ives and M.S. Leung, "Noncontact laminar-flow polishing for GaAs," *Rev. Sci. Instrum.*, Vol. 59, pp. 172-175, 1988.

[58] M.G. Mil'vidskii, V.B. Osvenskii, and T.G. Yugova, "Some peculiarities of the decomposition of supersaturated solid solutions of copper in gallium arsenide," *Fiz.*

Tverd. Tela, Vol. 10, pp. 2724-2730, 1968 [*Sov. Phys. - Solid State*, Vol. 10, pp. 2144-2148, 1969].

[59] L.M. Thomas and V.K. Lakdawala, "Influence of arsenic vapor pressure during copper diffusion on deep level formation in silicon-doped gallium arsenide," *J. Electron. Mater.*, Vol. 22, pp. 341-346, 1993.

[60] A. Goltzene, B. Meyer, and C. Schwab, "Electron paramagnetic resonance monitoring of recovery of fast neutron irradiated GaAs," *J. Appl. Phys.*, Vol. 57, pp. 1332-1335, 1985.

[61] A. Goltzene, C. Schwab, J.P. David, and A. Roizes, "Electrical behavior of fast neutron irradiated semi-insulating GaAs during thermal recovery," *Appl. Phys. Lett.*, Vol. 49, pp. 862-864, 1986.

[62] A. Goltzene, B. Meyer, and C. Schwab, "Persistent photoquenching and anion antisite defects in neutron-irradiated GaAs," *Appl. Phys. Lett.*, Vol. 54, pp. 907-909, 1989.

[63] R.L. Byer, *Quantum Electronics, Vol. I, part B*, R. Rabin and C.L. Chang, Eds., New York: Academic Press, 1975, Chap. 9.

[64] D.C. Stoudt, M.A. Richardson, H.D. Willie, and D.L. Demske, "A frequency-agile RF source using bistable optically controlled semiconductor switches (BOSS)," *Proc. 7th National Conf. on High Power Microwave Tech.*, Monterey, CA, 1994.

[65] J.I. Pankove, *Optical Processes in Semiconductors*, Englewood Cliffs: Prentice-Hall, 1971, p. 311.

[66] E. Yu. Brailovskii, V.N. Broudnyi, A.A. Groza, *Radiation Damage and Defects in Semiconductors*, University of Reading, Inst. Phys. Conf. Ser. 16, London and Bristol, 1973, pp. 121-128.

[67] R. Coates and E.W. Mitchell, "The optical and electrical effects of high concentrations of defects in irradiated crystalline gallium arsenide," *Adv. Phys.*, Vol. 24, D.H. Martin, Ed., London: Taylor & Francis, 1975, pp. 593-644.

[68] F.J. Zutavern and G.M. Loubriel, *High-Power Optically Activated Solid-State Swtiches*, A. Rosen and F. Zutavern, Eds., Boston: Artech House, 1994, Chap. 11.

[69] G.M. Loubriel, F.J. Zutavern, H.P. Hjalmarson, and M.W. O'Malley, "Closing photoconductive semiconductor switches," *Proc. 7th IEEE Pulsed Power Conf.*, Monterey, CA, 1989, pp. 365-367.

[70] S.T. Ko, *Study of Direct Semiconductor Materials for an Optically Controlled Switch*, Ph.D. Dissertation, Dept. of Electrical and Computer Eng., Old Dominion Univ., Norfolk, Virginia, 1989.

[71] M.S. Mazzola, *Experimental Studies of Bulk Optically Controlled GaAs Switches Utilizing Fast Infrared Quenching*, Ph.D. Dissertation, Dept. of Electrical and Computer Eng., Old Dominion Univ., Norfolk, Virginia, 1990.

[72] M.A. Lampert, "Double injection in insulators," *Phys. Rev.*, Vol. 125, pp. 126-141, 1962.

[73] K.L. Ashley and A.G. Milnes, "Double injection in deep-lying impurity semiconductors," *J. Appl. Phys.*, Vol. 35, pp. 369-375, 1964.

[74] A.M. Barnett and A.G. Milnes, "Filamentary injection in semi-insulating silicon," *J. Appl. Phys.*, Vol. 37, pp. 4215-4223, 1966.

[75] W.H. Weber and G.W. Ford, "Double injection in semiconductors heavily doped with deep two-level traps," *Solid State Electron.*, Vol. 13, pp. 1333-1356, 1970.

[76] R.P. Brinkmann, K.H. Schoenbach, M.S. Mazzola, R.A. Roush, and D.C. Stoudt, "Analysis of time-dependent current transport in an optically controlled, Cu-compensated GaAs switch," *Proc. SPIE, Vol. 1632, Optically Activated Switching II*, 1992, pp. 262-273.

[77] R.A. Roush, K.H. Schoenbach, and R.P. Brinkmann, "Bistable behavior of the dark current in copper-doped semi-insulating gallium arsenide," *J. Appl. Phys.*, Vol. 71, pp. 9-13, 1992.

[78] P.J. Stout, *Modeling Optically Activated High Power Semiconductor Switches*, Ph.D. Dissertation, Dept. of Electrical and Computer Eng., Univ. of Illinois at Urbana-Champaign, Urbana, Illinois, 1995.

[79] B.K. Ridley, "Specific negative resistance in solids," *Proc. Phys. Soc.*, Vol. 82, pp. 954-966, 1963.

[80] J.S. Blakemore, "Semiconducting and other major properties of gallium arsenide," *J. Appl. Phys.*, Vol. 53, pp. R123-R181, 1982.

APPENDIX A

POTENTIAL RF OUTPUT OF A PSO GENERATOR

Since the operation of the switch has been demonstrated at about 1 GHz, in a burst mode, and since the operation of two BOSS devices in a PSO generator has also been demonstrated, it is reasonable to examine the effect of generating a short burst of RF cycles at megahertz repetition rates. To accomplish this, a potential RF output from a PSO generator was simulated by replicating data similar to that shown in Fig. 21 for a laser pulse separation of 500 ps, and a time separation between RF cycles of 10 ns. The result of this data manipulation is shown below in Fig. A-1 where four RF cycles, at a 100-MHz repetition rate, are given with the total time window set at 80 ns. Figure A-1 is an illustration of the type of waveform that is expected to be generated by a PSO RF source once the laser system, which is currently being developed, becomes available.

The power spectra of a single monocycle as well as the waveform shown in Fig. A-1, corrected for a burst repetition rate of 1 kHz, are illustrated in Figures A-2 and A-3, respectively. The method by which the power spectrum is calculated is as follows. The data is first *padded* with zeros out to a total time window of 80 ns which corresponds to a 12.5-MHz burst repetition rate, as far as the FFT is concerned. Then an FFT is performed on the time-domain waveform of the voltage on the 50-Ω load. The amplitude of the resulting

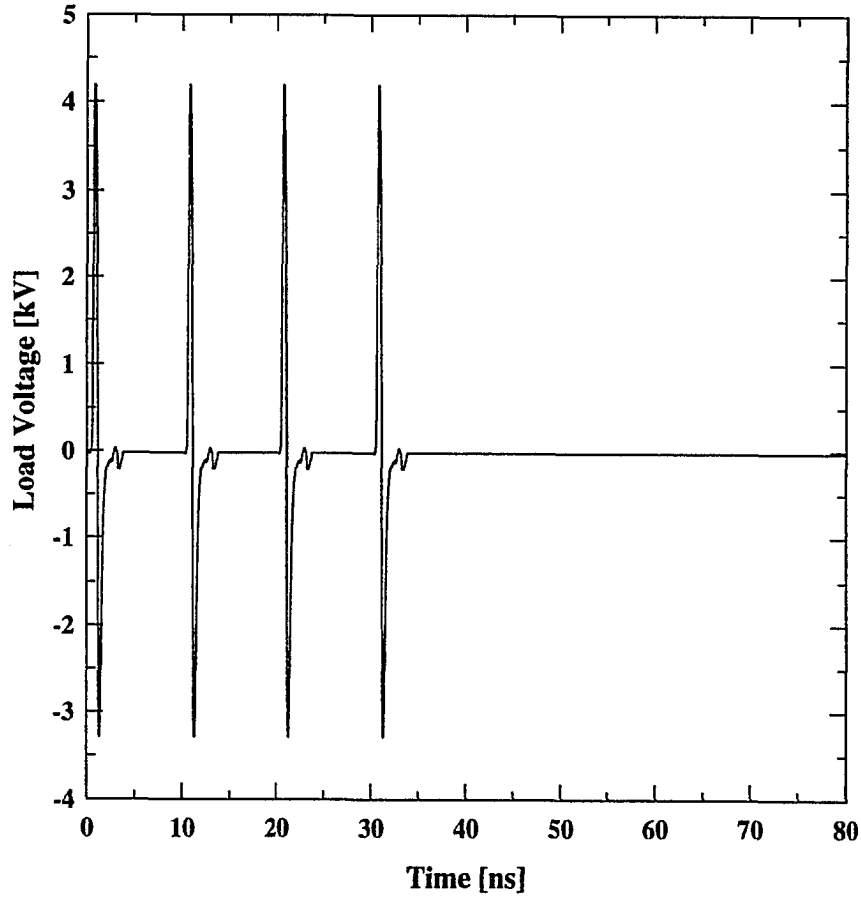

Figure A-1 Potential output of a PSO generator constructed by replicating data similar to that shown in Fig. 21 for a laser pulse separation of 500 ps.

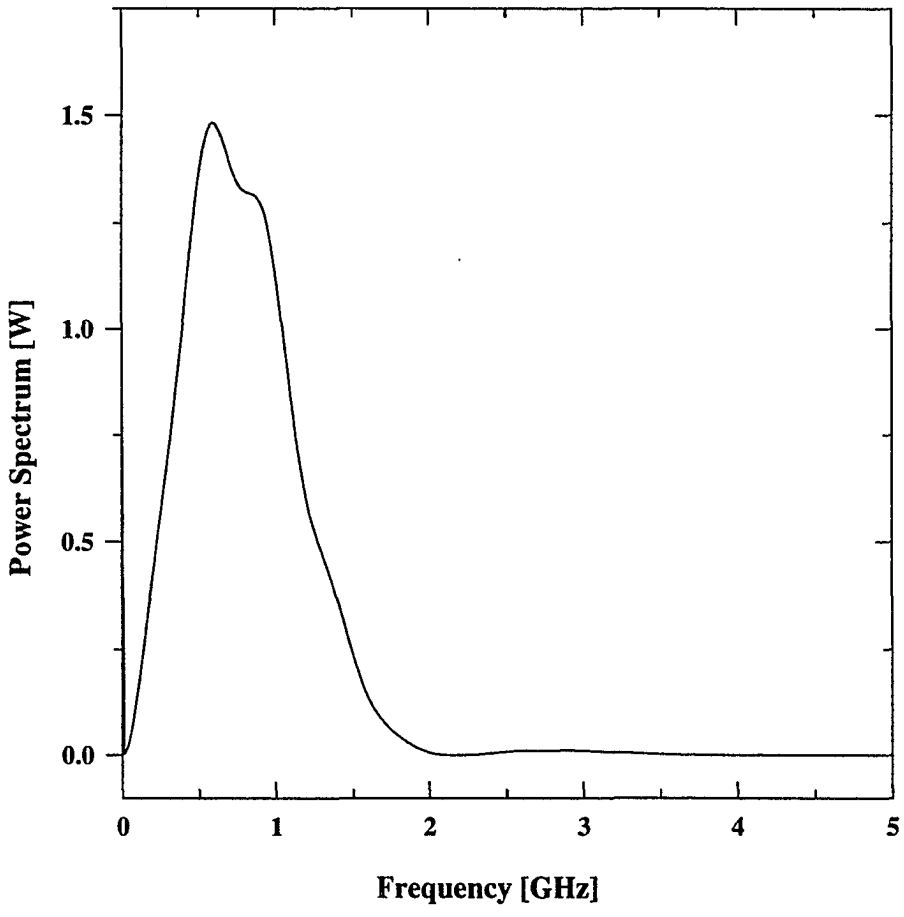

Figure A-2 Power spectrum of the single monocycle, for a repetition rate of 1 kHz, that was used to create the four-pulse burst shown in Fig. A-1.

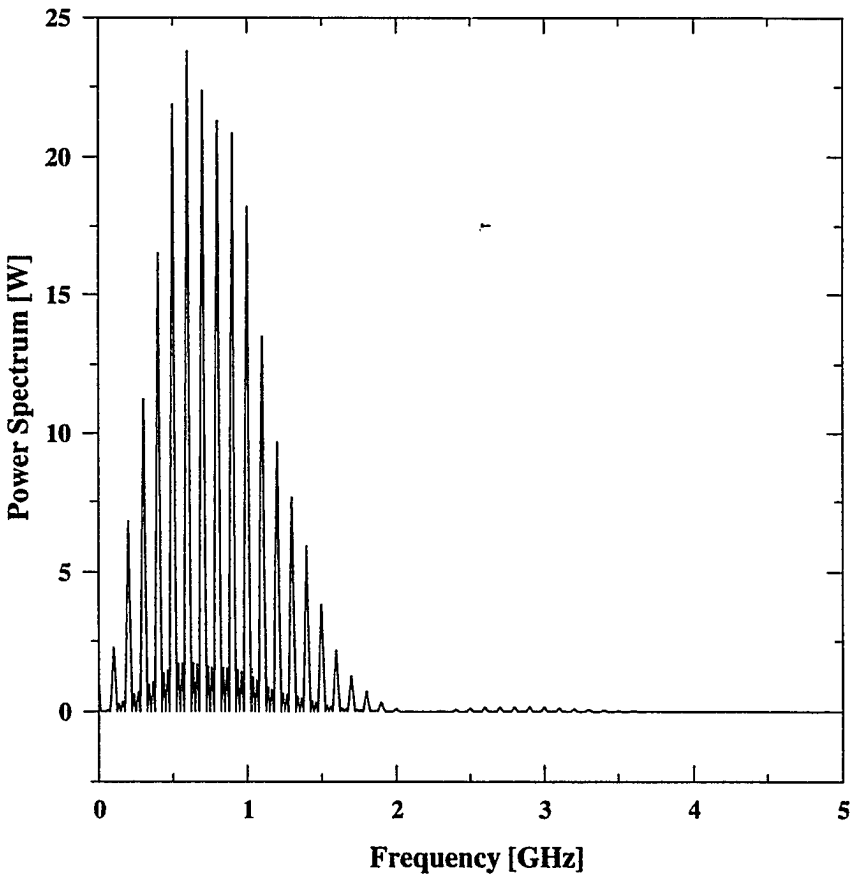

Figure A-3 Power spectrum of the waveform shown in Fig. A-1 for a 1-kHz burst-repetition rate.

frequency-domain data has units of volts. To obtain the power spectrum in the 50-Ω load, the amplitude is squared and subsequently divided by 50. The resulting spectral amplitude is now in units of watts, however, this amplitude corresponds to the 12.5-MHz repetition rate. To scale the data for a 1-kHz repetition rate, the data must be multiplied by the square of the ratio of 1 kHz over 12.5 MHz, or a factor of 6.4×10^{-9}.

The spectrum for the single monocycle, shown in Fig. A-2, has a maximum amplitude of about 1.5 W. However, as a result of the 10-ns spacing between the RF cycles, the spectrum for the four-pulse burst, shown in Fig. A-3, is further subdivided into peaks which occur every 100 MHz. As a result of the increased number of nulls in the spectrum, the power spectrum at each one of the peaks is increased considerably. In fact, the peak power increased from 1.5 W to about 24 W, or a factor of 16. There are basically two reasons for this increase in the power spectrum. First, since the power spectrum for both the monocycle and the four-pulse burst were calculated for a 1-kHz repetition rate, the total energy in the burst is a factor of four higher. The other factor of four comes from the subdivision of the spectrum into discrete peaks at every 100 MHz. In a similar manner, if ten pulses were generated within a single burst, the peak of the power spectrum would be increased by a factor of 100. A higher number if cycles in the burst would also have the effect of reducing the width of each one of the 100-MHz peaks.

The same type of results are obtained when using the waveform distorted by separating the positive and negative half cycles, as shown in Fig. A-4, to fabricate the four-pulse burst. Note that this distortion results in an additional increase in the peak of the power spectrum, at lower frequencies, as shown in Fig. A-5. These results indicate that the time

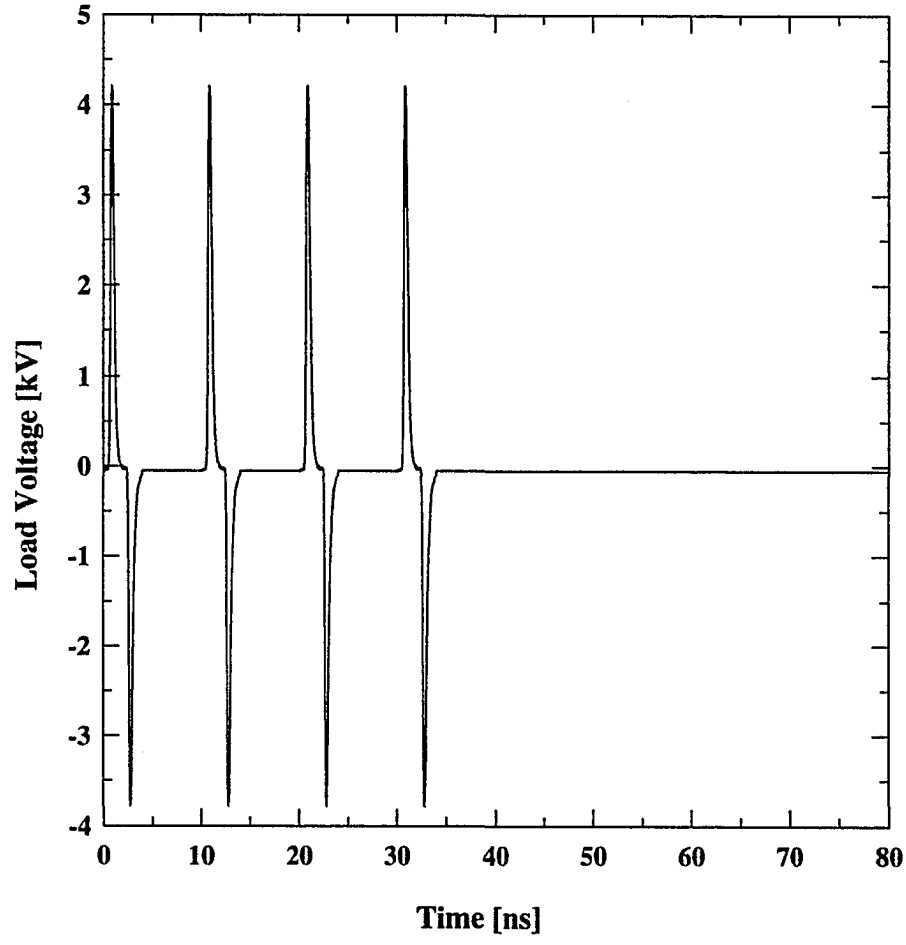

Figure A-4 Potential output of a PSO generator constructed by replicating the data shown in Fig. 21 for a laser pulse separation of 2.0 ns.

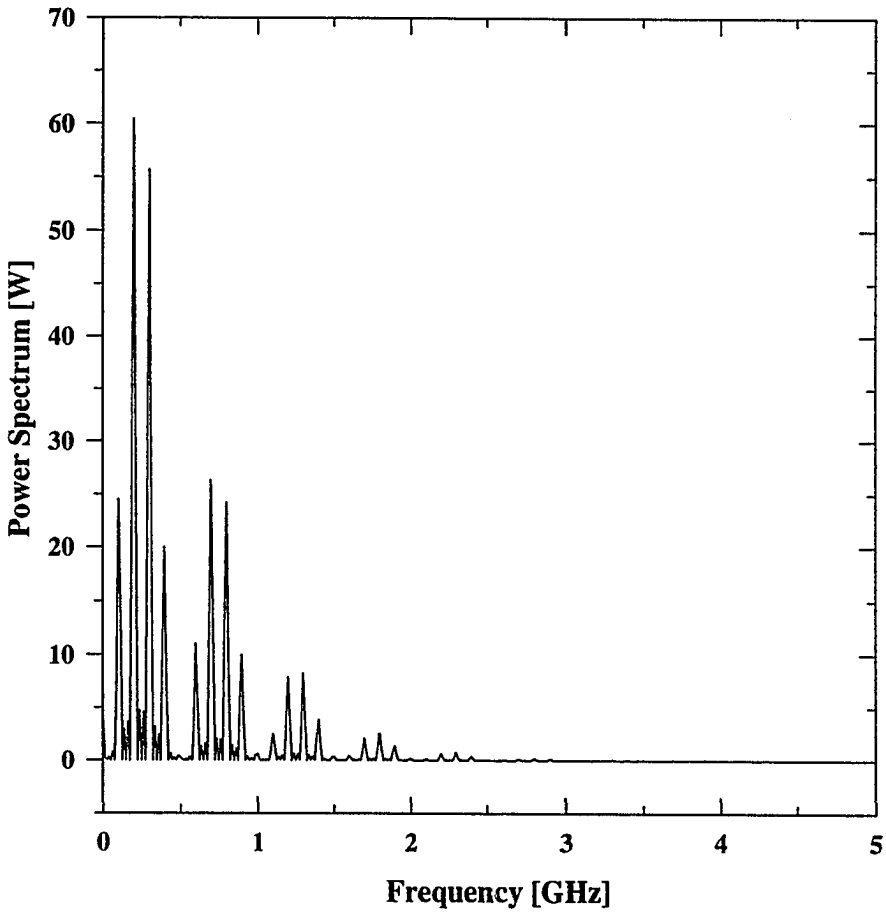

Figure A-5 Power spectrum of the waveform shown in Fig. A-4 for a 1-kHz burst-repetition rate.

delay between the positive and negative half-cycles dictates the shape of the envelope of the spectrum, while the cycle repetition rate within the burst dictates the placement of the various spectral peaks. The type of waveforms shown in Figs. A-1 and A-4, with their associated spectra shown in Figs. A-3 and A-5, respectively, may have considerable advantages for use in ultra-wide-band (UWB)-radar and other high-power microwave (HPM) applications.

David Clifton Stoudt was born in Abington, Pennsylvania, in 1959. From 1978 through 1984 he served in the U.S. Navy as a Nuclear Reactor Operator, and a U.S. Navy diver, aboard the fast-attack submarine USS Finback (SSN 670). He received the B.S.E.E. (summa cum laude) and M.S.E.E. degrees in 1987 and 1989, respectively, from Old Dominion University, Norfolk, VA. His Ph.D. degree was supported, at Old Dominion University, through the Navy Fellowship Program.

From 1987 through 1989 he worked as a Graduate Research Assistant at Old Dominion University where he conducted research on gallium arsenide material characterization and the development of a high-power electron-beam-controlled semiconductor switch. In 1990 he joined the Naval Surface Warfare Center in Dahlgren, VA, to continue his work on high-power semiconductor switches. His current research efforts include the effects of fast-neutron irradiation and contact configurations on the operation of photoconductive switches, the use of photoconductive switches in inductive-energy-storage and high-power microwave devices, and the transient response of dielectrics and poor conductors to fast microwave and optical pulses. In 1993 he was awarded the Pulsed Power Student Award at the Ninth IEEE International Pulsed Power Conference.

Mr. Stoudt is a member of the Eta Kappa Nu Electrical Engineering Honor Society, Tau Beta Pi Engineering Honor Society, the IEEE Electron Devices Society, and the IEEE Microwave Theory and Techniques Society.